The Sustainment and Consequences of Cytosolic Calcium Signals in Osteocytes

Genevieve N. Brown

Submitted in partial fulfillment of the
requirements for the degree of
Doctor of Philosophy
in the Graduate School of Arts and Sciences

COLUMBIA UNIVERSITY

2016

ABSTRACT

The Sustainment and Consequences of Cytosolic Calcium

Signals in Osteocytes

Genevieve N. Brown

Osteocytes are widely regarded as mechanosensors, capable of detecting changes in the mechanical environment of the bone tissue and modifying cellular responses accordingly. Indeed, an intact osteocyte network is required for bone changes in response to unloading, and studies have shown that loading/unloading influences osteocyte expression of proteins that modulate bone turnover, such as sclerostin and receptor activator of nuclear factor kappa B ligand (RANKL). However, mechanisms underlying osteocyte mechanotransduction remain unclear. For instance, one of the earliest responses of bone cells to mechanical stimuli is a rise in intracellular, or cytosolic, calcium (Ca^{2+}_{cyt}), but the mechanisms by which osteocytes generate or utilize Ca^{2+} signals to direct bone adaptation are largely unknown.

In this thesis, I explored the mechanisms underlying the sustainment of Ca^{2+}_{cyt} oscillations in osteocytes as well as downstream consequences of these patterns. I discovered that Ca^{2+}_{cyt} oscillations are generated in osteocytes by Ca^{2+} release from the endoplasmic reticulum and that the predominant expression of T-Type voltage sensitive Ca^{2+} channels in these cells facilitates this behavior. I also explored the role of the actin cytoskeleton – another prominent feature in osteocytes – and found that actin dynamics are important for the generation of Ca^{2+}_{cyt} signals. Furthermore, I confirmed that Ca^{2+}_{cyt} transients subsequently activate actomyosin contractions in osteocytes by monitoring interactions of osteocytes exposed to Ca^{2+} agonists on micropillar substrates.

With this information, I sought to relate Ca^{2+}_{cyt} signaling and actomyosin contractility in osteocytes to their roles as coordinators of bone adaptation. Ca^{2+}-dependent contractions have been shown to facilitate the release of extracellular vesicles, small membrane-enclosed packages of proteins that cells use for communication, in other cell types. I found that mechanical stimulation increased the production and release of extracellular vesicles in osteocytes, and this was dependent on Ca^{2+} signaling. These extracellular vesicles contained key bone regulatory proteins and were small enough to plausibly transport through the lacunocanalicular system. Thus, I uncovered a novel mechanotransduction pathway by which osteocytes may coordinate tissue-level adaptation. As an extension of this work, I also characterized these behaviors in new osteocyte cell lines which may better reflect native cell physiology.

The work in this thesis anchors Ca^{2+} signaling as a critical osteocyte response to mechanical loading and adds to the body of work exploring how and why these signals are generated. The results of these studies add new information to the still limited knowledge of this important bone cell and extend Ca^{2+} signaling research by connecting early mechanosensation events to subsequent protein responses to mechanical loading. Understanding the mechanisms behind the robust Ca^{2+}_{cyt} oscillations in osteocytes and how they relate to their roles as coordinators of bone adaptation may improve our ability to prevent or treat bone degeneration in diseases like osteoporosis where mechanosensitivity is impaired.

Table of Contents

List of Figures

Figure 6.8. Percent change in elastic modulus of devitalized bone cores loaded routinely and culture for 4 weeks. (A) 36 trabecular bone explants were randomly assigned to one of 6 groups (n=6/group): tissue culture control, non-loaded, and loaded for 1, 3, 5, and 10 days. Apparent elastic moduli were determined for each sample at Day 0, and a load level corresponding to 2400με was determined for each sample to apply similar strains across all specimens. The modulus was determined again after 4 weeks (Day 28), and a percent difference was calculated. (B) Average percent change in apparent elastic modulus for each group. Error bars are standard deviations. One sample was eliminated as an outlier from the 5 day loading group (gray italics). One-way ANOVA with Bonferroni's post hoc analysis was used to determine differences among groups, and $p<0.05$ was set to indicate significance. No differences were detected……...136

Figure 6.9. Influence of perfusion on osteocyte viability over long term culture. (A) Reconstructed confocal image of an explant perfused for 14 days in the loadable perfusion chamber. (B) Inset of the confocal slice corresponding to the bone surface. (C) Live osteocytes (green cells, white arrows) are observed 20μm below osteoblasts on the bone surface. (D) A number of dead osteocytes (red cells) can be observed in static cultures at the same time point…….138

Acknowledgements

I would first like to acknowledge the amazing help that I have had from high school, undergraduate, and M.S. students throughout the past six years. It has been a pleasure to work with some incredible students – each with their own skills and passions and personalities – and together generate the work that substantiates this thesis. I would like to thank Prajesh Desai (M.S. ’15) for helping with the ER depletion studies and the characterization of the MC3T3-E1 cell responses. He worked with me the longest of all my students, and it was so fun to have a research partner for that project. I also want to thank Walker Magrath (class of 2019) for performing the PLA and immunostaining and for working so diligently as my best-ever SURF student. I am extremely grateful to Victoria Dreyer and Navid Mousavi, both high school students starting college this year, for their help with immunostaining and flow studies and for our inspiring conversations about science. I want to thank Eamon Thomasson (B.S. ’16) for working out protocols for our new cell lines and Zac Sarish (M.S. ’14) for his help with the quasi-3D studies. I want to recognize Prashanthi Ravichandran, a current M.S. student, for working so thoroughly for her first time in a biology lab by helping with immunostaining and Western blots. I also want to thank Jonathan Guo and Reiji Mennitt, both high school students, for their help with preparing plasmids, running Western blots, analyzing images, and generally keeping the lab in good shape. And lastly, I want to acknowledge Donisha Das (M.S. ’12), Eugenia Gurvich (B.S. ’13, Brown University), and Alyce Ge for being among the first of my students, dedicating their time and energy to the explant project. It was a delight working with you all.

During the few times when I thought I might not make it through this process, I was comforted and encouraged by the amazing team of people I get to work with each day. I want to

thank my labmates for keeping me going. Bin Zhou is the most kind-hearted person I have ever met with the most outstanding work ethic, and I have learned how to be a little bit better with him as my friend. I continue to be amazed by Ji Wang's confidence and character, and I feel stronger myself having shared these past years together. For every mess of Eric Yu's I have had to clean up in the lab, he has helped me work through a mess in my personal life, and I am very grateful for his friendship. I want to thank Andrea Morrell for being such a gracious person, always offering her time and help and ideas. Having you as a sounding board for my ramblings about science has helped to expand a lot of this work. Thanks to Sam Robinson for being good at everything and therefore motivating me to try harder. And even though we only shared a short time together, I want to thank Jenny Hu for bringing such a calm and thoughtful character to the lab; you have impressed me so much with the way you handle your responsibilities. I want to acknowledge Eddie Zhang for the equal dedication he gives to his work and the people around him. And lastly, a huge thanks to Rachel Sattler for sharing her enthusiasm for science and for teaching me to think about, approach, and explain things differently.

Of course, the person that curated this amazing team is most deserving on my gratitude. I would like to thank my thesis advisor, X. Edward Guo, for pushing me to be a strong scientist and engineer – two titles each with their own mind- and skillsets that I believe he combines seamlessly. I have learned an incredible amount over the past 6 years about how to think about, approach, and solve problems, and I appreciate that you took the time to coach me into a better biomedical engineer. Thank you for showing me that a little bit of the right kind of confidence can go a long way.

I am fortunate to be surrounded by the very faculty that set the groundwork for my Ph.D. research. I would like to thank Professors Clark Hung and Chris Jacobs for inspiring many of

these studies and guiding their progress by serving on my committee. I would also like to thank Professor Lance Kam and his student Susie Jin for so graciously collaborating with me for part of this work. And lastly, I want to thank Henry Hess for jumping in when duty called. It has been wonderful to have all your support.

I would be remiss not to acknowledge the faculty and staff at Penn State that helped me get to Columbia in the first place. Thank you to Professors Erwin Vogler and Andrea Mastro for providing me with an incredible opportunity to work with you as an undergraduate. It was your research that sparked my first interest in this field and your guidance that helped me continue to grow as a researcher. I want to particularly thank Donna Sosnoski for taking the time to teach me every technique I know in the lab. I want to thank Professor Cheng Dong for guiding me in my decision to come to Columbia and for continuing to be so supportive throughout graduate school. I cannot properly express my gratitude to Melissa Marshall, Michael Alley, and Karen Thole for their immense support of my academic career and development with words alone. Thank you for shaping my skills as a communicator of science and engineering, and thank you for giving me so many opportunities over the past 6 years to grow into a professional. But mostly, thank you for all the little emails packed with big doses of encouragement; they meant so much to me. Finally, I would also like to thank the McNair program at Penn State for giving me the resources, mostly in the form of an incredible support network, to pursue a graduate degree.

A professor once told me that the best part about graduate school is that you form friendships that you will carry with you as you grow into adulthood, and I couldn't agree more. Thank you to Gwen Nero and Zen Liu for being my very best of friends. You are brilliant women that I respect and admire, and I am incredibly appreciative to have spent the last six years with you so close by.

I want to acknowledge my family for celebrating my successes and encouraging me through my struggles in school over the last ten years. I want to particularly thank my youngest sister, Kali, for always inspiring me to be better. It is my efforts to set a good example for your life that largely guide my approach to my own.

And finally, I thank my husband, Ian, for being so immensely supportive of this endeavor. I love you dearly.

Dedication

To my late grandfather, William Rudison, for his unending love and support. I hope this makes you proud.

Chapter 1

1.1 Background

1.1.1 Bone adaptation

Wolff's Law posits that bone adapts its internal structure to support and sustain external loads[1]. This is demonstrated by the enhanced bone strength in athletes[2,3] and the loss of bone in unloading conditions, such as extended bedrest[4] and microgravity[5,6]. Furthermore, it is believed that changes in the ability of bone to adapt to its mechanical environment underlie several skeletal pathologies, including osteoporosis[7]. A better understanding of the skeleton's ability to adapt to physiologic mechanical loads has potential to reveal new strategies for mitigating the more extreme demands placed on bones in pathologic conditions and to inform novel, innovative, and more precise treatments for patients with bone disease. Thus, there is considerable interest in studying the mechanisms of bone adaptation.

For these architectural changes to occur, one or more cells within the bone must be sensitive to mechanical stimulation. Bone is comprised of three major cell types (Fig. 1.1). Osteoblasts are cuboidal cells derived from the mesenchymal lineage responsible for matrix deposition. Osteoclasts are large, multi-nucleated cells of hematopoietic origin that resorb bone. The balanced activity of osteoblasts and osteoclasts, with bone formation following resorption on identical surfaces, is called remodeling. Imbalanced activities of osteoblasts and osteoclasts can result in either excess bone formation or resorption, both typically pathologic outcomes. Together, these cells make up less than 10% of the bone cell population and, with lifetimes estimated in only weeks, represent a transient population of cells.

The majority of bone cells are osteocytes – mature bone cells embedded within the bone matrix that can survive for decades[8]. Osteocytes mature from osteoblasts that become entombed in deposited matrix. Their function was enigmatic for a long time, largely due to their inaccessibility. While osteoblast and osteoclast populations were relatively easy to isolate and characterize, it was challenging to extract osteocytes from the bone and maintain their phenotype. However, with the introduction of an osteocyte-like cell line[9] and new technologies to probe their functions *in vitro* and *in vivo*[10], the role of osteocytes in bone adaptation has received considerable attention over the last few decades.

1.1.2 Osteocytes as mechanosensors

Osteocytes are considered ideal mechanosensors due to their abundance and intricate arrangement within the bone tissue[11-15]. They are stellate cells characterized by numerous cellular processes – or dendrites – emanating from the cell body and connecting cells with one another and with cells on the bone surface, such as osteoblasts and osteoclasts[16]. Osteocyte cell bodies reside in lacunae, and the dendrites extend through channels within the bone tissue called canaliculi. The extensive network created by these structures is called the lacunocanalicular system (LCS).

Mechanical loading of bone results in bending, with areas of compression and tension forming along the bone surfaces. Physiologic loads from activities such as running and jumping can engender strains in the range of 2000-3000με[17]. However, when similar strains were used to stimulate bone cells *in vitro*, they were not sufficient to engender a biological response[18], suggesting that cells embedded within the bone experience a different mechanical stimulus than strain on the whole bone surface. Using poroelastic models to relate whole bone strains to cell

level mechanical signals, it was proposed as early as the 1970s that small shear stresses acting on osteocytes within the LCS are induced by the flow of interstitial fluid[19-21]. In the 1990s, a seminal theoretical paper predicted that the relatively small deformations to the whole bone tissue could translate to fluid shear stresses similar to those in vascular tissues [19] (reviewed in [22]). It is therefore now widely accepted that the predominant stimulus experienced by osteocytes *in situ* is fluid shear stress that results from this interstitial fluid pressurization in the LCS upon dynamic deformation of the whole bone[20,22,23]. Indeed, this has been verified experimentally[24,25], and fluid shear is now extensively used as a stimulus for *in vitro* studies.

In vitro studies subjecting osteocytes to fluid shear have shown that loading can enhance the release of prostaglandin E_2 (PGE_2)[26-28], nitric oxide[29,30], osteopontin[31], Wnts[32], and modulate the ratio of receptor activator of nuclear factor kappa-B ligand (RANKL) and its decoy receptor osteoprotegerin (OPG)[33,34] over the course of hours and days. A few studies have also demonstrated that conditioned medium from osteocytes exposed to fluid flow decreases osteoclastogenesis[33,34], inhibits osteoclast resorptive activity[35], and promotes osteoblast differentiation[36]. Taken together, these studies demonstrate that osteocytes can respond to mechanical loads by adapting downstream protein responses.

In vivo studies have also demonstrated that osteocytes are sensitive to their mechanical environment and can orchestrate bone turnover in response to changing mechanical demands[14,15]. In transgenic mice with ablated osteocytes, bone resorption was enhanced due to an increase in the RANKL/OPG ratio, and mice were resistant to unloading-induced bone loss[37]. More recent studies using osteocyte-specific inducible knockouts of RANKL suggested that osteocytes are the primary source of RANKL for modulating osteoclast activity[38,39]. Loading has also been demonstrated to affect osteocyte control of osteoblast activity through the Wnt/β-catenin

inhibitor sclerostin, which suppresses the activity of osteoblasts. Studies of both ulnar and tibial loading in mice have been shown to decrease levels of the sclerostin protein expression, while unloading has been shown to increase levels of sclerostin[40]. These changes are highly correlated with sites of anabolic bone formation in these models [40-43]. Taken all together, these studies highlight the essential role of osteocytes in both immediate mechanosensation and the coordination of later adaptive responses (Figure 1.2).

1.1.3 Calcium signaling in bone cells

One of the earliest responses of bone cells to mechanical stimulation is a rise in Ca^{2+}_{cyt}[44]. Ca^{2+}_{cyt} signaling mediates a multitude of physiological processes in a wide range of tissues[45], including cell growth in cardiac progenitors[46], insulin production in pancreatic β cells[47], differential gene expression in T-cells[48], and migration in lung fibroblasts[49]. In the musculoskeletal system, Ca^{2+}_{cyt} signals affect the differentiation of mesenchymal stem cells[50] and contribute to RANKL-induced osteoclastogenesis[51-53].

In one of the earliest studies of real-time bone cell mechanotransduction, primary osteoblasts were demonstrated to exhibit heterogeneous Ca^{2+}_{cyt} responses to different fluid shear stress levels, with most cells exhibiting a single response to fluid flow with variable magnitude[44]. Further studies examined the effects of different flow profiles on osteoblast Ca^{2+}_{cyt} responses and found that osteoblasts are more responsive to steady and pulsatile flow than oscillatory flow[54]. Furthermore, cells exposed to multiple bouts of flow were found to exhibit similar response characteristics, suggesting an intrinsic mechanosensation response[55,56]. When cultured in micropatterned networks recapitulating the characteristic spacing and connectivity of osteocytes *in vivo*, osteoblasts exhibited subsequent, lower-magnitude responses to steady flow[57]. In

addition, osteoblasts cultured in these networks could propagate Ca^{2+}_{cyt} signals to neighboring cells when a single cell was stimulated by indentation[58].

The characterization of osteocyte Ca^{2+}_{cyt} responses to mechanical loading came nearly a decade later. In explanted fragments of chicken embryonic calvariae, bone cells were demonstrated to exhibit autonomous Ca^{2+} responses[59], and embedded osteocytes stimulated by microneedle displacement[60] or shear stress over the explant surface[61] were shown to exhibit Ca^{2+}_{cyt} responses that could be propagated to neighboring cells[62]. Furthermore, osteocytes were more responsive and more sensitive to microneedle displacement when stimulated along a dendritic process rather than at the cell body[63]. This result was confirmed by a later study using localized hydrodynamic forces[64].

When exposed to fluid shear *in vitro*, osteocytes cultured in micropatterned networks were discovered to exhibit unique patterns in Ca^{2+}_{cyt}; robust, un-attenuated oscillations in Ca^{2+}_{cyt} were observed in response to steady flow in MLO-Y4 osteocytes, with some cells exhibiting up to 17 Ca^{2+}_{cyt} transients in a 9-minute stimulation period[65]. These responses were distinct from the Ca^{2+}_{cyt} responses of osteoblast precursors[65,66] and more pronounced under steady than oscillatory flow[67].

This unique pattern in Ca^{2+}_{cyt} was recently confirmed in an *ex vivo* system where osteocytes and osteoblasts in native murine tibiae were subjected to dynamic deformational loading. Osteocytes, identified as cells residing in lacunae approximately 40 μm below the bone surface, exhibited robust oscillations in Ca^{2+}_{cyt} in response to load[68]. This pattern was more pronounced than the autonomous Ca^{2+}_{cyt} responses of osteocytes, which were undetectable, as well as the loading-induced and autonomous responses of cells on the bone surface[59,68]. Taken

together, these studies allude to a key role of Ca^{2+}_{cyt} signaling in osteocyte mechanosensation (Figure 1.3).

1.2 Motivations

While robust Ca^{2+}_{cyt} have been observed in osteocytes in response to mechanical loading, and mechanical loading has been demonstrated to affect the adaptive response of osteocytes through modulation of protein expression, to date no studies have connected Ca^{2+}-mediated mechanosensitivity to signal transduction in osteocytes. Furthermore, the mechanisms underlying the initiation and sustainment of Ca^{2+}_{cyt} oscillations have not been clearly identified. Ca^{2+}_{cyt} oscillations in osteocytes are dependent on ER stores and modulated by inhibition of membrane Ca^{2+} channels[65], but the exact nature of this interaction remains unknown. For instance, inhibition of T-Type voltage-sensitive calcium channels (VSCC) has similar effects as disruption of ER stores, yet no link has been demonstrated between them in osteocytes. Furthermore, the role of the ER has only been studied indirectly through the use of pharmacologic inhibitors.

A prominent feature of osteocytes is an actin-rich cytoskeleton. By tracking strains in the actin network within osteocytes subjected to fluid flow[69,70], our laboratory previously observed that development of tension in the actin precedes a Ca^{2+} response. We also discovered an immediate compression of the actin network following a Ca^{2+} signal, indicative of an actomyosin contraction. This is the first demonstration of a mechanical consequence of mechanotransduction in osteocytes and likely relates to the function of osteocytes as regulators of bone adaptation, but no studies have explored this phenomenon. This warrants a detailed investigation of the

interactions between the actin cytoskeleton and Ca^{2+}_{cyt} signals in osteocytes, which are so far largely unexplored.

Furthermore, Ca^{2+}_{cyt}-dependent contractions may facilitate the release of proteins from osteocytes within the bone to cells on the bone surface through the shedding of extracellular vesicles. Though vesicles have been identified in osteocytes[71] and shown to contain osteocyte proteins[72], to date no studies have explored their role in osteocyte mechanobiology.

1.3 Aims and Organization

The goal of this thesis is to extend the understanding of how Ca^{2+}_{cyt} signals in osteocytes are generated, sustained, and involved in adaptive protein responses.

In the first study presented in Chapter 2, we explored whether the ER sustains Ca^{2+}_{cyt} oscillations in osteocytes through interaction with T-Type VSCC. We hypothesized the predominant expression of T-Type channels in osteocytes may contribute to their unique Ca^{2+}_{cyt} patterns and further speculate that T-Type VSCC in osteocytes may interact with ER stores. Our efforts were guided by the following aims:

Specific Aim 1a: To determine the effects of VSCC inhibitors on Ca^{2+}_{cyt} signals and Ca^{2+}_{ER} dynamics in osteocytes and osteoblasts.

Specific Aim 1b: To investigate the physical association of T-Type VSCC with the ER in osteocytes and osteoblasts.

In the next study presented in Chapter 3, we explored how the dynamics of the actin cytoskeleton are coupled to Ca^{2+} signaling in osteocytes. Our first aim was to determine whether actin dynamics are important in sustaining Ca^{2+} oscillations in osteocytes. Next, we sought to confirm osteocytes exhibit Ca^{2+}-dependent contractions in an alternative experimental system by

chemically and mechanically inducing Ca^{2+}_{cyt} responses in osteocytes seeded onto micropillars. Finally, looking towards future studies in animal models, we sought to identify an inhibitor of this contractility that could be translated to *in vivo* studies.

Specific Aim 2a: To evaluate the influence of actin dynamics on Ca^{2+}_{cyt} oscillations in osteocytes under fluid shear stimulation.

Specific Aim 2b: To verify Ca^{2+}-dependent actomyosin contractility in osteocytes by measuring interactions with a deformable substrate.

Specific Aim 2c: To inhibit actin contractions independent of Ca^{2+} signals in osteocytes.

In Chapter 4, we wanted to link the observed Ca^{2+} oscillations and actin contractility to a functional consequence in osteocytes. There is a well-established role for Ca^{2+}/actin dynamics in promoting exocytosis, and recent research has highlighted the importance of exocytosis in the shedding of vesicles that serve to transport proteins from one cell to another. Thus, we hypothesized Ca^{2+}_{cyt} oscillations have a role in immediate osteocyte protein responses by facilitating the shedding of extracellular vesicles. This hypothesis was explored through the following aims:

Specific Aim 3b: To quantify mechanically-induced extracellular vesicle release in osteocytes with and without inhibition of Ca^{2+} oscillations.

Specific Aim 3c: To characterize the size and contents of osteocyte-derived extracellular vesicles.

The previous chapters use the MLO-Y4 osteocyte cell line, which, since its introduction in 1997[9,73], has revolutionized the study of osteocytes. However, as our studies begin to link behaviors in MLO-Y4 osteocytes to their protein responses, it is important to evaluate how well they recapitulate native osteocyte physiology. Recently, two new osteocyte cell lines – IDG-SW3

and Ocy454 – have been developed to address the lack of sclerostin expression in MLO-Y4[74,75]. Sclerostin is expressed almost exclusively in osteocytes and serves to inhibit bone formation, therefore it is a specific and effective target of current therapies for osteoporosis. In order to rely on these new cell lines for experimental studies linking Ca^{2+} responses to changes in sclerostin expression, we sought to characterize these responses in Chapter 5. Given the consistency among our prior *in vitro* and *ex vivo* studies, we hypothesized mature osteocytes would exhibit oscillations in Ca^{2+}_{cyt} in response to fluid shear, while immature cells would be less sensitive. The following aims reflect the characterization of these two cell lines:

Specific Aim 4a: To evaluate the percentage of responsive cells and number of Ca^{2+} peaks in immature and differentiated Ocy454 cells subjected to fluid shear.

Specific Aim 4b: To evaluate the percentage of responsive cells and number of Ca^{2+} peaks in immature and differentiated IDG-SW3 cells subjected to fluid shear.

Lastly, though the final study in Chapter 6 was actually developed prior to the start of the other studies presented herein, it represents an important move in extending that work to inter-cellular communication dependent on these processes. A loadable perfusion chamber was developed to simultaneously load and perfuse explanted bovine bone cores. These bone cores are organotypic, with preserved osteocytes in the lacunocanalicular system connected with osteoblasts on the bone surface. This system also has the singular advantage to generate an experimental group that cannot be made *in vitro* or *in vivo*: genetically modified osteoblasts with intact osteocytes. Culturing these bone cores in a loadable perfusion bioreactor thus enables precise mechanical interventions and long-term culture of these critical samples. This work was guided by the following aims:

Specific Aim 5a: To design a loadable perfusion chamber for the long-term culture of bovine trabecular bone.

Specific Aim 5b: To evaluate the accuracy of the mechanical properties of bone tissue calculated from samples inside the chamber.

Specific Aim 5c: To confirm that perfusion of bovine trabecular bone in could maintain osteocyte viability for up to 4 weeks in culture.

Chapter 7 summarizes the conclusions of this thesis work and suggests future studies to expand on these findings.

1.4 Figures

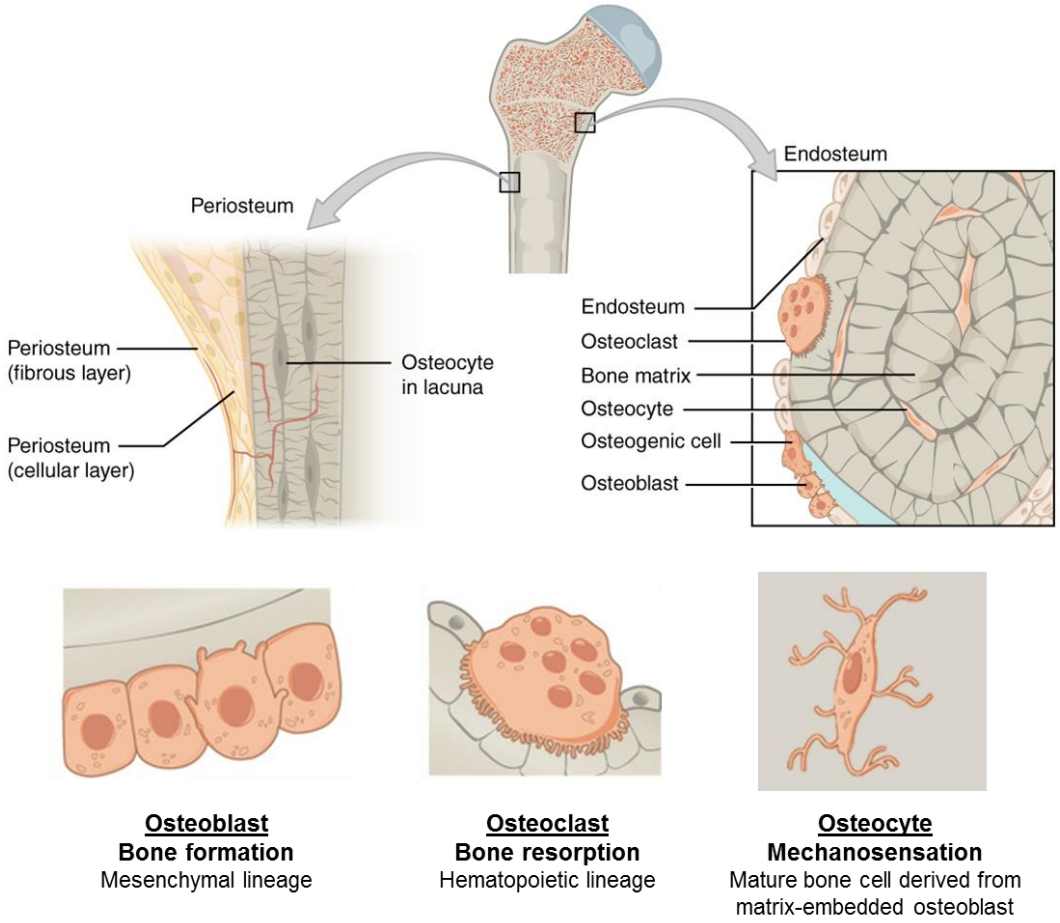

Figure 1.1 Types of bone cells and their primary functions. Bone is comprised of three major cell types that work in concert to maintain the skeleton. Osteoblasts are responsible for matrix deposition, while osteoclasts are responsible for matrix resorption. Osteocytes are the most abundant cells thought to primarily function as mechanosensors. Osteoblasts that become embedded in their deposited matrix can mature into osteocytes. Osteocytes are characterized by numerous dendrites emanating from the cell body that connect cells to one another and to osteoblasts and osteoclasts on the bone surface. *Images adapted from OpenStax, Anatomy & Physiology. OpenStax CNX. May 18, 2016 http://cnx.org/contents/14fb4ad7-39a1-4eee-ab6e-3ef2482e3e22@8.25*

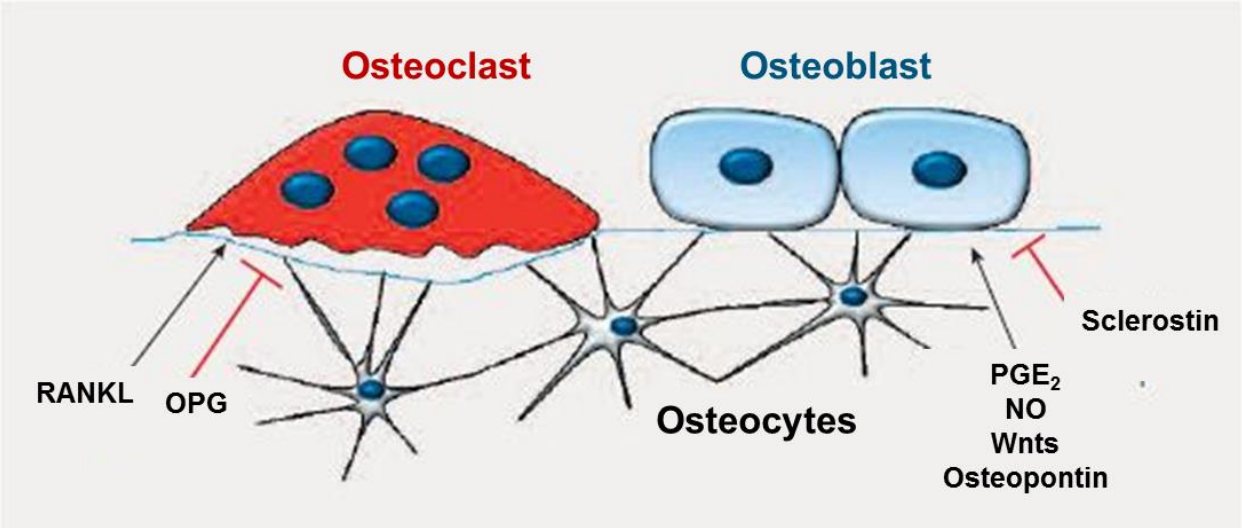

Figure 1.2 Osteocyte regulation of osteoblast and osteoclast activities. Summary of the various biochemical responses of osteocytes to mechanical loading and how these function to promote or inhibit bone formation and resorption. *Image adapted from: "The osteocyte: doing the hard work backstage." M. Prideaux and L. Bonewald, Medicographia. 2012; 34:228-235*

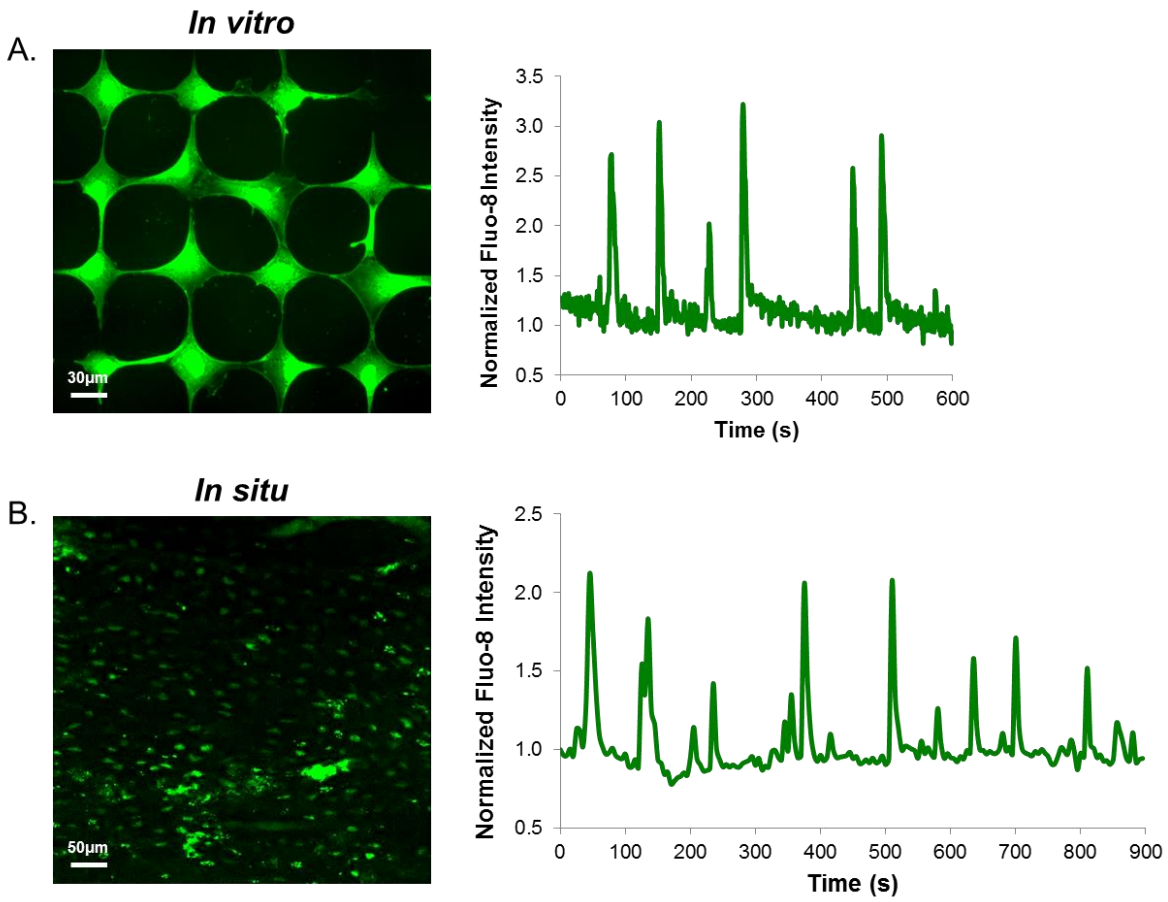

Figure 1.3 Mechanically-induced calcium oscillations in *in vitro* and *in situ* osteocytes. (A) MLO-Y4 osteocytes cultured in micropatterned cell networks exhibit repetitive, spike-like changes (oscillations) in Ca^{2+}_{cyt} levels when exposed to steady fluid shear. (B) Osteocytes embedded in an explanted murine tibia exhibit similar patterns in Ca^{2+}_{cyt} when subjected to dynamic, deformational loading of the whole bone. *Images adapted from references 65 and 68*.

Chapter 2

Interactions between the endoplasmic reticulum and T-Type voltage-sensitive calcium channels in osteocytes to sustain mechanically-induced calcium oscillations

This thesis chapter has been previously published, in part, in the manuscript:

> Genevieve N. Brown, *Pui L. Leong, and X. Edward Guo. "T-Type voltage-sensitive calcium channels mediate mechanically-induced intracellular calcium oscillations in osteocytes by regulating endoplasmic reticulum calcium dynamics." Bone 88, 2016.*

2.1 Introduction

Osteocytes are widely regarded as mechanosensors, capable of detecting changes in the mechanical environment of the bone tissue and modifying cellular responses accordingly[11,14]. Osteocytes exhibit robust oscillations in Ca^{2+}_{cyt} in response to mechanical stimulation, a pattern distinct from their osteoblast precursors and attributed to their mechanosensitivity[65,68]. Prior *in vitro* work from our laboratory concluded that Ca^{2+}_{cyt} transients depend on both the extracellular reservoir of Ca^{2+} ions (with Ca^{2+} transported through channels on the plasma membrane) and intracellular storage organelles, in particular the endoplasmic reticulum (ER)[65] (Figure 2.1).

Indeed, prior studies in osteoblasts alluded to the importance of the ER as a subcellular store of Ca^{2+} for flow-induced Ca^{2+} responses in bone cells. Block of Ca^{2+}_{ER} release by TMB-8[44] or neomycin[76] dramatically reduced the number of osteoblasts capable of exhibiting Ca^{2+}_{cyt} transients, and thapsigargin treatment eliminated the lower magnitude subsequent peaks in micropatterned osteoblasts[57].

In osteocytes, depletion of ER stores abrogates oscillations. Treatment with the drug thapsigargin to block ER Ca^{2+} reuptake significantly reduced the number of Ca^{2+}_{cyt} transients from an average of five down to a single response. A similar effect was observed in *in situ* osteocytes, where thapsigargin treatment abolished multiple Ca^{2+} responses induced by dynamic loading of a murine tibia[68].

The distinct Ca^{2+} oscillations in osteocytes, which are absent in osteoblasts and inhibited by ER disruption[65], suggest that a phenotypic difference between these two cells may explain this behavior. Ca^{2+}_{cyt} oscillations in osteocytes are also affected by inhibition of a number of membrane channels involved in Ca^{2+} transport, and targeting channels expressed primarily in osteocytes should clarify some mechanisms underlying this unique behavior. For instance, the expression of voltage-sensitive calcium channel (VSCC) subtypes changes as osteoblasts differentiate into osteocytes[77]. Osteoblasts express both low threshold T- and high threshold L-type VSCC, whereas osteocytes predominantly express T-Type VSCC[78]. Previous studies published from our laboratory explored the effects of VSCC inhibitors when added to the flow medium after shear stimulation[65]. The addition of the T-Type inhibitor NNC 55-0396 interrupted Ca^{2+}_{cyt} responses in osteocytes, preventing subsequent Ca^{2+} transients, but had little observable effect on osteoblasts. Treatment of *in situ* osteocytes with the T-Type inhibitor prior to mechanical stimulation also significantly reduced the number of Ca^{2+} responses[68]. Interestingly, inhibition of these channels in both systems had similar effects as disruption of ER stores, though no link has been demonstrated between them in osteocytes. This suggests that T-Type VSCC may interact with the ER in osteocytes, with the ER possibly relying on T-Type VSCC to replenish Ca^{2+} following Ca^{2+} release.

VSCC have been shown to interact with the ER and Ca^{2+}_{ER} release pathways in other cells. A direct association of T-Type VSCC with the ER has been previously demonstrated in arterial smooth muscle, where $Ca_V3.2$ channels were found to be localized to ER caveolae by transmission electron microscopy and to bind to ryanodine receptors (RyR) on the ER by a proximity ligation assay[79]. In a previous study, blocking RyR by tetracaine did not abolish Ca^{2+}_{cyt} oscillations in osteocytes, but inhibition of inositol triphosphate (IP3) generation by treatment of cells with neomycin, which prevents IP3 receptor (IP3R)-mediated release of Ca^{2+} from the ER, abolished multiple responses[65]. Thus, a similar association may exist between T-Type VSCC and IP3R in osteocytes. In addition, a number of proteins participate in Ca^{2+} release from ER stores and Ca^{2+} entry triggered by this release – a phenomenon referred to as store-operated calcium entry (SOCE) – such as Stromal Interaction Molecules (STIMs) and Ca^{2+}-Release Activated Channels (CRACs)[80]. In particular, STIM1 has been shown to interact with L-Type VSCC in rat cortical neurons[81] and vascular smooth muscle cells[82] and $Ca_V3.1$ T-Type VSCC in cardiac myocytes[83]. The potential role of SOCE-related proteins in osteocyte Ca^{2+} signaling have not yet been explored.

Though our previous studies implicate roles for both the ER and T-Type VSCC in osteocyte Ca^{2+}_{cyt} responses, their relative contributions or any interactions between the ER and T-Type VSCC remain unknown. This is largely due to an inability to observe ER Ca^{2+} dynamics in the same way that we can probe Ca^{2+}_{cyt} events[84,85], i.e. to monitor Ca^{2+} localized to the ER separately from Ca^{2+} entering the cell from the extracellular fluid. However, advances in genetically encoded Ca^{2+} biosensors now enable the targeting of these sensors to subcellular organelles, including the ER[86-88].

Thus, the focus of this work is to observe Ca^{2+}_{ER} dynamics in bone cells to better understand the role of ER stores in the unique Ca^{2+} oscillations in osteocytes. We hypothesized that an ability to refill ER stores results in Ca^{2+}_{cyt} oscillations in osteocytes. We also hypothesized that the predominant expression of T-type channels in osteocytes may contribute to their unique Ca^{2+}_{cyt} patterns and further speculated that T-type VSCC in osteocytes may interact with ER stores.

2.2 Materials and Methods

2.2.1 Cell culture

Osteocyte-like MLO-Y4 cells (a gift from Dr. Lynda Bonewald, University of Missouri-Kansas City, Kansas City, MO) were cultured on 0.15 mg/ml collagen (rat tail type I, BD Biosciences, San Jose, CA) coated culture dishes in minimum essential alpha medium (α-MEM, Life Technologies, Carlsbad, CA) supplemented with 5% fetal bovine serum (FBS, Hyclone Laboratories Inc., Logan, UT) and 5% calf serum (CS, Life Technologies, Carlsbad, CA). MC3T3-E1 pre-osteoblasts (ATCC, Manassas, VA) were cultured in α-MEM supplemented with 10% FBS. Cells were maintained at 5% CO_2 and 37°C in a humidified incubator. MLO-Y4 cells were sub-cultured prior to reaching 70-80% confluence in order to maintain an osteocyte-like phenotype.

2.2.2 Inhibitors

All inhibitors used in this study were purchased from Sigma-Aldrich (St. Louis, MO). Thapsigargin is an inhibitor of the Ca^{2+}-ATPase pump on the ER (SERCA) which facilitates the reuptake of Ca^{2+} into the ER, and thapsigargin treatment (1μM) thereby results in ER depletion.

Two VSCC inhibitors were used in this study: the T-Type inhibitor NNC 55-0396 (20 μM) and the L-Type specific inhibitor nifedipine (10μM). MLO-Y4 cells were also treated with the following inhibitors related to SOCE: YM58483 (3μM), a CRAC inhibitor[89]; SKF-96365 (50μM), a SOCE inhibitor that inhibits STIM1 (similar effects as STIM1 silencing)[90] but exhibits off-target effects on VSCC activity[91]; and 2-APB (50μM), a reliable inhibitor of SOCE and IP_3R[91,92]. Cells were incubated in the inhibitors for 15 minutes prior to flow exposure, and the inhibitors remained in the flow medium for the duration of the experiment.

2.2.3 Ca^{2+}_{cyt} indicators and Ca^{2+}_{ER} visualization

To observe Ca^{2+}_{cyt} changes only, MLO-Y4 and MC3T3-E1 cells were stained with Fluo-8 AM (AAT Bioquest, Sunnyvale, CA) dissolved in 20% Pluronic F-127 in DMSO (Invitrogen, Carlsbad, CA). To visualize ER calcium levels in osteocytes and osteoblasts, cells were transiently transfected with the D1ER plasmid (plasmid #36325, Addgene, Cambridge, MA)[93] using standard non-liposomal techniques (Fugene 6, Promega Corporation, Madison, WI). D1ER is a second generation cameleon Ca^{2+} fluorescence resonance energy transfer (FRET) sensor targeted to the ER with a retention sequence. To simultaneously visualize Ca^{2+}_{cyt} and Ca^{2+}_{ER}, cells were transfected with D1ER and then stained with the red-shifted Ca^{2+}_{cyt} indicator Fura Red-AM (20μM, Life Technologies, Carlsbad, CA) in DMSO and Kolliphor® EL (Sigma-Aldrich, St. Louis, MO) prior to fluid flow stimulation.

To verify the localization of the D1ER plasmid, transfected cells were stained with ER-Tracker Red (Molecular Probes, Eugene, OR). Cells were rinsed and incubated with a warmed 1μM working solution of ER-Tracker Red for 30 minutes at 37ºC. Cells were rinsed with fresh medium and post-incubated for 15 minutes prior to imaging. The FRET biosensor was excited at

430nm, and fluorescence emission of YFP (530nm) was collected as the FRET image. The ER Tracker Red dye was imaged using 568nm excitation/660nm emission.

2.2.4 Fluid flow stimulation

Prior to staining with appropriate Ca^{2+} indicators, cells were plated onto 10μg/mL fibronectin (Corning, Corning, NY) coated glass slides at ~80% confluency to establish cell-cell contact. Slides were then stained and assembled into a custom parallel-plate flow chamber with a glass bottom that permits live cell imaging under fluid shear stimulation. For single cell studies, cells were plated onto 500μm thick glass slides (Delta Technologies, Loveland, CO) to accommodate the shorter working distance of the higher magnification objectives. The chamber was placed on the stage of an inverted microscope (Olympus, Waltham, MA) and attached to a magnetic gear pump (Scilog, Madison, WI) for the application of steady, laminar, unidirectional flow at a shear stress of 35 dynes/cm^2, which has been shown to induce multiple Ca^{2+}_{cyt} responses in osteocytes and fewer, weaker responses in osteoblasts in our previous studies[65]. In addition, the Ca^{2+}_{cyt} patterns observed *in vitro* under this flow profile are consistent with those observed in *ex vivo* mouse tibia under physiologic dynamic loads[68], while oscillatory flow induces fewer responses[67]. Baseline fluorescence intensity was captured for 1 minute prior to fluid shear stimulation for 9 minutes.

2.2.5 Imaging and image analysis

For monitoring ER depletion, time-lapse images were collected 36-48 hours post transfection at 40X magnification. The FRET biosensor was excited at 430nm using a Lambda DG-4 xenon lamp (Sutter Instruments, Novato, CA), and fluorescence emissions of YFP

(530nm) and CFP (470nm) were captured simultaneously using a quadview beamsplitter (Photometrics, Tucson, AZ) and custom quad-band polychroic (Chroma, Bellows Falls, VT)[69]. To monitor ER depletion, cells were imaged for 20 minutes following the addition of thapsigargin (1μM). Images were acquired every 3 seconds to minimize photobleaching. The FRET ratio was calculated on a pixel-by-pixel basis using cross-correlation based image registration of the FRET and donor emissions to obtain relative Ca^{2+}_{ER} levels. The time to depletion was defined as the time at which the normalized FRET ratio fell below 0.8[94].

To monitor the effects of VSCC and SOCE inhibitors on Ca^{2+}_{cyt} responses, time-lapse images of cells were collected at 20X magnification for 9 minute periods of fluid flow stimulation. The Fluo-8 Ca^{2+} indicator was excited at 488nm, and fluorescence emissions were collected at 527nm. A Ca^{2+}_{cyt} transient was defined by an increase Fluo-8 intensity at least 4 times the magnitude of noise prior to flow onset[55].

To simultaneously monitor Ca^{2+}_{cyt} and Ca^{2+}_{ER}, single cells expressing Fura Red and the D1ER FRET sensor were identified at 60X magnification. Single excitation (430nm) was used to excite the dye and FRET biosensor, and fluorescence emissions of YFP, CFP, and Fura Red (641nm) were captured separately and simultaneously. Images were acquired every 3 seconds. Ca^{2+}_{cyt} time-courses were extracted from the Fura Red image. Photobleaching was corrected in this channel using an exponential fit of the baseline Ca^{2+}_{cyt} levels. The FRET ratio was determined from registered FRET/donor emissions. Regions of interest were selected to capture Ca^{2+} micro-domains within the cell based on the location of the initiation of a Ca^{2+}_{cyt} response[95]. To investigate the relationship between Ca^{2+} activity in the cytosol and the ER, we defined a percentage synchrony as the number of coincident Ca^{2+}_{cyt} and Ca^{2+}_{ER} transients divided by the total number of transients (peaks and inverse peaks). Ca^{2+}_{cyt} peaks and decreases in Ca^{2+}_{ER} were

identified as transient responses (i.e. decrease and recovery) with a magnitude greater than four times the magnitude of the noise in the baseline images.

2.2.6 Immuno-detection

For immunostaining, cells were rinsed in Dulbecco's Phosphate Buffered Saline (DPBS, Gibco, Carlsbad, CA), fixed in 4% paraformaldehyde (Sigma Aldrich, St. Louis, MO) in DPBS, and permeabilized with 0.2% Triton^{TM} X-100 (Sigma-Aldrich, St. Louis, MO). Non-specific protein antibody interactions were blocked using 2.5% Normal Horse Serum for 30 minutes (Vector Laboratories, Burlingame, CA). A rabbit polyclonal antibody to IP3R (ab5804, Abcam, Cambridge, MA) and a goat polyclonal antibody to α1H subunits of T-Type VSCC (sc-16261, Santa Cruz Biotechnology, Dallas, TX). Cells were incubated overnight at 4°C with antibodies diluted in 1% Bovine Serum Albumin (BSA, Vector Laboratories). Detection was achieved using anti-rabbit IgG and anti-goat IgG secondary antibody solutions conjugated to Dylight 594 (VectaFluor, Vector Laboratories). Following antibody incubations, the plasma membrane was labeled with 5 µg/ml Wheat Germ Agglutinin (WGA) AlexaFluor 488 conjugate (Invitrogen, Carlsbad, CA), which also stains the Golgi apparatus in permeabilized cells. Samples mounted with DAPI mounting medium (Vector Laboratories). Negative controls with no primary antibody were prepared to evaluate non-specific binding. We observed considerable non-specific staining in MLO-Y4 cells probed with the goat polyclonal antibody and isolated the calf serum used in cell culture as the primary contributor to this non-specific staining. Subsequently, cells were cultured for 48 hours prior to fixation in CS-free medium to eliminate this effect. Images were taken on a FV1000 confocal microscope (Olympus, Waltham, MA).

2.2.7 Proximity ligation assay

To evaluate a functional interaction between T-Type VSCC and the ER in osteocytes, we used a proximity ligation assay (PLA). In this assay, primary antibodies raised in two different species are bound by two different PLA probes against those species. Each PLA probe is a secondary antibody conjugated to a DNA strand. In close proximity (<40nm), the DNA strands from each probe can ligate, forming a closed-loop DNA oligonucleotide which exhibits fluorescence.

For this assay, we used the Duolink In Situ Red PLA kit recognizing goat and rabbit primary antibodies (Sigma Aldrich, St. Louis, MO) to detect interaction events between the T-Type VSCC and IP3R on the ER, respectively. The assay was performed according to the manufacturer's protocol. Blocking and primary antibody procedures were performed as in 2.2.7. Samples were incubated with the PLA probes for 1 hour at 37°C, washed in buffer, and treated with ligation solution for 30 minutes at 37°C. Cells were washed again and then exposed to an amplification-polymerase solution for 100 minutes at 37°C. Samples were mounted with DAPI mounting medium contained in the kit and imaged by confocal microscopy.

Controls were used to evaluate non-specific interaction events by also preparing samples without any primary antibody and with only one of each of the primary antibodies. For comparing the number of interaction events between the two cell types, an adjusted number of interaction events per cell was calculated by subtracting the average number of non-specific reactions per cell from the number of interaction events per cell for each sample. To facilitate the counting of interaction events, PLA images were thresholded in Image J (NIH, Bethesda, MD) such that interaction events appeared as black dots on a white background.

2.2.8 Data analysis

The data presented herein analyzes only responsive cells, though responsive percentages were greater than 80% for all experiments, except for SKF-96365 and 2-ABP treatment, which reduced the number of responsive MLO-Y4 cells to ~60% and 50%, respectively in cell populations. A cell was defined as responsive if the magnitude of the first Ca^{2+}_{cyt} response was at least four times higher than fluctuations in intensity during baseline measurements. Student's t-tests were used to determine significant differences for the number of Ca^{2+}_{cyt} peaks at a specific experimental condition and for differences in mean interaction events between the two cell types. All data are shown as mean ± standard deviation. Multi-factorial analysis of variance (ANOVA) with Bonferroni's post hoc analysis was performed to determine statistical differences between mean values of inhibitor treatments on the two cell types. Statistical significance can be observed when $p<0.05$.

2.3 Results

2.3.1 Effects of L- and T-Type VSCC inhibitors on bone cell Ca^{2+}_{cyt} responses to fluid flow

Osteocytes (n=480 cells, 18 slides) exhibited numerous Ca^{2+}_{cyt} oscillations under fluid flow, and these multiple responses were significantly reduced by treatment with the T-type inhibitor NNC 55-0396 (n= 201 cells, 10 slides) (Figure 2.2A). The L-type inhibitor had no effect on the number of Ca^{2+}_{cyt} responses in osteocytes (n=187 cells, 8 slides). Osteoblasts were less responsive than osteocytes, exhibiting less than two Ca^{2+}_{cyt} peaks on average for all groups (n=237, 53, 79 cells; 8, 2, 3 slides for control, L- and T-Type inhibitors, respectively) (Figure 2.2B).

2.3.2 Effects VSCC inhibitors on ER dynamics in bone cells

The localization of the D1ER plasmid to the ER was verified by staining D1ER-transfected osteocytes with ER Tracker Red (Figure 2.3). Transfected cells were imaged for 20 minutes following the addition of thapsigargin to deplete the ER. Representative FRET ratios of a single osteocyte treated with thapsigargin is shown in Figure 2.4A.

Though osteocytes express little to no L-Type VSCC, in an earlier study the inhibitor amlodipine influenced Ca^{2+} baseline levels in both cells types. Further study found that amlodipine is actually a non-specific VSCC inhibitor with an off-target effect of rapidly depleting the ER (Figure 2.5). We therefore confirmed that the VSCC inhibitors used in this study had minimal effect on ER depletion.

The time to deplete the ER under the outlined conditions is shown in Figure 2.4. The scatter plots show representative depletion curves for MLO-Y4 cells (Figure 2.4B) and MC3T3-E1 cells (Figure 2.4C). The small difference (3%) between untreated MLO-Y4 cells (n=14) and MC3T3-E1 cells (n=6) in the time to depletion did not reach significance. Similarly, the effect of VSCC inhibitors had on the time to depletion in osteoblasts was not significant (Figure 2.4C; n=5, 4 cells for L- and T-Type inhibition, respectively), and the L-Type VSCC inhibitor had no effect in osteocytes (Figure 2.4B, n=5 cells). Treatment of MLO-Y4 cells with the T-Type VSCC inhibitor prior to the addition of thapsigargin resulted in a significantly faster time to depletion compared to untreated controls (Figure 2.4B, n=6 cells). On average, it took ~300s longer for Ca^{2+}_{ER} levels to deplete in control cells than those with disrupted T-Type VSCC.

2.3.3 Simultaneous imaging of Ca^{2+}_{cyt} and Ca^{2+}_{ER} in bone cells under fluid flow

To simultaneously image Ca^{2+}_{cyt} and Ca^{2+}_{ER}, bone cells were transfected with D1ER, stained with Fura Red-AM, and imaged using a quadview beamsplitter (Figure 2.6A). The FRET ratio was calculated from the FRET and donor images, and in some cells, a subregion corresponding to Ca^{2+}_{cyt} spike initiation was selected for analysis (Figure 2.6B). Representative time courses for MLO-Y4 and MC3T3-E1 cells under control (untreated), L-Type inhibitor treated, and T-Type inhibitor treated conditions is shown in Figure 2.7. In osteocytes, elevations of Ca^{2+}_{cyt} coincided with depression of Ca^{2+}_{ER}, with subsequent peaks occurring after recovery of Ca^{2+}_{ER} levels (n=10 cells). In osteoblasts, significantly fewer Ca^{2+}_{cyt} responses were observed, and while the ER contributed to these responses, a depression in Ca^{2+}_{ER} was often not recovered in the course of the experiment (n=11 cells). Treatment of either cell type with the L-Type VSCC inhibitor nifedipine had no detectable effect on the number of Ca^{2+}_{cyt} peaks (n=8 osteocytes, 5 osteoblasts), and the T-Type VSCC inhibitor NNC 55-0396 had no detectable effect on responses in osteoblasts (n=6 cells). Treatment of MLO-Y4 cells with the T-Type VSCC inhibitor significantly reduced the number of Ca^{2+}_{cyt} responses (Figure 2.8A, n=9 cells).

The percentage of synchronous responses was defined as the number of coincident Ca^{2+}_{cyt} and Ca^{2+}_{ER} transients divided by the total number of transients (peaks and inverse peaks). The synchronous response percentage was high in control osteocytes, with more than 80% of Ca^{2+}_{cyt} peaks corresponding to dynamic changes in Ca^{2+}_{ER} (Figure 2.8B). MC3T3-E1 cells exhibited few Ca^{2+}_{cyt} peaks in response to flow (Figure 2.8A), and more often than not those peaks were not synchronous with a transient drop in Ca^{2+}_{ER} (Figure 2.8B). Inhibition of T-Type VSCC significantly reduced the synchrony in osteocytes to similar levels observed in osteoblasts, with an average of ~20%.

2.3.4 Effects of SOCE inhibitors on osteocyte Ca^{2+}_{cyt} responses

MLO-Y4 cells were subjected to fluid flow stimulation in the presence of three different SOCE-related inhibitors to inform the mechanism of Ca^{2+} exchange with the ER. These inhibitors were first used on osteocyte populations (YM58483: n=223 cells, 7 slides; SKF-96365: n=231 cells, 4 slides; 2-APB: n=84 cells, 5 slides) to evaluate their effects on the percentage of responsive cells (Figure 2.9A) and the number of Ca^{2+}_{cyt} peaks (Figure 2.9B).

Treatment of single osteocytes transfected with D1ER resulted in similar effects (Figure 2.10). The number of Ca^{2+}_{cyt} peaks (Figure 2.10A) and the synchronous response percentage (Figure 2.10B) were determined for each group. YM58483 had no effect on Ca^{2+}_{cyt} responses in osteocytes (n=3 cells), and though SKF-96365 reduced the number of Ca^{2+}_{cyt} responses, the effect was not significant (n=4 cells). Neither treatment influenced synchrony. Treatment with 2-APB significantly reduced the number of Ca^{2+}_{cyt} responses and the percent of synchronous responses (n=5 cells). Again, the effect on Ca^{2+}_{cyt} responses was consistent with Fluo-8 experiments on larger cell populations. Representative curves of Ca^{2+}_{cyt} and Ca^{2+}_{ER} in MLO-Y4 cells treated with these inhibitors showed high synchrony in YM58483 and SKF-96365 treated cells (Figure 2.10C,D), whereas 2-APB treatment resulted in no recovery of ER levels following a Ca^{2+}_{cyt} transient (Figure 2.10E).

2.3.5 Interaction between T-Type VSCC and the ER

Immunostaining for T-Type VSCC revealed punctate staining in osteocytes, with some regions of dense staining along the border of the cell membrane (Figure 2.11). Staining for T-Type VSCC in osteoblasts revealed weaker, more diffuse staining (Figure 2.12). Staining for

IP3R in osteocytes showed strong nuclear localization and striated patterns of staining throughout the cell (Figure 2.13). Osteoblasts exhibited similar IP3R staining patterns, though the striations were less pronounced (Figure 2.14). Specificity of staining was confirmed with negative controls for each antibody (Figure 2.15).

The PLA revealed a considerable number of interaction events between T-Type VSCC and IP3R in osteocytes (n=5, Figure 2.16), with some images showing over 100 interaction events for as few as 6 cells. Controls revealed only minor non-specific interactions. Far fewer interactions were detected in osteoblasts (n=3, Figure 2.17). Quantitative comparisons of adjusted interaction events between cell types revealed significantly greater proximity between T-Type VSCC and IP3R in osteocytes (Figure 2.18).

2.4 Discussion

The purpose of this study was to uncover mechanisms underlying the generation of Ca^{2+}_{cyt} oscillations in osteocytes. Previous studies have implicated the ER as an important source of Ca^{2+} for transient Ca^{2+} signals in osteocytes responding to mechanical stimuli, however to date no study has precisely identified the mechanisms by which the ER enables Ca^{2+}_{cyt} oscillations in osteocytes. This study represents the first attempt to visualize the dynamics of Ca^{2+} specifically in the ER in osteocytes. Using a FRET biosensor localized to the ER, we were able to simultaneously observe Ca^{2+} exchange between the ER and the cytosol. We found high synchrony between rises in Ca^{2+}_{cyt} and depressions in Ca^{2+}_{ER}, with subsequent Ca^{2+}_{cyt} responses occurring after a recovery of Ca^{2+}_{ER} levels, suggesting that ER dynamics dictate osteocyte Ca^{2+} responses to fluid flow. Additionally, a major goal of this study was to link a phenotypic difference between osteocytes and osteoblasts in the expression of VSCC to the mechanobiology

of these cell types. Indeed, we found that challenging T-Type VSCC alters the kinetics of ER depletion in osteocytes and that the predominant expression of T-Type VSCC in osteocytes sustains Ca^{2+}_{cyt} oscillations by facilitating $Ca^{2+}_{cyt}/Ca^{2+}_{ER}$ synchrony. Using inhibitors of various SOCE-related pathways, we determined that this exchange of Ca^{2+} between the cytosol and the ER is likely not a result of STIM proteins or transport of Ca^{2+} through CRACs, but rather through an interaction of the ER with T-Type channels on the osteocyte cell membrane.

Previous studies detected little to no L-Type VSCC expression in MLO-Y4 osteocytes, but found detectable levels of T-Type VSCC[77]. Furthermore, a pattern of development suggested a loss of L-Type VSCC with the differentiation of osteoblasts to osteocytes. A later study confirmed this finding and additionally reported that T-Type channels mediated mechanically-induced ATP release in osteocytes[78]. Most recently, a study in IDG-SW3 osteocytes found that parathyroid hormone treatment increased the expression of L-Type VSCC and decreased T-Type VSCC in osteocyte-stage cells to revert them to a less mature phenotype[96]. Our results are consistent with the role of VSCC in the differentiation of osteoblasts to osteocytes and additionally suggest the predominant expression of T-Type VSCC in osteocytes is important for their distinct role as mechanosensors. Indeed, T-Type VSCC have been shown to associate with integrins in a mechanoreceptor complex in osteocytes, lending credence to the role of these channels in osteocyte mechanobiology[97].

As previous studies resulted in similar effects of VSCC and ER antagonists on osteocyte Ca^{2+}_{cyt} responses, we sought to determine whether there was any interaction between T-Type VSCC and the ER in osteocytes. The time to depletion was very similar (within 3%) in untreated MLO-Y4 and MC3T3-E1, suggesting that ER release kinetics alone cannot account for the Ca^{2+}_{cyt} oscillation behavior in osteocytes. Treatment of MLO-Y4 with a T-Type VSCC inhibitor

prior to thapsigargin resulted in a significantly faster time to depletion compared to untreated controls. This suggests that the presence of T-Type VSCC may serve to refill ER stores in osteocytes, which may explain the ability of osteocytes to sustain Ca^{2+}_{cyt} oscillations.

Though inhibitor studies challenging the ER allude to a mechanism involving Ca^{2+}_{ER} release and refilling in sustaining Ca^{2+}_{cyt} oscillations in osteocytes, these conclusions are speculative without the direct measurement of Ca^{2+}_{ER} dynamics under flow. This is also true for measurements of ER depletion, where only a single induction of Ca^{2+}_{ER} release is monitored. In this study, by simultaneously monitoring Ca^{2+} separately in the cytosol and ER in osteocytes, we found that most rises in Ca^{2+}_{cyt} were accompanied by a corresponding decrease and recovery in Ca^{2+}_{ER}. This supports the hypothesis that osteocytes are capable of generating Ca^{2+}_{cyt} oscillations by an ability to refill the ER stores. The effects of T-Type VSCC inhibition implicate T-Type channels in this process.

Though the T-Type inhibitor had a large suppressive effect on $Ca^{2+}_{cyt}/Ca^{2+}_{ER}$ synchrony in osteocytes, there are other possible mechanisms linking the exchange of Ca^{2+} between these two spaces. However, the lack of a pronounced suppression between control cells and those treated with YM58483 on the number of Ca^{2+}_{cyt} responses and the percentage of synchronous responses indicates that CRACs are not involved. While SKF-96365 treatment mildly decreased the number of responses, this reduction is likely due to reported off-target effects on VSCC[91]. The only inhibitor that produced similar effects as the T-Type antagonist was the IP_3R inhibitor 2-APB, which blocks IP_3-mediated release of Ca^{2+} from the ER. Thus, the exchange of Ca^{2+} between the cytosol and the ER is likely not a result of Ca^{2+} transport through CRAC or STIM1 involvement, but rather through the IP_3-mediated release of Ca^{2+}_{ER}.

The results of the proximity ligation assay further support the hypothesis that T-Type VSCC interact with the ER to facilitate IP_3-mediated Ca^{2+}_{ER} release. Immunostaining for T-Type VSCC revealed strong presence of this channel in osteocytes and weaker staining in osteoblasts, consistent with prior work from our laboratory[98]. IP3R staining patterns were similar between cell types, with striated staining throughout the cell and expression in the nucleus. The large number of interaction events between T-Type VSCC and IP3R in osteocytes is likely in part due to stronger presence of T-Type VSCC.

There are a few limitations to the current study. First, the small sample sizes, though consistent with our experiments on large cell populations, mean our study was only designed to detect relatively large effects of the investigated treatments. Future studies looking for more subtle differences will require a larger sample size. In addition, our conclusions are drawn from experiments using small molecule inhibitors, which often have incomplete or off-target effects. Thus, future studies could be aimed at genetic modifications of cells to alter the expression of VSCC to investigate their role in osteocyte Ca^{2+} signaling. The average synchrony in osteoblasts was also approximately 20%, though standard deviations were somewhat high due to the limited number of responses. As all T-Type treated MC3T3-E1 cells analyzed in this study had only one response with no coincident inverse response from the ER, the synchrony in the T-Type treated osteoblasts was zero, though this value was still not statistically different from MC3T3-E1 untreated controls. Although the present study indicates that the first Ca^{2+}_{cyt} response in both cells can have some contribution of the ER, it is known that extracellular Ca^{2+} is also required, thus this effect is likely due to differences between the first and subsequent Ca^{2+}_{cyt} transients in these cells. Future work could explore these differences. Finally, the aim of the proximity ligation assay was to evaluate a functional interaction between T-Type VSCC and the ER. IP3R

were targeted due to the numerous pathway studies indicating their importance in regulating Ca^{2+} release from the ER in osteocytes; however, strong staining was also observed in the nucleus. The lack of nuclear expression of T-Type VSCC and range of the assay suggests that any interaction events detected here indeed represent proximity between T-Type VSCC on the plasma membrane and IP3R on the ER, but future studies could aim to clarify the cellular localization of these structures. Furthermore, whether the differences in interactions between cells is simply a result of the abundance of T-Type VSCC in osteocytes remains unclear, but could be explore in future work by overexpressing T-Type VSCC in osteoblasts.

2.5 Conclusions

The sustainment of robust oscillations in Ca^{2+}_{cyt} under mechanical loading is a hallmark of osteocytes both *in vitro* and *ex vivo*, thus the primary goal of this study was to uncover the mechanism by which osteocytes rely on specific subcellular stores of Ca^{2+} to generate these multiple responses. By observing Ca^{2+} dynamics in both cytosolic and ER spaces, this study demonstrated that osteocytes generate multiple responses through an ability to refill ER stores. Our data suggests that T-type VSCC facilitate the recovery of Ca^{2+}_{ER} through a functional interaction in osteocytes to permit this behavior. We uncovered a new mechanism involving T-type VSCC underlying the unique behavior of osteocytes as mechanosensors.

2.6 Figures

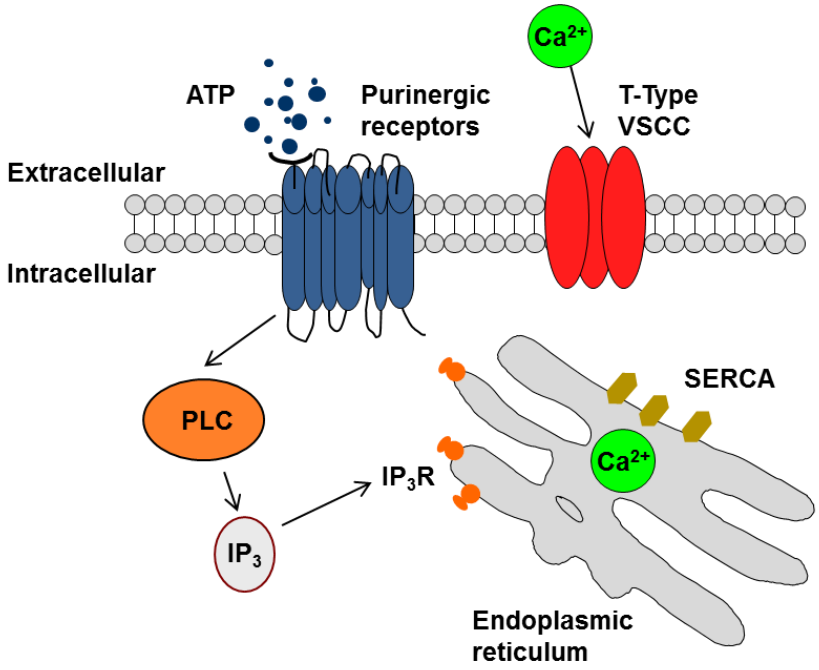

Figure 2.1. Pathways involved in intracellular Ca^{2+} signaling in osteocytes. Both the extracellular reservoir and intracellular storage organelles contribute to Ca^{2+} signaling in osteocytes. Channels along the cell membrane facilitate Ca^{2+} transport from these spaces. Purinergic receptors and T-Type VSCC are the most critical channels in osteocytes. Activation of purinergic signaling generates phospholipase C (PLC), which generates inositol triphosphate (IP_3), which can bind to the IP_3 receptors (IP_3R) on the membrane of the endoplasmic reticulum (ER), resulting in Ca^{2+} release from the ER. Sarcoplasmic/endoplasmic reticulum Ca^{2+} ATP-ase (SERCA) pumps on the ER membrane serve to refill the ER with Ca^{2+} ions. Ca^{2+} from the extracellular environment can be transported directly through T-Type VSCC upon activation. *Image adapted from Reference 67.*

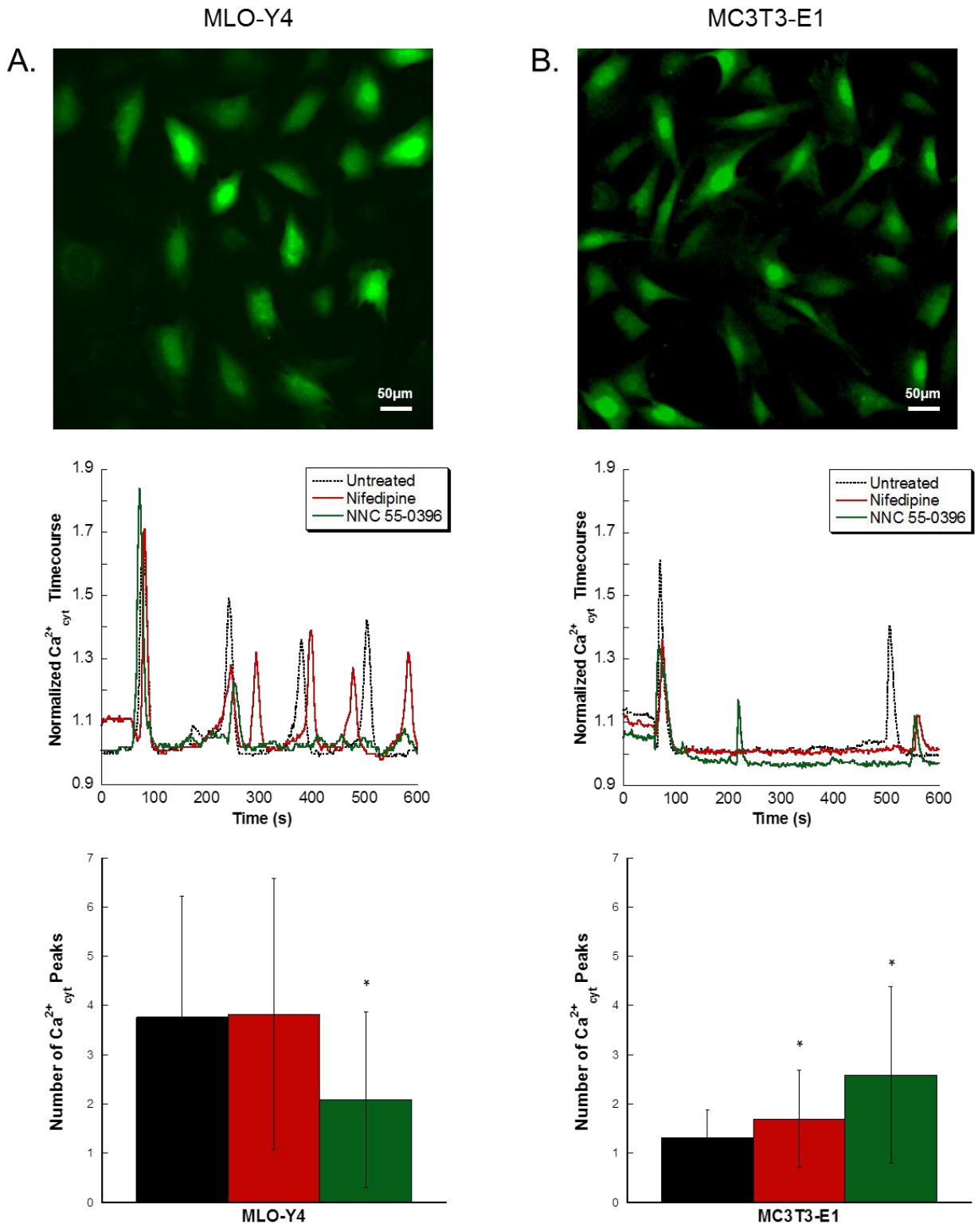
MLO-Y4
MC3T3-E1
A.
B.
50μm
50μm
Untreated
Nifedipine
NNC 55-0396
Normalized Ca2+cyt Timecourse
Time (s)
Number of Ca2+cyt Peaks
MLO-Y4
MC3T3-E1

Figure 2.2. The effects of VSCC inhibitors on Ca^{2+}_{cyt} responses in osteocytes and osteoblasts. Representative images of Fluo-8 stained cells, Ca^{2+}_{cyt} time courses, and quantification of the number of Ca^{2+}_{cyt} peaks are shown for (A) MLO-Y4 and (B) MC3T3-E1 cells treated with the L-Type inhibitor nifedipine or the T-Type inhibitor NNC 55-0396 prior to exposure to fluid flow. Ca^{2+}_{cyt} transients are shown as intensity changes of the fluorescent indicator Fluo-8 normalized to intensity at baseline prior to fluid flow exposure. Error bars are standard deviations. *$p<0.05$ compared to controls within each group.

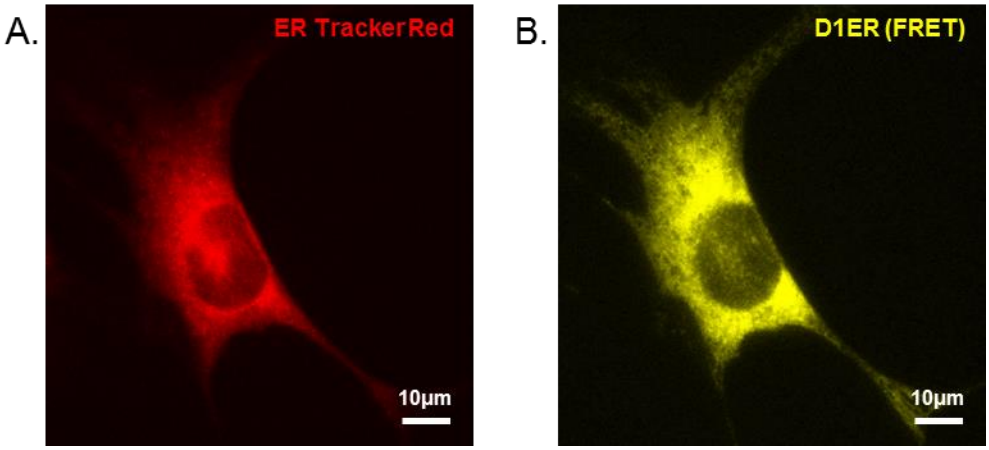

Figure 2.3. Localization of D1ER to the ER. Live, transfected cells were stained with (A) ER-Tracker Red to show localization of the (B) D1ER plasmid (yellow = FRET) to the ER. This image is a representative osteocyte.

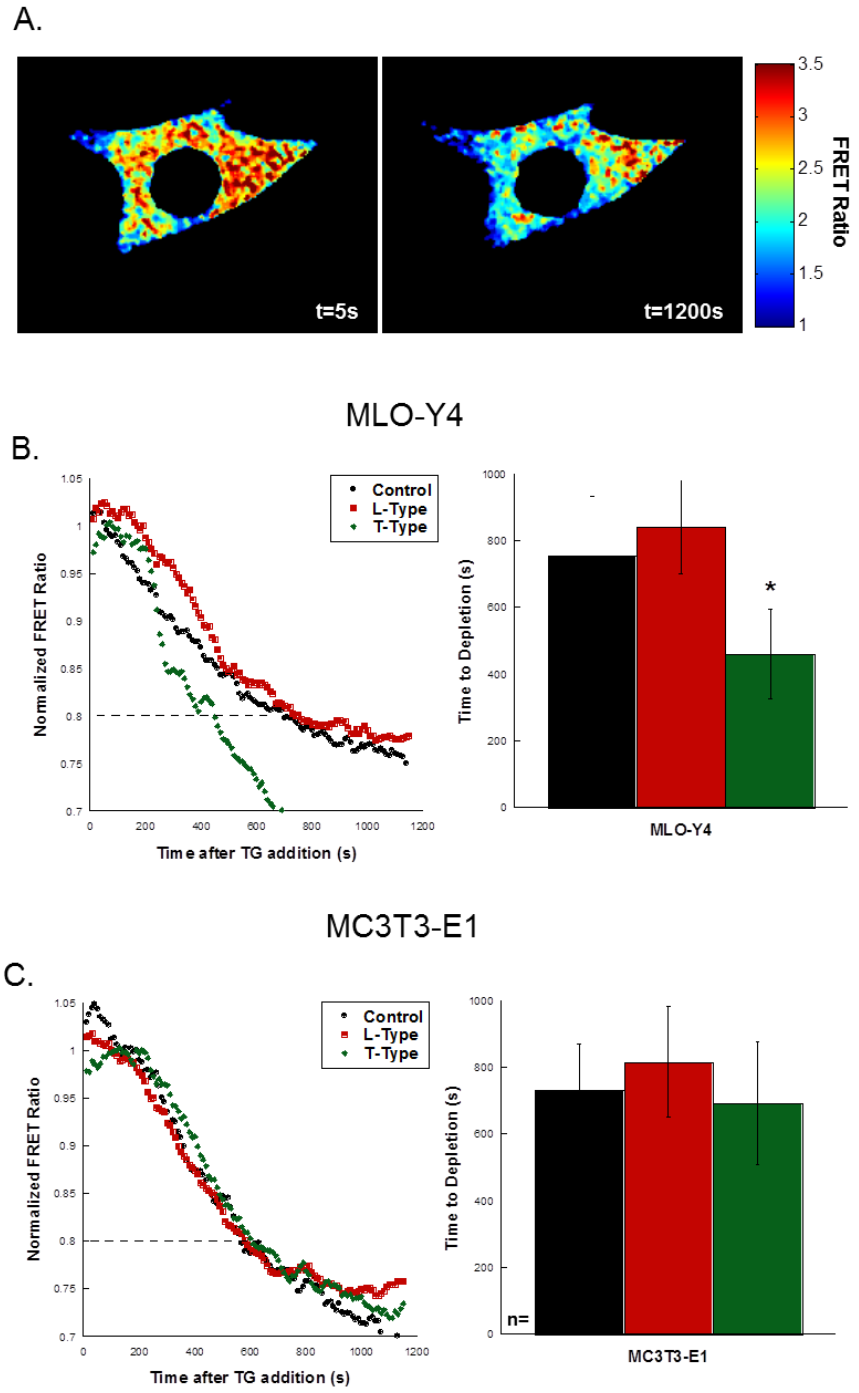

Figure 2.4. The effects of VSCC inhibitors on Ca^{2+} dynamics in the ER. (A) Thapsigargin was used to induce depletion of the ER over the time course of the experiment. The FRET ratio was calculated by registering and dividing the FRET and donor images and calculating the ratio

within the cell. Depletion was determined by a reduction in the normalized FRET ratio to below 0.8. (B) Untreated MLO-Y4 exhibited similar depletion characteristics as those treated with an L-Type inhibitor. Treatment with the T-Type inhibitor resulted in significantly faster depletion, quantified in the bar graph. (C) In MC3T3-E1, no differences were detected in the depletion times among all groups. Error bars are standard deviations. Significance was assessed by one-way ANOVA. *$p<0.05$ compared to control.

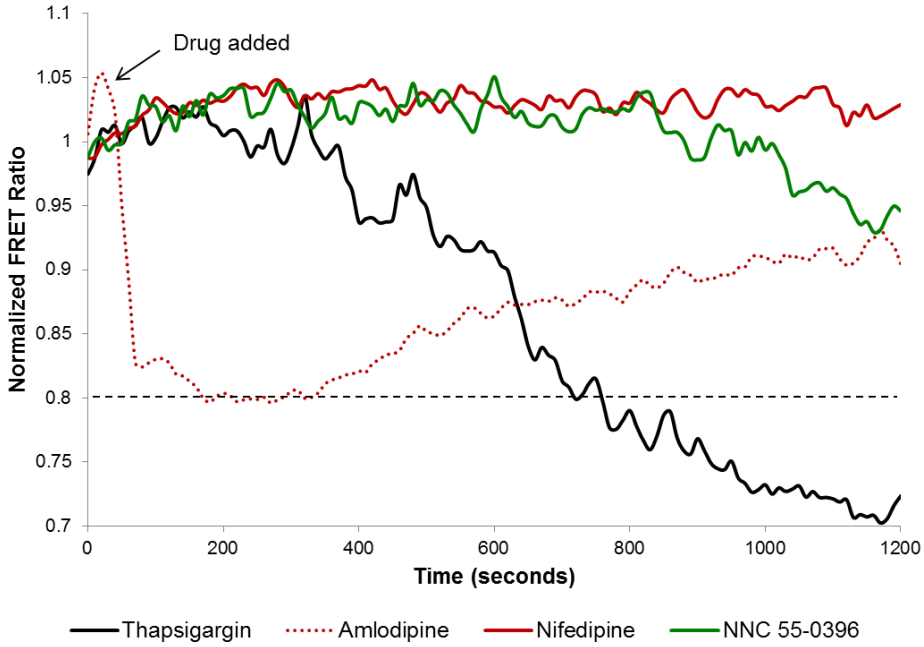

Figure 2.5. Effects of inhibitors alone on Ca^{2+}_{ER} levels. MLO-Y4 cells were imaged for 20 minutes, and drug was added after 1 min. Drugs were used at the following concentrations: thapsigargin (1µM); amlodipine (10µM); nifedipine (10µM); NNC 55-0396 (20µM). Note the rapid depletion of the ER (ratio below 0.8) upon addition of amlodipine. No other drugs showed off-target effects.

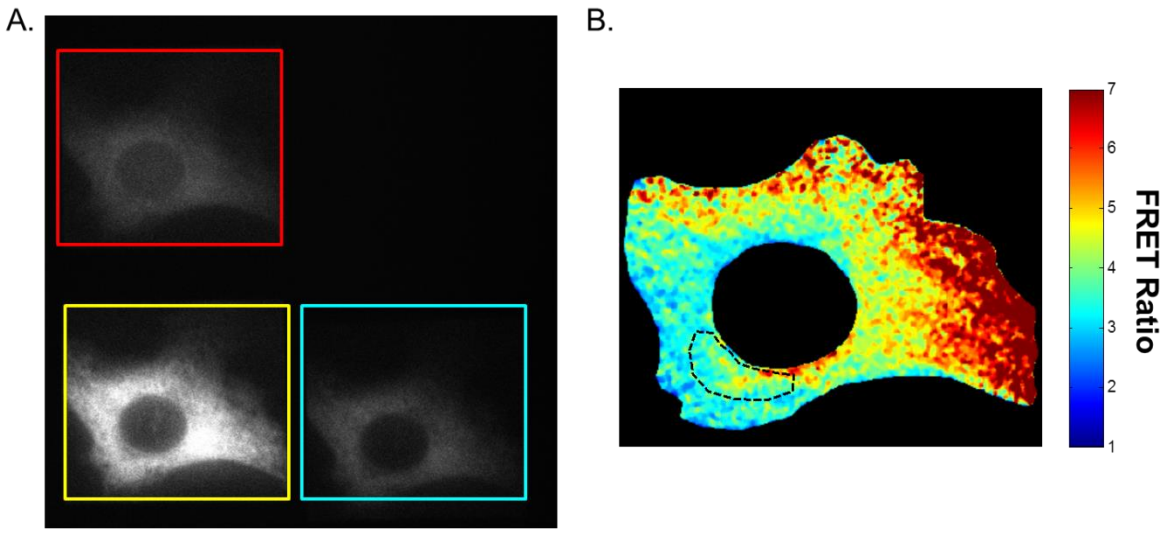

Figure 2.6. Simultaneous measurement of Ca^{2+}_{cyt} and Ca^{2+}_{ER} dynamics. To simultaneously monitor Ca^{2+} in the cytosol and the ER, cells were transfected with D1ER and stained with the red-shifted fluorescent Ca^{2+}_{cyt} indicator Fura Red-AM. Single cells at 60X were imaged using a quadview beamsplitter with single excitation of both indicators to achieve simultaneous, real-time measurements of Ca^{2+}_{cyt} and Ca^{2+}_{ER}. A representative image is shown in (A). The FRET ratio was calculated from the FRET and donor images, and (B) shows the selection of a subregion to determine the changes in Ca^{2+}_{ER} microdomains corresponding to Ca^{2+}_{cyt} spike initiation.

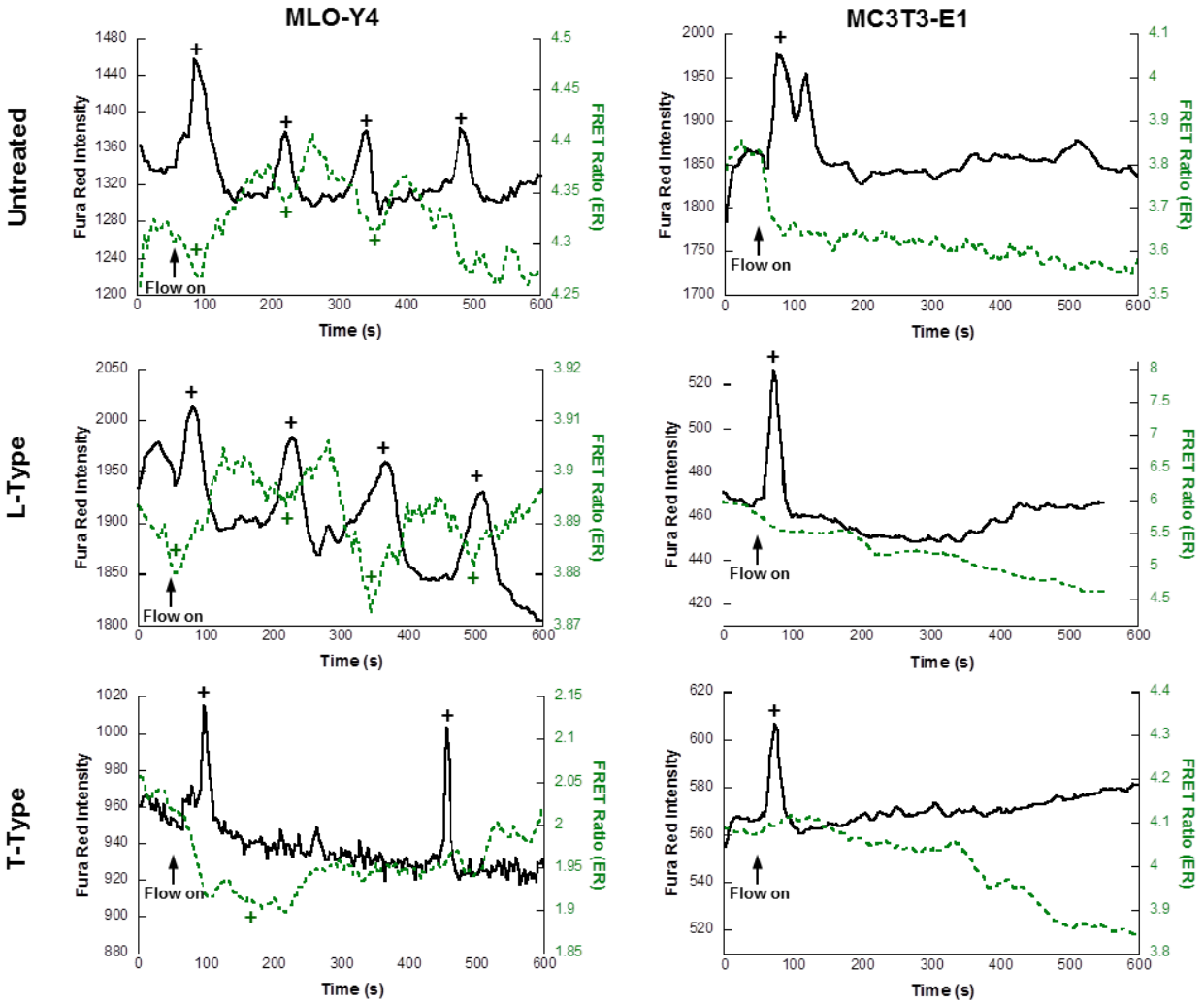

Figure 2.7. The effects of VSCC inhibitor treatment on Ca^{2+}_{cyt} responses and $Ca^{2+}_{cyt}/Ca^{2+}_{ER}$ synchrony in MLO-Y4 osteocytes and MC3T3-E1 osteoblasts. Representative time courses from MLO-Y4 and MC3T3-E1 cells imaged at 60X magnification under fluid flow exposure in the presence or absence of L- and T-Type VSCC inhibitors. Flow was started after the collection of 60s baseline. Detected peaks and valleys are indicated by "+".

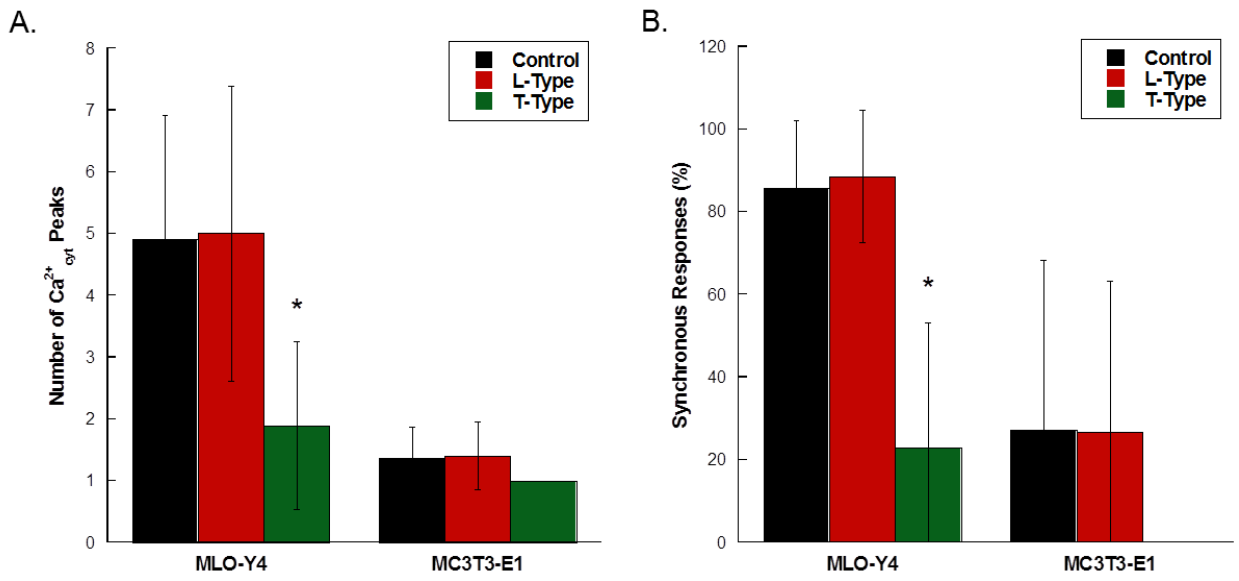

Figure 2.8. Quantification of the effects of VSCC inhibitors on the number of Ca^{2+}_{cyt} responses and $Ca^{2+}_{cyt}/Ca^{2+}_{ER}$ synchrony in MLO-Y4 osteocytes and MC3T3-E1 osteoblasts. (A) The number of Ca^{2+}_{cyt} responses in untreated, L-Type inhibitor treated, and T-Type inhibitor treated bone cells. (B) The percentage of synchronous responses in MLO-Y4 and MC3T3-E1 treated with VSCC inhibitors. The percentage of synchronous responses was defined as the number of coincident Ca^{2+}_{cyt} and Ca^{2+}_{ER} transients divided by the total number of transients (peaks and inverse peaks). Error bars are standard deviation. Significance was assessed by multi-factorial ANOVA with Bonferroni's post hoc analysis. *$p<0.05$ compared to control.

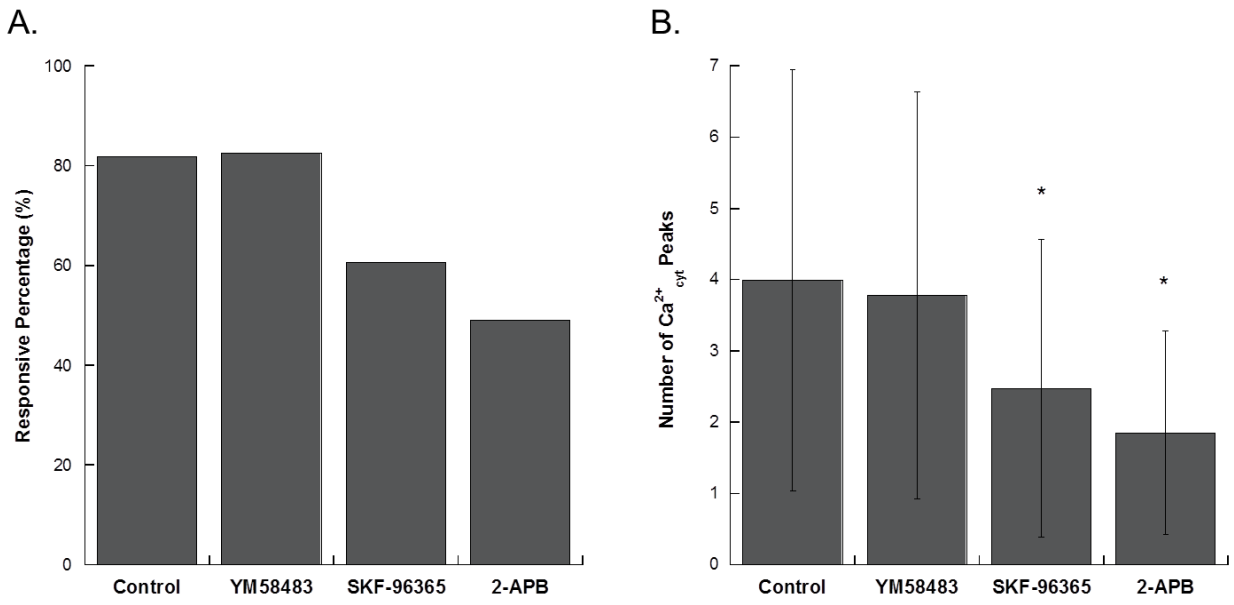

Figure 2.9. Inhibition of SOCE in MLO-Y4 cell populations. (A) Percentage of responsive cells and (B) number of Ca^{2+}_{cyt} peaks in control and treated groups. Error bars are standard deviations. *$p<0.05$ compared to control

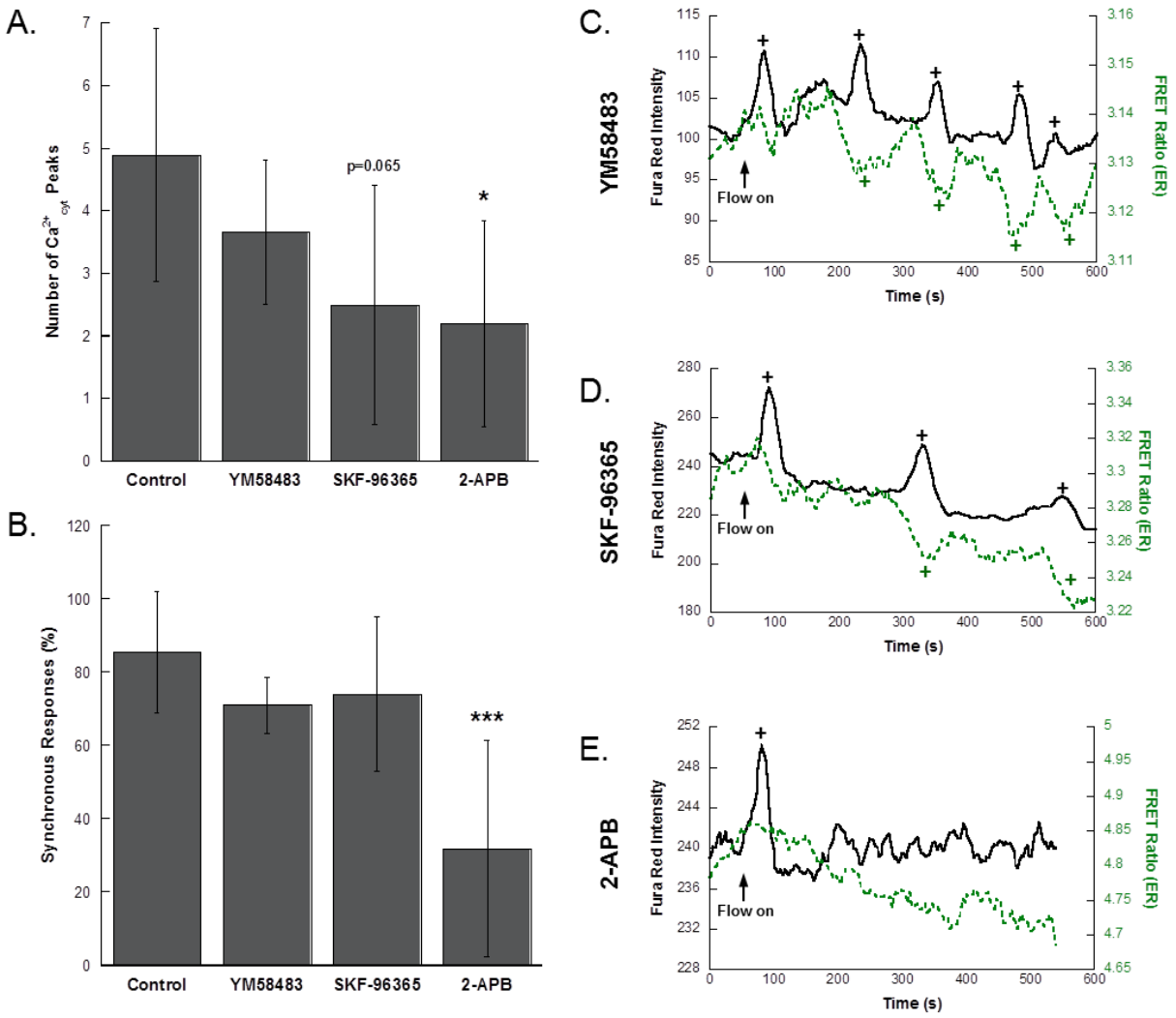

Figure 2.10. Pharmacologic inhibition of SOCE in single MLO-Y4 osteocytes. (A) Number of Ca^{2+}_{cyt} peaks in control and inhibitor treated groups. (B) The percentage of synchronous responses in MLO-Y4 treated with SOCE inhibitors. Simultaneous measurement of Ca^{2+}_{cyt} and Ca^{2+}_{ER} in MLO-Y4 cells exposed to fluid shear pre-treated with (C) YM58483, (D) SKF-96365, and (E) 2-APB. Flow was started after the collection of 60s baseline. Detected peaks and valleys are indicated by "+". Significance was assessed by one-way ANOVA. Error bars are standard deviations. *p<0.05, ***p<0.001 compared to control.

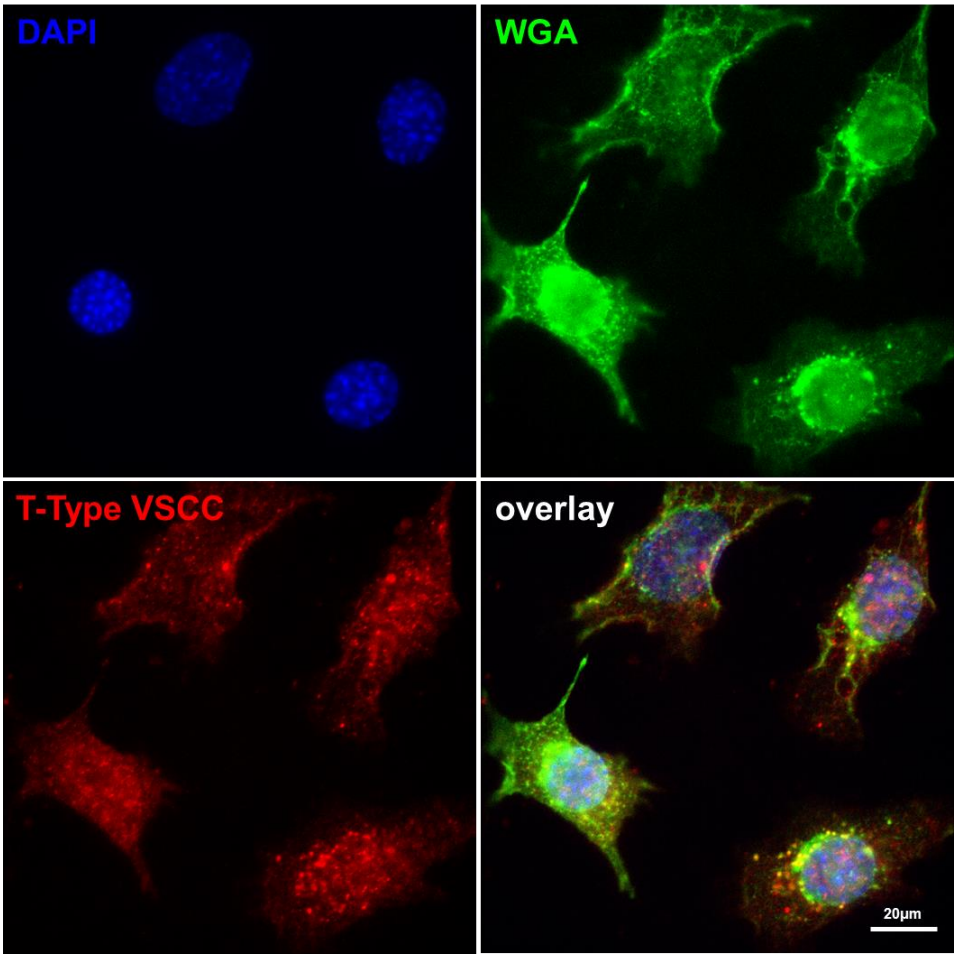

Figure 2.11. Immunostaining of T-Type VSCC in MLO-Y4 osteocytes. Representative images of osteocytes probed for T-Type VSCC (red) and counterstained with WGA (green) to indicate the plasma membrane and DAPI (blue) to indicate nuclei.

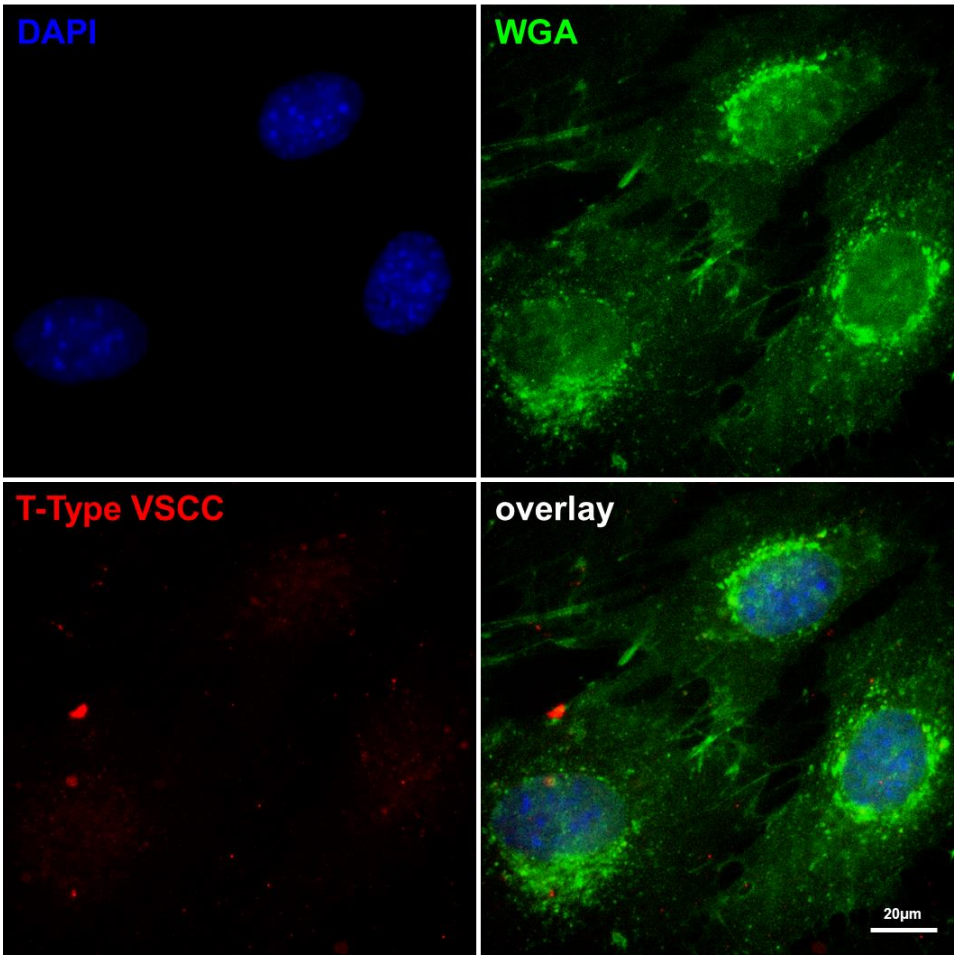

Figure 2.12. Immunostaining of T-Type VSCC in MC3T3-E1 osteoblasts. Representative images of osteoblasts probed for T-Type VSCC (red) and counterstained with WGA (green) to indicate the plasma membrane and DAPI (blue) to indicate nuclei.

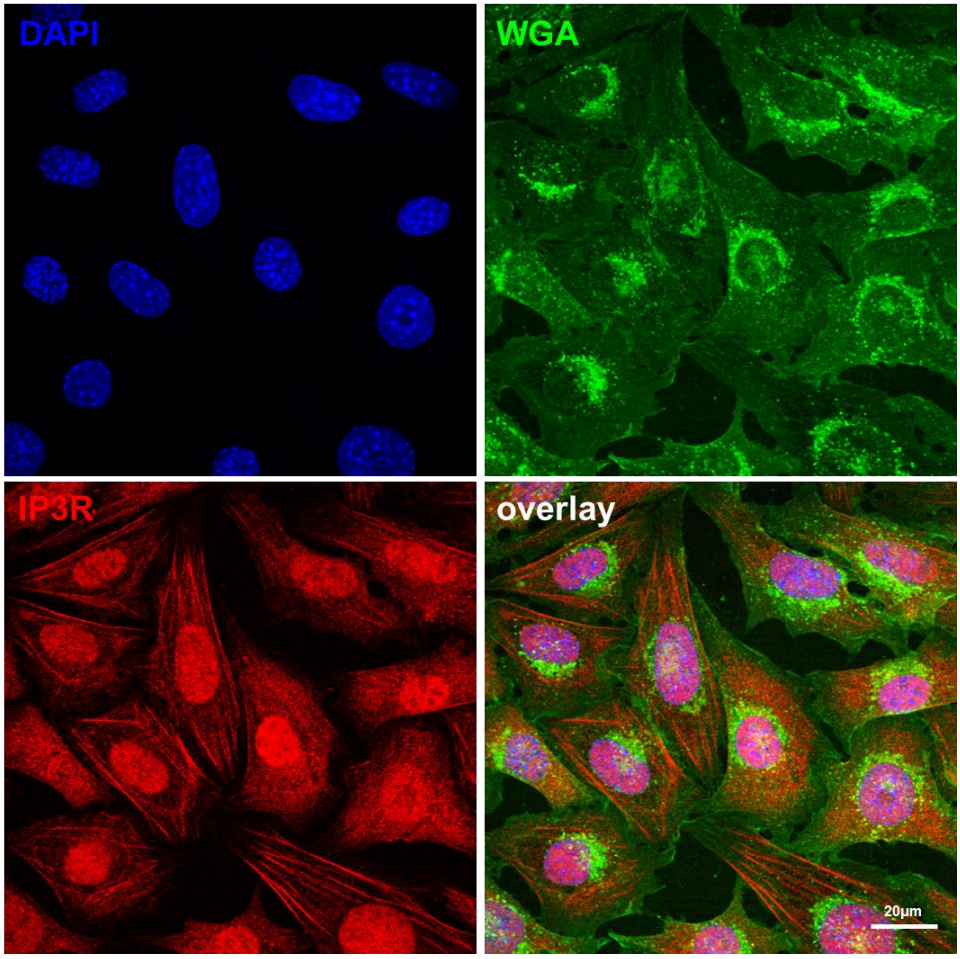

Figure 2.13. Immunostaining of IP_3R in MLO-Y4 osteocytes. Representative images of osteocytes probed for IP3R (red) and counterstained with WGA (green) to indicate the plasma membrane and DAPI (blue) to indicate nuclei.

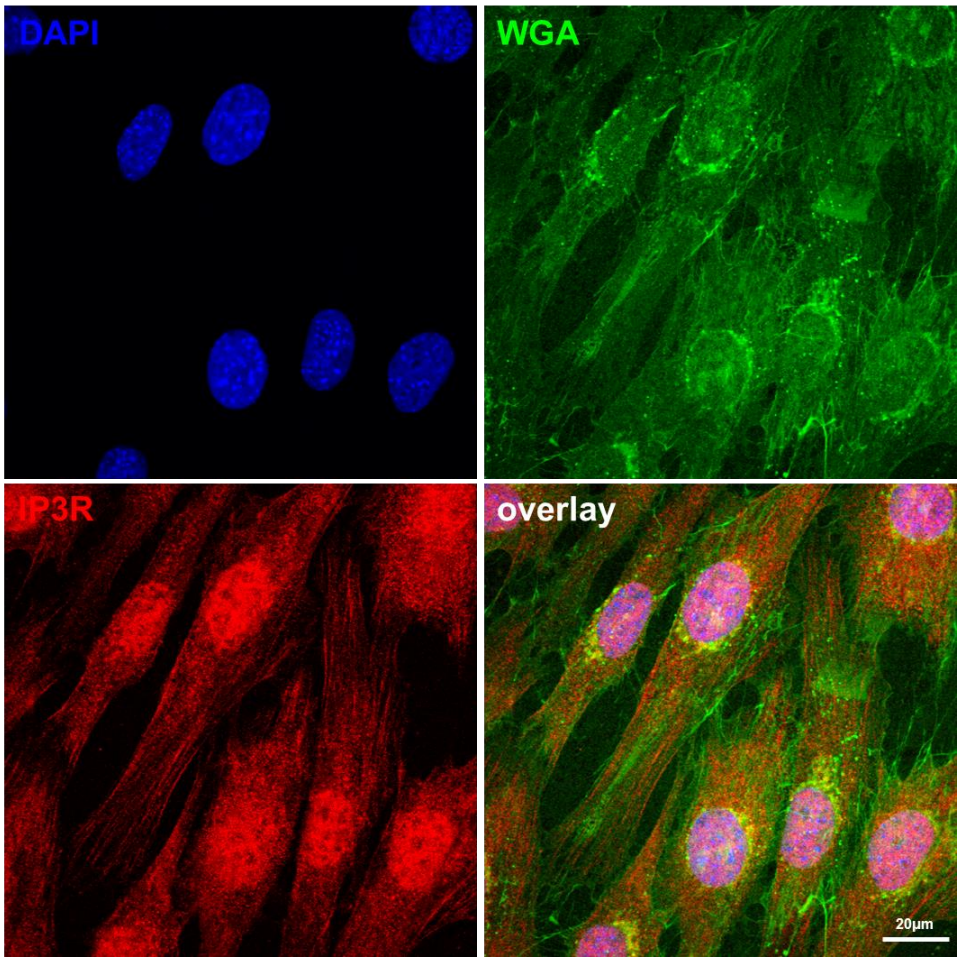

Figure 2.14. Immunostaining of IP_3R in MC3T3-E1 osteoblasts. Representative images of osteoblasts probed for IP3R (red) and counterstained with WGA (green) to indicate the plasma membrane and DAPI (blue) to indicate nuclei.

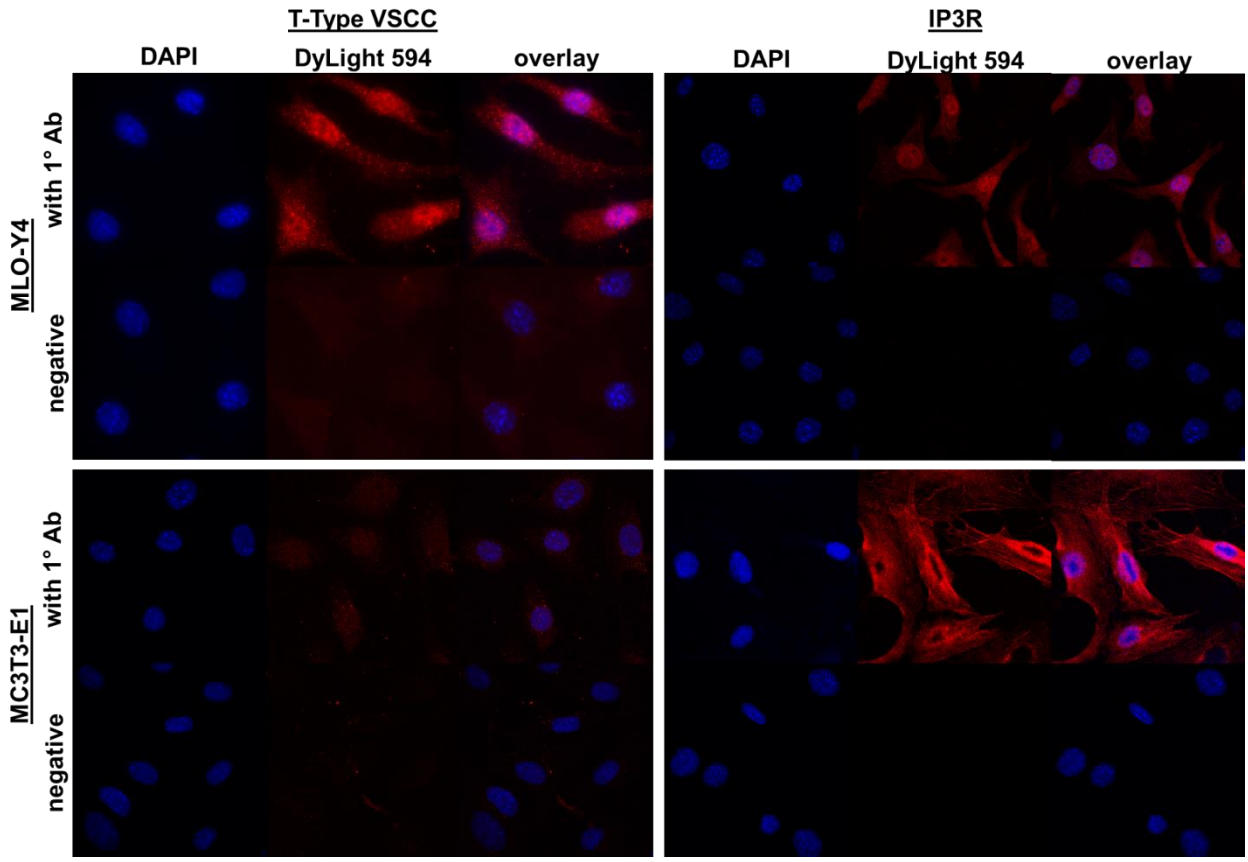

Figure 2.15. Positive and negative staining of T-Type VSCC and IP3R in bone cells. Representative images of cells stained with and without (negative) primary antibodies (1° Ab) for T-Type VSCC and IP3R.

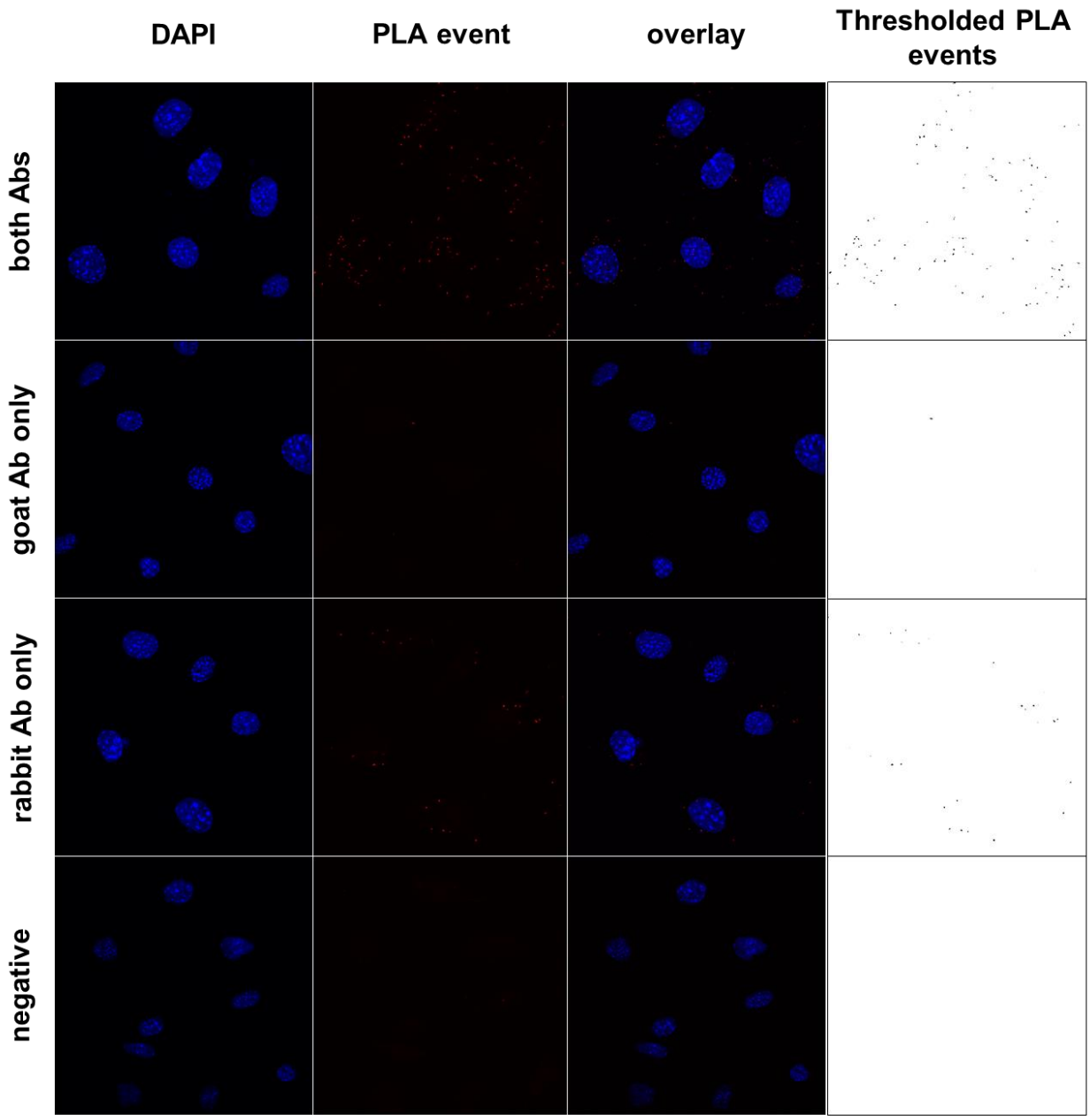

Figure 2.16. Proximity ligation assay between T-Type VSCC and IP_3R in MLO-Y4 osteocytes. Representative images of interaction events (red dots) between anti-goat and anti-rabbit PLA probes in fixed osteocytes. The top panel represents interaction events between probes targeting T-Type VSCC and IP3R antibodies raised in goat and rabbit, respectively. Nuclei are indicated by counterstaining with DAPI. Representative images are also shown for

controls with either antibody alone or absence of both primary antibodies (negative). The right column is a threshold image of the interaction events in red.

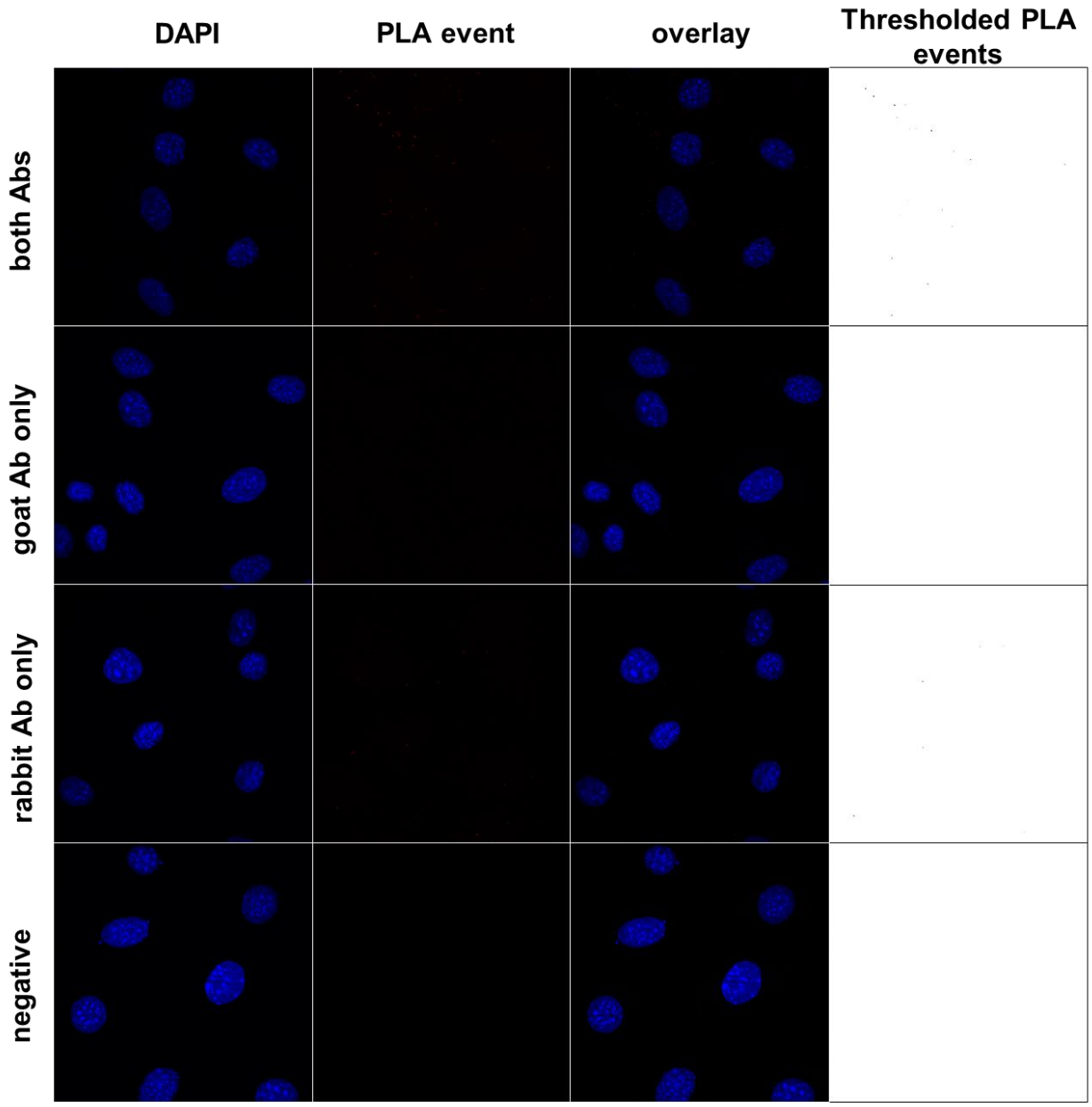

Figure 2.17. Proximity ligation assay between T-Type VSCC and IP_3R in MC3T3-E1 osteoblasts. Representative images of interaction events (red dots) between anti-goat and anti-rabbit PLA probes in fixed osteoblasts. The top panel represents interaction events between probes targeting T-Type VSCC and IP3R antibodies raised in goat and rabbit, respectively. Nuclei are indicated by counterstaining with DAPI. Representative images are also shown for

controls with either antibody alone or absence of both primary antibodies (negative). The right column is a threshold image of the interaction events in red.

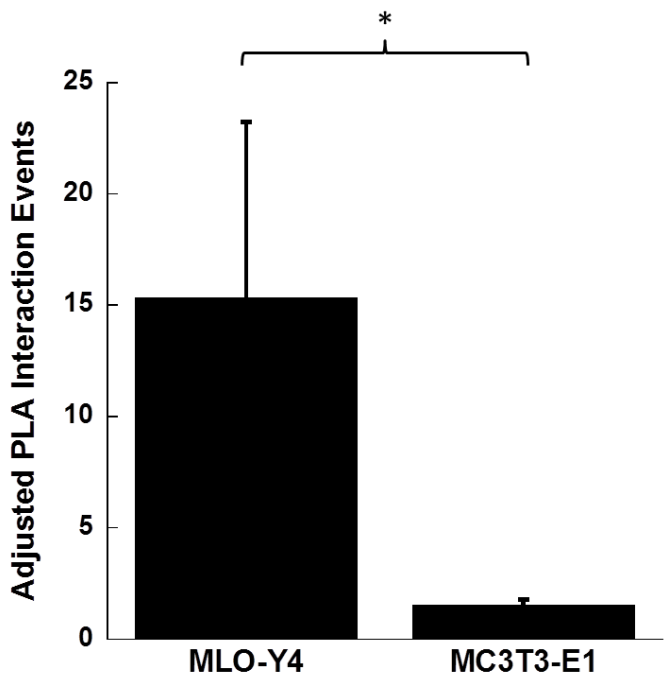

Figure 2.18. Comparison of PLA interaction events between T-Type VSCC and IP_3R in osteocytes and osteoblasts. An adjusted number of PLA interaction events was determined for each cell type by counting the number of interaction events in samples probed for both antibodies, normalizing by the total number of cells, and subtracting an average number of non-specific interactions per cell from the images with either antibody alone. Error bars are standard deviations. Student's t-test was used to determined differences between cell types. *$p < 0.05$

Chapter 3

Actin cytoskeletal dynamics and Ca^{2+} signaling in osteocytes

This thesis chapter, in part, is being prepared for submission as the manuscript:

Genevieve N. Brown, Andrea E. Morrell, Samuel T. Robinson, Rachel L. Sattler, Andrew D. Baik, and X. Edward Guo. "Calcium-dependent contractility and vesicle release in osteocytes mediate bone mechanoadaptation." Science, in preparation.

3.1 Introduction

Many *in vitro* studies have explored the role of subcellular organelles in contributing to the biochemical responses of osteocytes to mechanical stimulation. For instance, both the primary cilium[95] and the endoplasmic reticulum (ER) have been demonstrated to contribute to Ca^{2+} signaling in osteocytes, and mechanosensitive channels within the cell membrane have also been shown to contribute to these responses[27]. Furthermore, subcellular structures influence the transmission of mechanical forces to cells from the extracellular environment. The cell cytoskeleton and its associated molecules relay this mechanical information to locations within the cell containing mechanosensitive proteins, such as the nucleus or the ER[99]. Thus, the cytoskeleton of osteocytes likely plays a critical role in flow-induced mechanosensing[100-102].

The actin cytoskeleton is very pronounced in osteocytes, with dense perinuclear actin networks and actin filaments extending along the entire length of osteocytes processes[103]. Actin filaments maintain cell shape, dendritic morphology, and support membrane tension in osteocytes as evidenced by studies using latrunculin B to depolymerize actin[103,104]. Indeed, the dramatic differences in cytoskeletal components between osteocytes and osteoblasts, particularly

in dendrites, suggest that actin may play a critical role in osteocyte mechanosensory function[104]. Furthermore, differences in osteocyte morphology in long bones compared with those that experience relatively mild mechanical environments[105] suggests the importance of the cell cytoskeleton and conferred cell shape in bone adaptation.

Many studies have explored the role of the actin cytoskeleton in bone cells exposed to loading[106], with a particular focus on cytoskeletal rearrangement following fluid flow stimulation. Fluid flow induced stress fiber formation in osteoblasts and osteocytes, with differential effects of flow profile (unidirectional or oscillatory) and duration on the fiber arrangement[31]. Stress fiber formation in osteoblasts was dependent on Ca^{2+}_{cyt} signaling, as disruption of ER stores prevented flow-induced stress fiber formation, though stretch-activated Ca^{2+} channel (SACC) inhibition had no effect[107]. Cytoskeletal rearrangement in response to loading can even be observed *in situ*, where osteocyte cell bodies align along the principal loading direction[108].

Fewer studies have investigated the role of cytoskeletal deformation/dynamics in initiating the responses of bone cells to mechanical stimuli, though many studies have alluded to its importance. Spontaneous oscillations in Ca^{2+}_{cyt} in mesenchymal stem cells were found to be dependent on the small GTPase protein RhoA and Rho-associated protein kinase (ROCK) signaling, but not the cytoskeleton[109]. The expression of RhoA and ROCK in osteoprogenitors are modulated by fluid flow, and inhibition of ROCK was able to prevent flow-induced Runx2 expression in these cells[100]. Furthermore, an intact actin cytoskeleton was necessary for this response, suggesting that cytoskeletal tension maintained by ROCK is necessary for flow-induced osteogenic differentiation of mesenchymal stem cells[100]. Inhibition of actin was also found to decrease Ca^{2+}_{cyt} oscillation frequency in myofibroblasts[110]. In osteoblasts, fluid-shear

induced COX-2 expression was dependent on an intact actin cytoskeleton[111], but PGE_2 release and Ca^{2+}_{cyt} were actually increased by actin disruption[112].

In osteocytes, flow-induced PGE_2 release was inhibited by actin disruption, supposedly through effects on SACC[102]. The actin cytoskeleton was also shown to be important in hypotonicity-induced Ca^{2+}_{cyt} rises in osteocytes[113], which was previously demonstrated to depend on SACC[114]. In another study, cell strain was found to increase with increasing fluid shear stress over osteocytes, and this was correlated with increases in Ca^{2+}_{cyt}[115]. However, this study did not measure Ca^{2+} dynamics simultaneously with deformation and did not track the deformation of a specific cytoskeletal element. To date, no studies have investigated the role of the actin cytoskeleton in initiating Ca^{2+} responses in osteocytes under physiologic mechanical loads.

Our laboratory developed a technique to observe the deformation of cytoskeletal elements in rounded osteocytes under fluid flow at high temporal resolution in both bottom- and side-view [69]. Using this technique, we reconstruct a quasi-three-dimensional (quasi-3D) image of the cell under fluid flow. Traditional bottom-view imaging of osteocytes transfected with a fluorescent protein tagged to the actin cytoskeleton showed time-dependent deformation of the cytoskeleton under loading, with moderate creep and recovery of the actin cytoskeleton in the normal strain directions. The addition of side-view imaging revealed more pronounced cytoskeletal deformations and the observation of a shear strain. In a later study, the cortical actin network in osteocytes was found to be more responsive to oscillatory flow than microtubule networks when the temporal resolution was sufficient to probe subcellular responses within a single oscillation period[70]. Taken together, these studies suggest that actin dynamics are important for bone cell responses to mechanical loading, and thus likely influence Ca^{2+} signaling in these cells.

In addition, in unpublished work from laboratory, we discovered that the actin cytoskeleton compresses, or contracts, following a Ca^{2+}_{cyt} transient. This contraction was phasic, with strains in the cytoskeleton recovering to baseline levels in approximately the same period we observe between Ca^{2+}_{cyt} oscillations in osteocytes. Furthermore, we detected smooth muscle contraction-related proteins in osteocytes and found that inhibition of myosin light chain kinase (MLCK) by ML-7 significantly delayed the contraction, suggesting a smooth muscle mechanism underlying this contractility.

For this study, we hypothesized that the actin cytoskeleton is tightly coupled to Ca^{2+} signaling in osteocytes to effect a mechano-transduction-mechano process in which actin dynamics facilitate Ca^{2+} entry, and Ca^{2+}_{cyt} rises result in an actomyosin contraction. We first explored the role of actin dynamics in the generation of Ca^{2+}_{cyt} oscillations. Though previously examined, we also sought to verify that osteocytes exhibit this Ca^{2+}_{cyt}-dependent contractility in an alternative system. Micropillar substrates are commonly used to investigate cellular force generation and dynamic substrate interactions[116], so we next translated our Ca^{2+} signaling experiments to this experimental setup. To our knowledge, this is the first study to explore Ca^{2+}-dependent dynamics of cells on micropillars. Furthermore, since ML-7 only delayed contractions in our earlier quasi-3D work, we sought to identify an inhibitor of contractility that could be used in future work to delineate the roles of Ca^{2+}_{cyt} signaling and concomitant contractions in osteocyte responses to mechanical loading.

3.2 Methods

3.2.1 Cell culture

Osteocyte-like MLO-Y4 cells (a gift from Dr. Lynda Bonewald, University of Missouri-Kansas City, Kansas City, MO) were cultured on 0.15 mg/ml collagen (rat tail type I, BD Biosciences, San Jose, CA) coated culture dishes in minimum essential alpha medium (α-MEM, Life Technologies, Carlsbad, CA) supplemented with 5% fetal bovine serum (FBS, Hyclone Laboratories Inc., Logan, UT) and 5% calf serum (CS, Life Technologies, Carlsbad, CA). Cells were maintained at 5% CO_2 and 37°C in a humidified incubator. MLO-Y4 cells were sub-cultured prior to reaching 70-80% confluence in order to maintain an osteocyte-like phenotype.

3.2.2 Inhibitors

Cytochalasin D (CytoD) prevents actin polymerization[117] and was used in this study to explore the role of actin dynamics on the generation of Ca^{2+}_{cyt} signals in osteocytes (3μM in DMSO, Sigma Aldrich, St. Louis, MO). Thapsigargin is an inhibitor of the Ca^{2+}-ATPase pump on the ER (SERCA) which facilitates the reuptake of Ca^{2+} into the ER, and thapsigargin treatment (1μM) thereby results in ER depletion (Sigma Aldrich). Cells were treated for 15 minutes prior to assembly in the flow chamber, for an additional 15 minutes prior to flow onset, and throughout the experiment. Jasplakinolide is an F-actin stabilizing agent that has been used both *in vitro* and *in vivo* to disrupt cortical actin networks[118-121]. It was used in this study (1μM in DMSO) to evaluate its potential as an inhibitor of Ca^{2+}_{cyt}-dependent contractility. Cells prepared for quasi-3D studies were assembled into flow chambers with drug-containing medium and incubated with the drug for 15 minutes prior to flow exposure.

3.2.3 Ca^{2+}_{cyt} indicators and cell transfections

To observe Ca^{2+}_{cyt} changes only, MLO-Y4 were stained with Fluo-8 AM (AAT Bioquest, Sunnyvale, CA) dissolved in 20% Pluronic F-127 in DMSO (Invitrogen, Carlsbad, CA). To visualize the actin cytoskeleton, cells were transiently transfected with a LifeAct-GFP plasmid using standard non-liposomal techniques (Fugene 6, Promega Corporation, Madison, WI). To simultaneously visualize the actin cytoskeleton and measure Ca^{2+}_{cyt}, cells were dual-transfected with a LifeAct-mkate2 plasmid and a cameleon Ca^{2+} fluorescence resonance energy transfer (FRET) sensor[84,122].

3.2.4 Fluid flow stimulation on osteocyte populations

Prior to staining with Fluo-8, cells were plated onto 10μg/mL fibronectin-coated glass slides at ~80% confluency to establish cell-cell contact. Slides were then stained and assembled into a custom parallel-plate flow chamber with a glass bottom that permits live cell imaging under fluid shear stimulation. The chamber was placed on the stage of an inverted microscope (Olympus, Waltham, MA) and attached to a magnetic gear pump (Scilog, Madison, WI) for the application of steady, laminar, unidirectional flow at a shear stress of 35 dynes/cm^2. Baseline fluorescence intensity was captured for 1 minute prior to fluid shear stimulation for 9 minutes.

3.2.5 Micropillar fabrication and cell stimulation

Micropillars were fabricated from PDMS with 1μm diameter and 7μm height according to previously published methods[116,123]. PDMS micropillars were demolded in isopropanol and

then gradually switched to PBS to prevent dehydration and collapse. Pillars were coated with 10 μg/ml rhodamine fibronectin (Cytoskeleton, Inc., Denver, CO) overnight at 4°C.

To evaluate actin morphology in osteocytes seeded onto the pillars, LifeAct-GFP transfected MLO-Y4 cells were seeded onto fibronectin-coated micropillars for 30 minutes prior to imaging.

To simultaneously image pillars and Ca^{2+}_{cyt} dynamics, pillars were rinsed gently in PBS, and MLO-Y4 cells were seeded onto the pillars in Fluo-8 staining solution with reduced-serum medium (2.5% CS, 2.5% FBS in αMEM). After 30 minutes, cells were rinsed gently with reduced serum medium and then set up for imaging. Ca^{2+} was elevated by chemical induction using 50μM ATP (Sigma Aldrich, St. Louis, MO) or 5μM ionomycin (Sigma Aldrich) infused gently into the dish with a syringe.

3.2.6 Single cell quasi-3D microscopy

For quasi-3D studies, cells were plated onto fibronectin-coated glass microslides fabricated by laser-cutting glass coverslips and inserted into a square glass flow chamber (Vitrocom, Mountain Lakes, NJ) mounted on a microscope stage. Bottom- and side-view images of single cells were collected simultaneously by acquiring images from an inverted microscope (Olympus, Waltham, MA) and a 45° mirror (Red Optronics, Mountain View, CA) in the light path of an upright microscope (Olympus, Waltham, MA), respectively. Steady, laminar, unidirectional flow at a shear stress of 20 dynes/cm^2 was applied by a syringe pump (Kent Scientific, Torrington, CT). Baseline fluorescence intensities were captured for 5 seconds prior to fluid shear stimulation for an additional 55s.

3.2.7 Imaging and image analysis

To monitor the effects of CytoD on Ca^{2+}_{cyt} responses, time-lapse images of cells were collected at 20X magnification for 9 minute periods of fluid flow stimulation. The Fluo-8 Ca^{2+} indicator was excited at 488nm, and fluorescence emissions were collected at 527nm. A Ca^{2+}_{cyt} transient was defined by an increase Fluo-8 intensity at least 4 times the magnitude of noise prior to flow onset[55].

Separate images of Fluo-8 stained MLO-Y4 cells and rhodamine-fibronectin micropillars were captured every 10 seconds on an inverted microscope with a stage warmer at 100X using an oil objective. Baseline images were collected for 60 seconds prior to the addition of medium or agonists.

The actin probe and FRET biosensor were excited simultaneously by a custom triple exciter (Chroma, Bellows Falls, VT) capable of 430nm and 570nm excitations on a Lambda DG-4 xenon lamp (Sutter Instruments, Novato, CA), and fluorescence emissions of YFP (530nm), CFP (470nm), and mkate2 (641nm) were captured simultaneously using a quadview beamsplitter (Photometrics, Tucson, AZ) and custom quad-band polychroic (Chroma)[69]. Stage movement was corrected for using cross-correlation based image registration of the first frame with remaining frames in the image stack. The FRET ratio was calculated on a pixel-by-pixel basis using image registration of the FRET and donor emissions to obtain relative Ca^{2+}_{cyt} levels. Whole-cell strains in the actin cytoskeleton were determined by digital image correlation of the fluorescent F-actin image according to previously described methods[69,70].

3.2.8 Pillar deflection

Images were first registered using cross-correlation to account for stage movement during acquisition. Uneven illumination intensity was adjusted by subtracting a heavily blurred image from the original, and adaptive filtering was used to smooth the pillar boundaries. Pillar displacements were then analyzed from these processed images by tracking pillar positions in image stacks using the "Tracking Objects" feature in MetaMorph (Molecular Devices, Sunnyvale, CA). A threshold-based tracking algorithm was used to determine the location of pillar centroids in each image of the stack. Maximum displacements following the addition of medium with or without Ca^{2+} agonists were recorded for 7 pillars under the cell periphery and 7 static pillars away from the cell for each image.

3.3 Results

3.3.1 CytoD impairs Ca^{2+}_{cyt} responses in osteocytes

We first sought to determine whether dynamics of the actin cytoskeleton were critical to the generation of Ca^{2+}_{cyt} responses by treating MLO-Y4 cells with 3μM CytoD to disrupt actin polymerization prior to fluid flow. Actin inhibition significantly reduced both the number of flow-induced Ca^{2+}_{cyt} spikes and the peak magnitude of Ca^{2+}_{cyt} spikes, but it did not abolish the ability of cells to generate multiple responses (control: n=88 cells, 82% responsive; cytoD: n=70 cells, 39% responsive; Figure 3.1). We hypothesized that the remaining responses could be due to the release of Ca^{2+} from ER stores, which may or may not be disrupted with actin inhibition. Indeed, treatment of cells with both CytoD and thapsigargin completely abolished the multiple responses (n=19 cells, 5% responsive).

3.3.2 Chemically-induced Ca^{2+}-dependent contractions of osteocytes on micropillar substrates

By controlling the plating time, osteocytes were found to exhibit cortical actin arrangement on micropillars (Figure 3.2A), recapitulating the morphology preserved in quasi-3D. We seeded Fluo-8 stained MLO-Y4 cells on rhodamine-fibronectin coated micropillars, and chemical induction was used to elevate Ca^{2+}_{cyt} levels by adding Ca^{2+} agonists in solution and focusing on the pillar heads during image acquisition. Pillar positions were tracked over time to determine displacements following Ca^{2+} induction (Figure 3.3). Addition of media alone (n=2, Figure 3.4) had no effect on pillar displacements. Following addition of 5μM ionomycin (n=3, Figure 3.5) or 50μM ATP (n=3, Figure 3.6), Ca^{2+}_{cyt} was elevated, and pillars near the periphery of the cell deflected further inward, suggesting a contraction. Particle tracking using a threshold-based algorithm demonstrated that the maximum displacement of pillars below an osteocyte was significantly higher than static pillars away from the cell in both agonist conditions.

3.3.3 Inhibition of actomyosin contractility by jasplakinolide

As in our previous work, fluid shear in cells imaged by quasi-3D microscopy (Figure 3.7) induced Ca^{2+}_{cyt} transients which were often coupled to compressions in the E_{zz} strain (n=5 cells, Figure 3.8). We next explored whether the actin stabilizing agent jasplakinolide could permit Ca^{2+}_{cyt} responses in cells but inhibit actomyosin contractions. Cells treated with 1μM jasplakinolide were capable of generating Ca^{2+}_{cyt} transients, but decreases in E_{zz} strains were not observed (n=2 cells, Figure 3.9).

3.4 Discussion

We have shown now in two separate experimental systems that osteocytes exhibit contractions following Ca^{2+}_{cyt} induction. Quasi-3D studies confirmed that rises in Ca^{2+}_{cyt} occur with decreases in E_{zz} strain in actin networks, and inward deflection of pillars following a rise in Ca^{2+}_{cyt} levels suggest contractile behavior. Though the micropillar studies cannot confirm that this is an actomyosin contraction, the cortical actin arrangement of cells plated on the pillars corroborates this hypothesis. Furthermore, we now have evidence that an actin stabilizing compound can prevent these contractions in quasi-3D. Though preliminary, these results are encouraging. We have yet to determine a function for actomyosin contractility in osteocytes, though in other cells, Ca^{2+} oscillations and corresponding actin dynamics facilitate exocytosis of important chemical signals[124,125]. Indeed, jasplakinolide has been used both *in vitro* and *in vivo* to prevent exocytosis. These results suggest it is a promising agent for future studies aimed at delineating the roles of Ca^{2+} oscillations and contractility in downstream osteocyte functions.

We have previously reported the development of viscoelastic strains in cytoskeletal networks of osteocytes under fluid shear stimulation and have shown that tensile strains occur prior to calcium spike initiation (unpublished work). This study demonstrates that actin dynamics are important for osteocyte Ca^{2+}_{cyt} oscillations, but other mechanisms of Ca^{2+} mobilization, such as release from ER stores, can still enable Ca^{2+} transients in the absence of actin polymerization or in the presence of actin stabilization. Whether actin dynamics interfere with Ca^{2+}_{ER} release is unclear from this study. Alteration in the expression of actin-associating proteins has been shown to accompany the differentiation of osteoblasts to osteocytes[104,126]. For instance, osteocytes express much more villin than osteoblasts, and its expression is primarily contained within the cell body[126]. Furthermore, previous studies have shown that the activity of phospholipase C

(PLC), which generates IP3 to release Ca^{2+} from ER stores, is regulated by villin[127]. Thus, it is plausible for actin dynamics to be coupled to the ER in osteocytes, and future studies simultaneously measuring Ca^{2+}_{ER} and actin dynamics, as in using the D1ER FRET sensor, could help elucidate this mechanism.

A major limitation to these studies is the small sample sizes, partially because these measurements are made on single cells. Methods of extrapolating these results to population studies would prove valuable. For instance, though our preliminary data and the work of others[125] suggests that Ca^{2+} signals are not impaired by jasplakinolide treatment, the drug should be evaluated on cell populations exposed to flow, as in the CytoD treatment. Conversely, the role of actin dynamics in Ca^{2+}_{cyt} spike initiation could be more thoroughly explored in quasi-3D, where the temporal resolution may unveil interesting differences in the time it takes for Ca^{2+} signals to initiate when actin dynamics are impaired.

3.5 Conclusions

We demonstrated that the prominent actin cytoskeleton in osteocytes is indeed involved in biochemical responses of these cells. We confirmed that osteocytes exhibit a mechano-transduction-mechano process in which actin dynamics facilitate Ca^{2+} entry, and Ca^{2+}_{cyt} rises result in actomyosin contractions. Future work exploring the mechanisms involved in actin-mediated responses to load may improve our understanding of mechanosensation and mechanotransduction in bone.

3.6 Figures

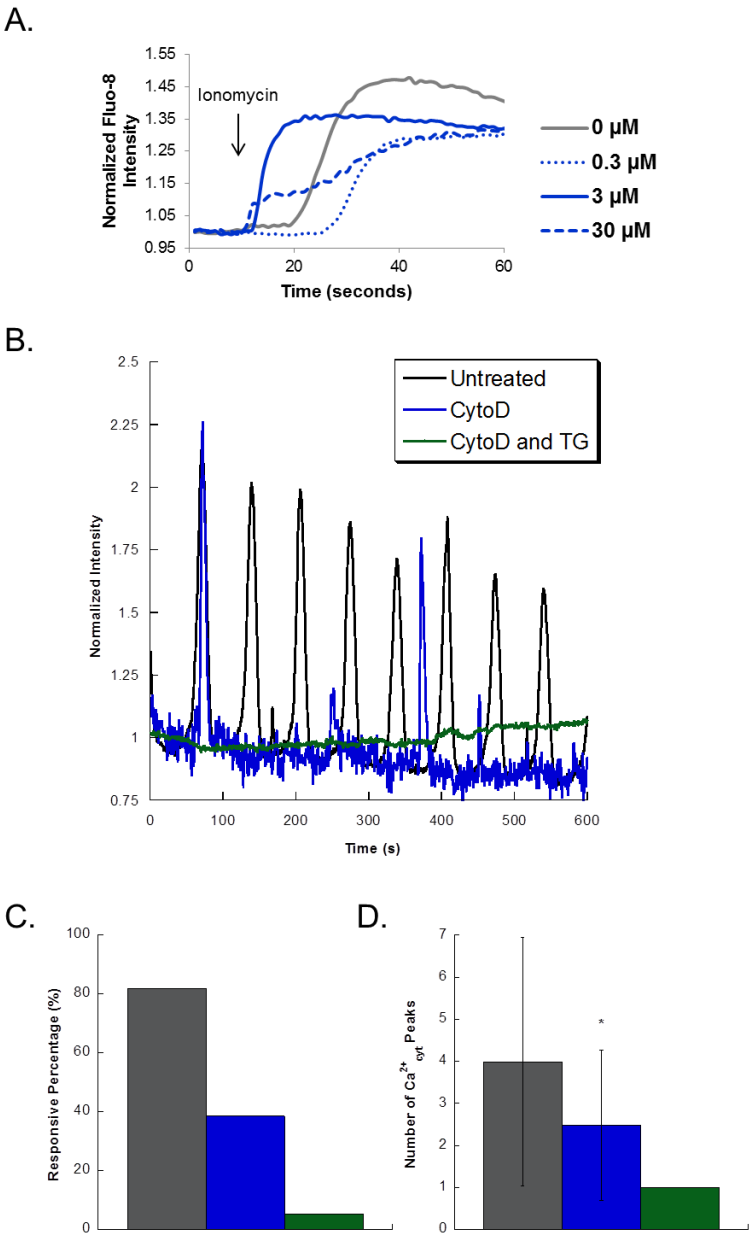

Figure 3.1. Effects of cytoskeletal disruption on Ca^{2+}_{cyt} oscillations in osteocytes. (A) A dose study demonstrated that cells exposed to varying concentrations of CytoD could still respond to Ca^{2+} elevations by ionomycin. (B) Representative traces of Ca^{2+}_{cyt} transients in untreated osteocytes and cells treated with CytoD or CytoD and thapsigargin. (C) Percentage of responsive

cells under each condition. (D) Number of Ca^{2+}_{cyt} peaks under each condition. Error bars are standard deviations. *$p<0.05$ compared to untreated cells

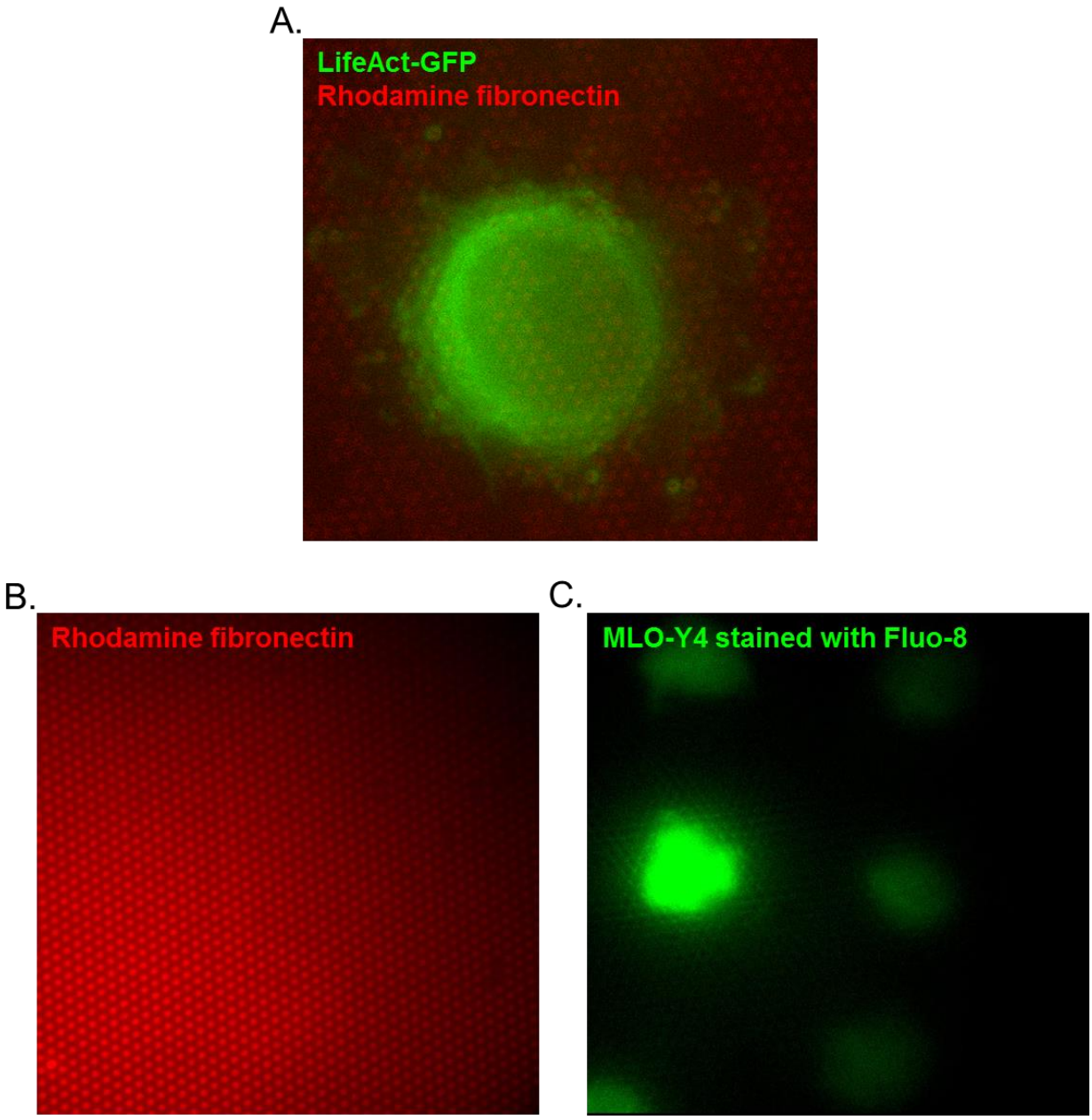

Figure 3.2. MLO-Y4 osteocytes on PDMS micropillars. (A) Cortical actin morphology of MLO-Y4 osteocytes seeded onto micropillars. (B) Micropillars coated with rhodamine fibronectin and (C) seeded MLO-Y4 stained with the Ca^{2+}_{cyt} indicator Fluo-8.

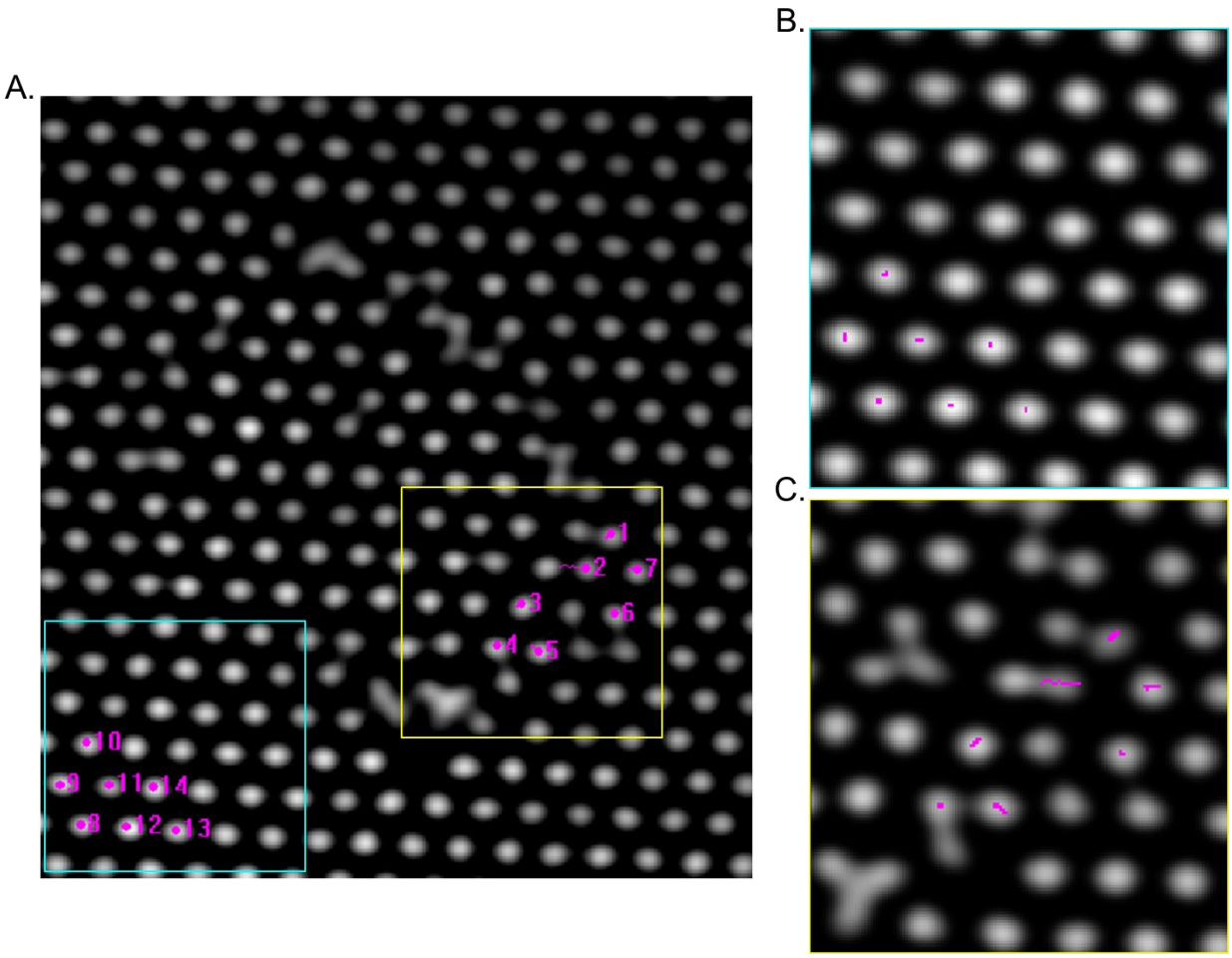

Figure 3.3. Particle tracking to determine pillar displacements. (A) Representative image of particle tracking in image stacks from experiments using Fluo-8 stained MLO-Y4 cells seeded onto fluorescent micropillars. For each image, the positions of 7 pillars at the cell periphery and 7 pillars away from the cell were tracked over time, and maximum displacements following Ca^{2+}_{cyt} induction were calculated from the pillar position data. (B) Tracking of static pillars away from the cell. (C) Tracking of pillars beneath the cell periphery. Lines indicate positions over the entire imaging period.

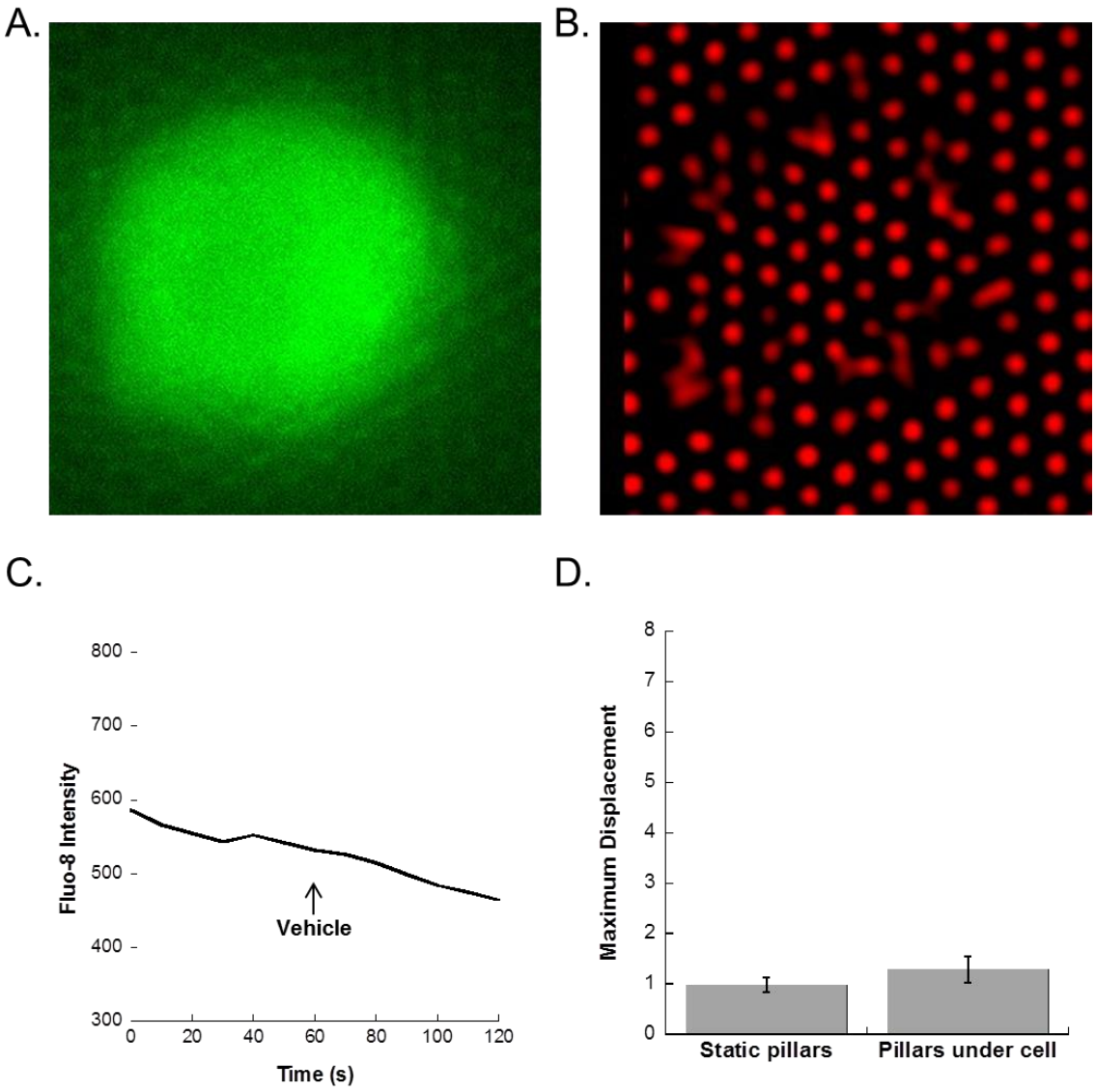

Figure 3.4. Effects of addition of vehicle (media alone) on Ca^{2+} responses and pillar displacements. (A) Representative osteocyte stained with Fluo-8. (B) Rhodamine micropillars beneath the cell. (C) Time course of Fluo-8 intensity. (D) Maximum displacement following the addition of vehicle of pillars under the cell periphery and static pillars away from the cell. A Student's t-test was used to determine differences between groups.

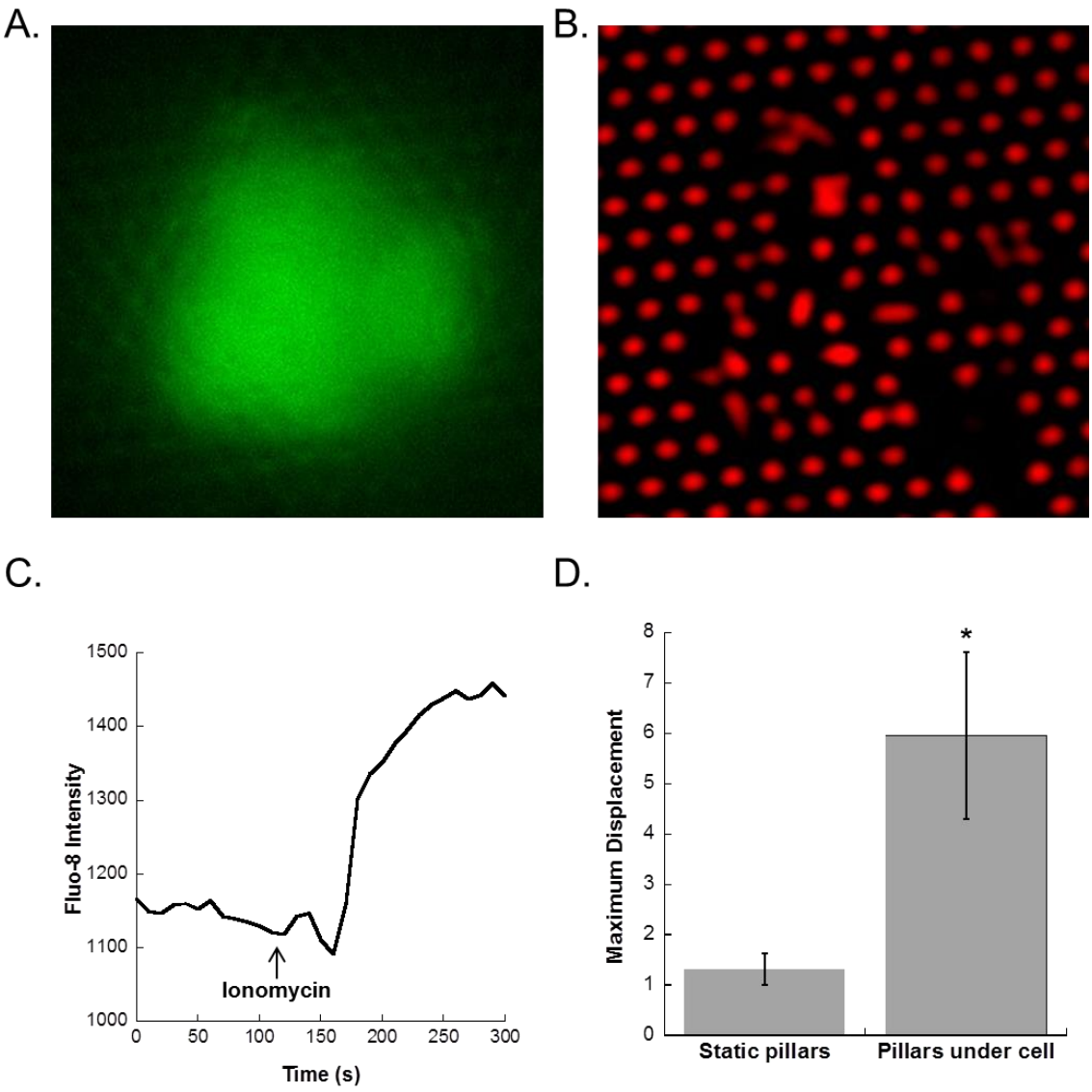

Figure 3.5. Effects of addition of ionomycin on Ca^{2+} responses and pillar displacements. (A) Representative osteocyte stained with Fluo-8. (B) Rhodamine micropillars beneath the cell. (C) Time course of Fluo-8 intensity. (D) Maximum displacement following the addition of ionomycin of pillars under the cell periphery and static pillars away from the cell. A Student's t-test was used to determine differences between groups. *$p<0.05$

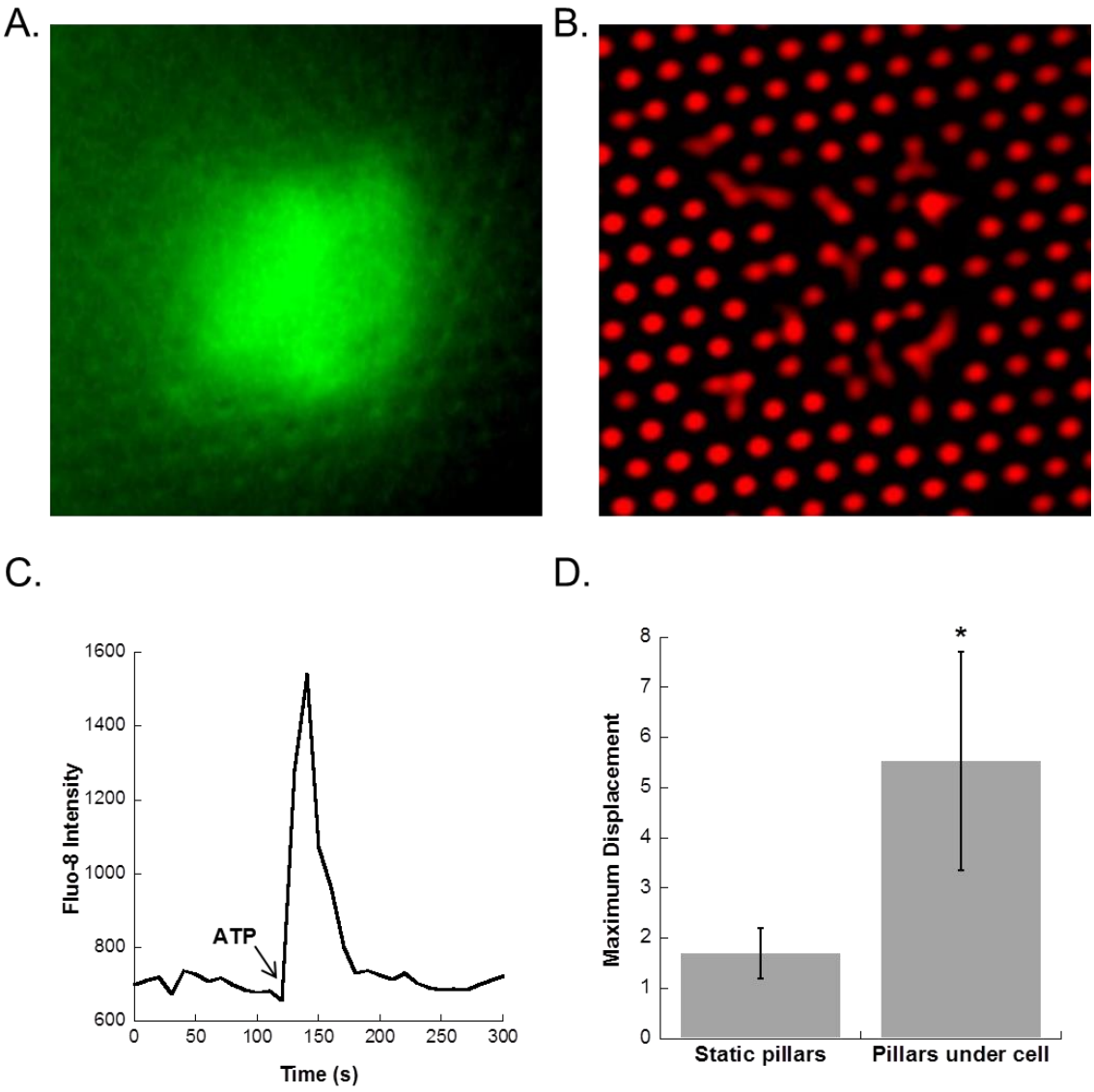

Figure 3.6. Effects of addition of ATP on Ca^{2+} responses and pillar displacements. (A) Representative osteocyte stained with Fluo-8. (B) Rhodamine micropillars beneath the cell. (C) Time course of Fluo-8 intensity. (D) Maximum displacement following the addition of ATP of pillars under the cell periphery and static pillars away from the cell. A Student's t-test was used to determine differences between groups. *$p<0.05$

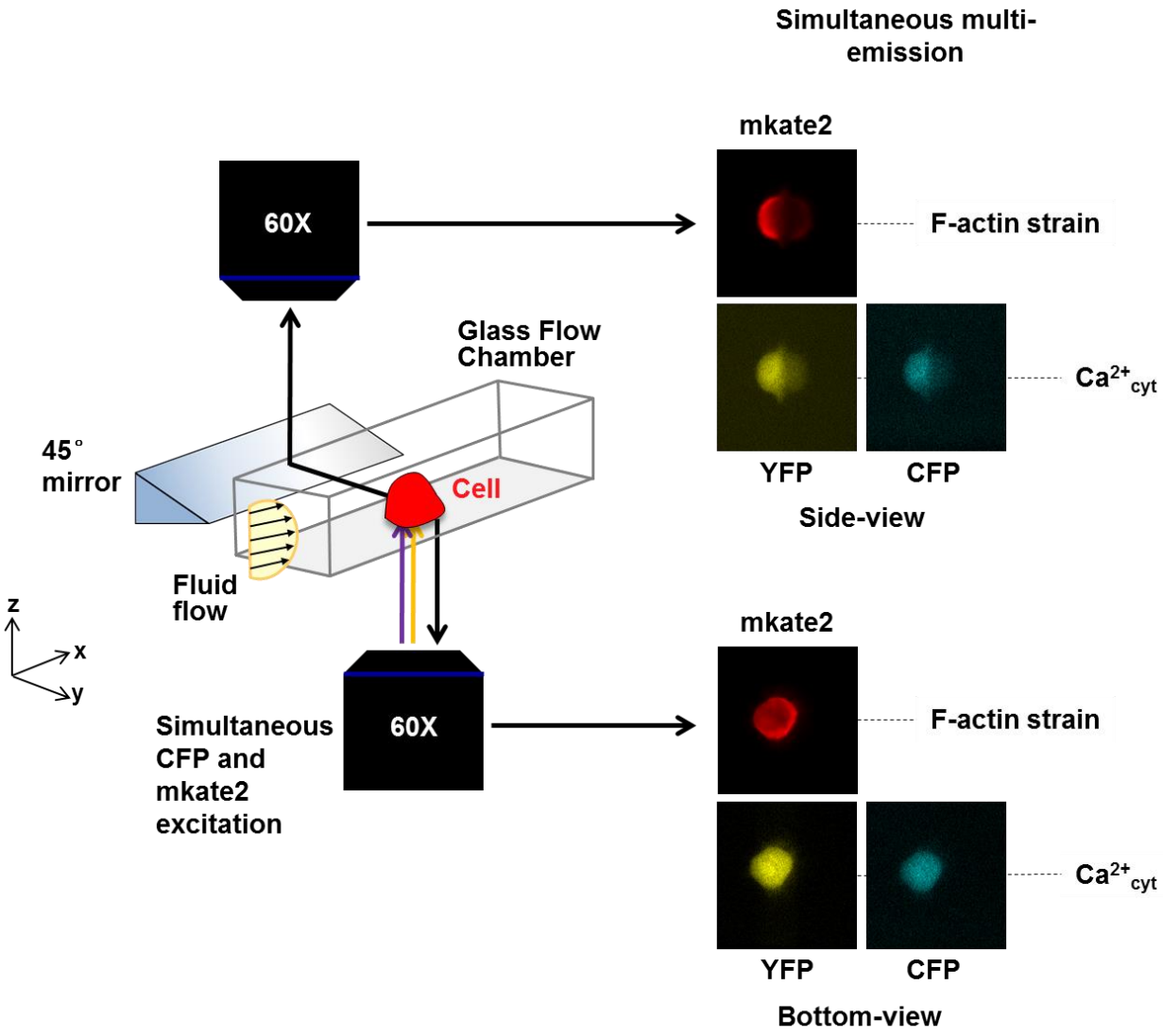

Figure 3.7. Quasi-3D microscopy. Single osteocytes with rounded morphology are imaged in a square glass flow chamber at 60X. Dual-excitation and a custom quadview emission filter allow for simultaneous collection of three fluorescence channels: YFP and CFP of the FRET sensor and mkate2. An inverted microscope provides a traditional bottom-view image. A 45° mirror in the light path directs emissions to an upright microscope to also provide a side-view image.

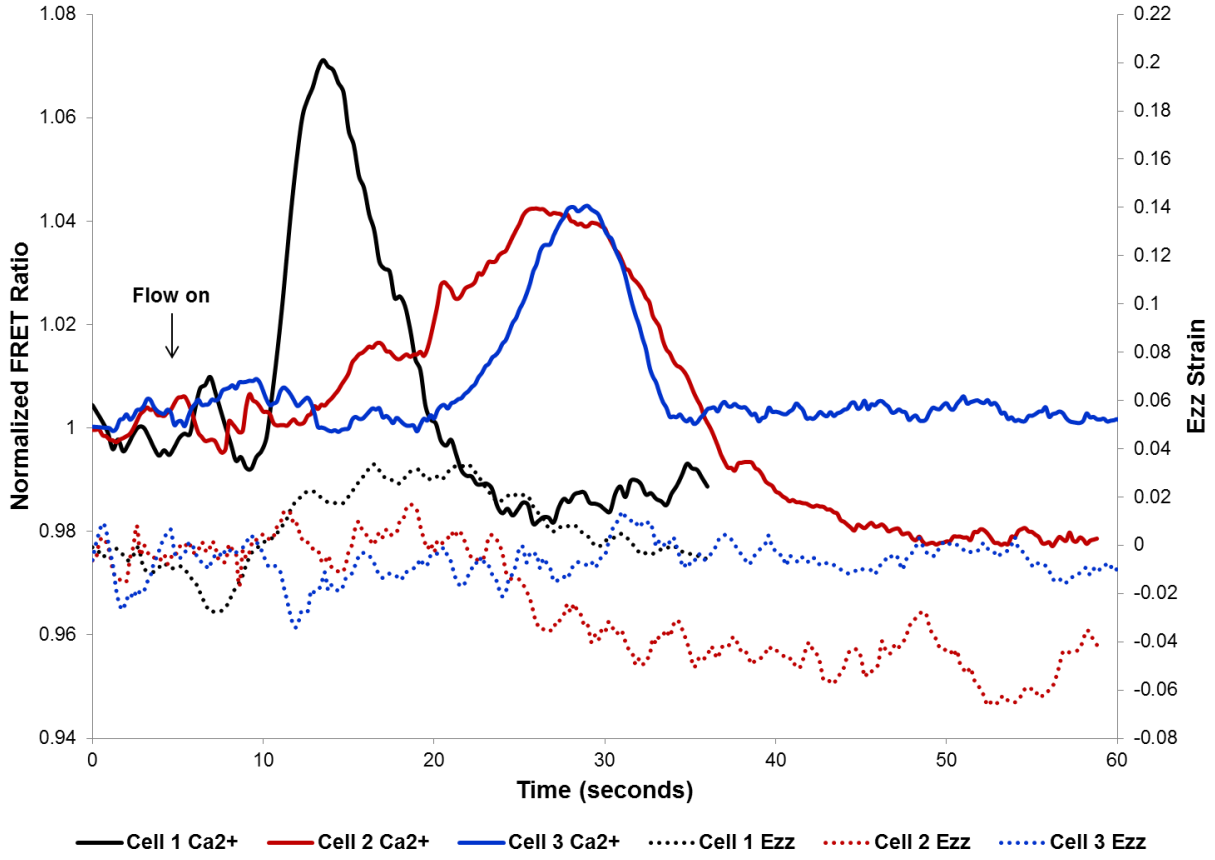

Figure 3.8. Ca^{2+}_{cyt} responses and E_{zz} strain measurements in osteocytes exposed to steady fluid shear. Ca^{2+}_{cyt} transients are displayed as solid lines, while E_{zz} strains are shown as dotted lines. Flow was started at 5 seconds.

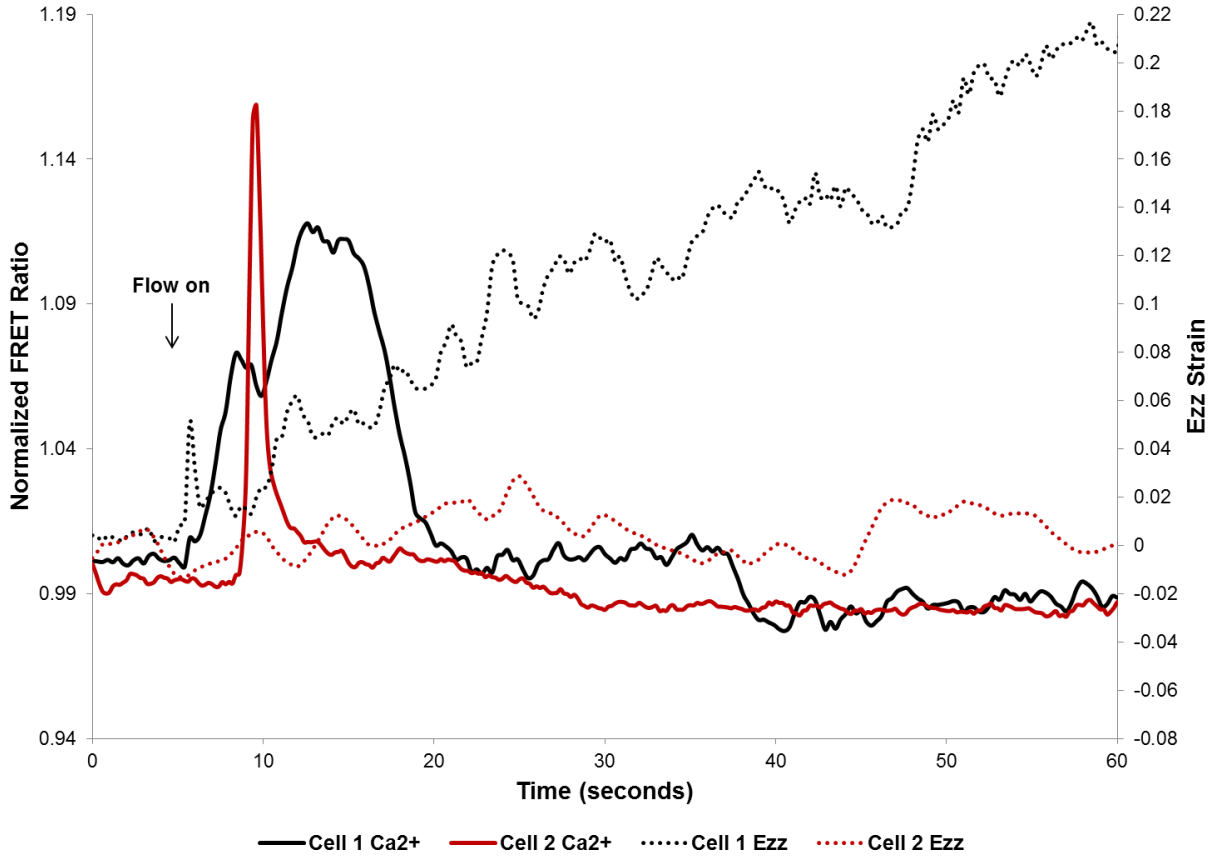

Figure 3.9. Ca^{2+}_{cyt} responses and E_{zz} strain measurements in osteocytes exposed to steady fluid shear following pre-treatment with jasplakinolide. Ca^{2+}_{cyt} transients are displayed as solid lines, while E_{zz} strains are shown as dotted lines. Cells were treated for 15 minutes prior to flow with 1µM jasplakinolide, and the drug was included in the flow medium. Flow was started at 5 seconds.

Chapter 4

Mechanically-Induced Calcium Oscillations in Osteocytes Facilitate the Release of Extracellular Vesicles Containing Proteins Involved in Bone Adaptation

This thesis chapter, in part, is being prepared for submission as the manuscript:

> *Genevieve N. Brown, Andrea E. Morrell, Samuel T. Robinson, Rachel L. Sattler, Andrew D. Baik, and X. Edward Guo. "Calcium-dependent contractility and vesicle release in osteocytes mediate bone mechanoadaptation." Science, in preparation.*

4.1 Introduction

Osteocytes are the most abundant bone cells, making up more than 90% of the cell population buried in the bone matrix. They are highly dendritic cells, interconnected by cellular processes emanating from cell bodies through an extensive network called the lacunocanalicular system (LCS)[128-130]. In this respect, osteocytes form cellular networks that are ideally situated to sense and respond to mechanical events that arise from physiological loading conditions[20,22,131-136]. Studies have demonstrated that the loss of osteocytes alone by targeted ablation will induce osteoporosis[37]. Interestingly, these transgenic mice with ablated osteocytes were also resistant to unloading-induced bone loss, and numerous studies have demonstrated osteocytes can orchestrate bone turnover in response to changing mechanical demands[14,15], illustrating their critical role in detecting mechanical signals and maintaining skeletal integrity.

Mechanotransduction refers to the conversion of a physical stimulus, such as applied load, to a biochemical response[137]. Over time, these biochemical responses act on osteoblasts, osteoclasts, and other supporting cell types to modulate the tissue composition and architecture,

resulting in adaptation of the whole bone. In health, these processes are coordinated to maintain tissue homeostasis. In disease, alterations in these biochemical responses and/or reduction in sensitivity to the applied forces may lead to the overall pathologies that present at the tissue level. Thus, there is considerable motivation to reveal mechanisms of mechanosensation and mechanotransduction in order to more effectively understand bone adaptation in health and disease.

The most promising osteoporosis treatments are in fact targeted at osteocyte biology[138]. Osteocytes are the primary source of RANKL[38,39,139], which stimulates bone resorption, and sclerostin[140,141], which inhibits bone formation. The anti-RANKL antibody denosumab and anti-sclerostin antibody romosozumab have both shown osteoanabolic effects in the clinic and in clinical trials[142,143], respectively. However, prolonged inhibition of RANKL signaling disrupts routine remodeling of the skeleton, and the anabolic effects of anti-sclerostin antibody attenuate with repeated administration[142-145]. An underlying factor may be the desensitization of mechanotransduction[146], warranting further study of osteocyte modulation of these key drug-targeted proteins. Previous studies have shown mechanical loading downregulates (and unloading upregulates) gene and protein expression of sclerostin both *in vivo* and *in vitro*[75]. However, recent studies indicate that sclerostin knockout mice still respond to anabolic loading *in vivo*[42], and wild-type animals treated with anti-sclerostin antibody can still sense disuse environments[43,75]. Studies of the regulation of RANKL and its decoy receptor OPG by loading have also produced conflicting results, though most suggest that anabolic levels of fluid shear reduce RANKL/OPG gene expression[33,34,75,147-149]. Notably, few studies have examined protein production of RANKL or OPG, and no *in vivo* experiments have examined gene or protein

changes of RANKL or OPG under physiological mechanical loads, only overloading or unloading[150-152].

The sustainment of robust oscillations in Ca^{2+} is a hallmark of osteocytes responding to mechanical stimuli[59-63,65,68,153,154]. Ca^{2+} signaling can regulate many cellular functions, including gene and protein expression, but no studies have explored the role of osteocyte Ca^{2+} signaling in the regulation of RANKL, OPG or sclerostin expression over time. To our knowledge, only two studies have even linked Ca^{2+} signaling in bone cells to protein responses. In a study on osteoblasts, fluid flow was shown to induce actin stress fiber formation and the production of COX-2[107]. Pre-treatment of cells with the intracellular Ca^{2+} chelator BAPTA-AM prior to flow abolished these responses. In another study, treatment of osteoblasts with thapsigargin prevented flow-induced upregulation of osteopontin[155]. However, to date no studies have investigated the role of osteocyte Ca^{2+} oscillations in protein modulation by mechanical loading.

Furthermore, though the actin cytoskeleton has been implicated in mechanically-induced protein responses in osteocytes[27,101,102,106,111], no studies have connected Ca^{2+}-dependent actin dynamics to osteocyte signal transduction. In myofibroblasts, spontaneous Ca^{2+} oscillations and Ca^{2+}-dependent contractions are critical for cellular communication in remodeling tissue[156], though this study focused on force communication rather than biochemical signaling.

Recently, vesicle release has been highlighted as an important means of intercellular communication[157,158], where cells package proteins and mRNAs in membrane-enclosed extracellular vesicles (EVs) to shuttle their contents among one another[158,159]. Actomyosin contractility has been shown to facilitate EV release in endothelial cells[124], and actin/Ca^{2+} oscillations are coupled to vesicle secretion in mast cells[125]. Interestingly, vesicle-like structures have been detected in osteocyte networks *in situ*[71], and osteocyte-like cells were found to

produce EVs enriched in proteins related to bone adaptation, including RANKL and sclerostin[72]. It is still unknown how osteocytes send biochemical signals from within the bone matrix to cells on the bone surface, and microvesicle trafficking could be an explanation.

The overall purpose of this study is to demonstrate the importance of the unique Ca^{2+}_{cyt} oscillations in osteocytes in their role as coordinators of bone adaptation. We hypothesize that load-induced Ca^{2+}_{cyt} oscillations facilitate the production and release of EVs containing proteins involved in bone adaptation and posit this as a means by which osteocytes coordinate bone responses to mechanical loading.

4.2 Methods

4.2.1 Cell culture

Osteocyte-like MLO-Y4 cells (a gift from Dr. Lynda Bonewald, University of Missouri-Kansas City, Kansas City, MO) were cultured on 0.15 mg/ml collagen (rat tail type I, BD Biosciences, San Jose, CA) coated culture dishes in minimum essential alpha medium (α-MEM, Life Technologies, Carlsbad, CA) supplemented with 5% fetal bovine serum (FBS, Hyclone Laboratories Inc., Logan, UT) and 5% calf serum (CS, Life Technologies, Carlsbad, CA). Cells were maintained at 5% CO_2 and 37°C in a humidified incubator. MLO-Y4 cells were sub-cultured prior to reaching 70-80% confluence in order to maintain an osteocyte-like phenotype.

Cells were plated onto 10μg/ml fibronectin (Corning, Corning, NY) coated large (38 x 75mm) glass slides at a density of $30x10^4$ cells/slide and cultured for 36 hours. Prior to fluid shear exposure, MLO-Y4 cells were rinsed 3 times for 5 minutes each in phosphate buffered saline (PBS, Gibco, ThermoFisher Scientific, Waltham, MA) and pre-incubated with minimum essential medium alpha supplemented with exosome-depleted fetal bovine serum (System

Biosciences, Palo Alto, CA) to remove contaminating bovine exosomes. Exosome-depleted serum had no effect on the ability of cells to exhibit Ca^{2+}_{cyt} responses (Figure 4.1).

4.2.2 Fluid shear stimulation

Cells were assembled into a custom parallel-plate flow chamber. Fluid shear was applied at 35 dynes/cm^2 for two 10-minute bouts of steady flow separated by a 15 minute rest period, which has been shown to induce Ca^{2+} oscillations in earlier studies[65]. Flow was driven by a magnetic gear pump (Ismatec, Cole-Parmer, Vernon Hills, IL). To inhibit Ca^{2+} oscillations, cells were pre-treated for 30 mins prior to flow onset with 15mM neomycin (Sigma Aldrich, St. Louis, MO), which has been shown in earlier studies of micropatterned cells to reduce the number of Ca^{2+} transients to a single response. This experimental design is summarized in Figure 4.2.

4.2.3 Isolation and characterization of extracellular vesicles

Conditioned medium from flow experiments was collected immediately after experiments and frozen at -20°C prior to analysis. Exosomes were purified from conditioned medium by differential ultracentrifugation[160] on a Beckman L8-M ultracentrifuge (Beckman Coulter, Brea, CA) with a 50.2 Ti fixed-angle rotor (Figure 4.3). Conditioned medium samples were centrifuged at 2000 x g to pellet dead cells, and the supernatants were transferred to polycarbonate ultracentrifuge tubes (Beckman Coulter). Samples were massed to within 0.02 g to ensure balance. First, samples were centrifuged at 10,000 x g for 30 minutes to remove any cell debris. Supernatants were further spun at 100,000 x g for 70 minutes to pellet out extracellular vesicles. As this fraction often contains contaminating protein aggregates, pellets were rinsed and resuspended in PBS and centrifuged once again at 100,000 x g for 70 mins. Pellets from 6

independent slides exposed to one of the experimental conditions (control, steady flow, or steady flow with neomycin treatment) were combined to generate one sample for analysis. Pellets were resuspended in 1 ml PBS for particle characterization or 150 µl RIPA buffer for Western blot.

Particle concentration and size distribution were analyzed by Nanoparticle Tracking Analysis on a Malvern NanoSight (Malvern, United Kingdom) at the Cornell Nanobiotechnology Center (Ithaca, NY). Samples were diluted in PBS, and data from 5 separate measurements of the same sample were averaged to determine the sample concentration and average particle size. The average of n=4 samples per group were analyzed.

4.2.4 Immuno-detection

Immediately following flow exposure, cells were fixed and permeabilized in ice-cold acetone. Cells were probed for the expression of the secretory exosome marker lysosomal associated membrane protein 1 (LAMP1) using standard immunocytochemistry techniques. Briefly, cells were blocked in 5% BSA (Sigma Aldrich, St. Louis, MO) and incubated overnight with a rabbit polyclonal anti-LAMP1 antibody (ab24170, Abcam, Cambridge, MA). The VectaFluor Detection system with DyLight 594 Anti-rabbit Ig reagent (Vector Laboratories, Burlingame, CA) was used to probe the antibody for LAMP1.

Exosome contents were assessed by Western blot. Exosome protein lysates were prepared by lysing vesicle preparations in RIPA lysis and extraction buffer supplemented with protease and phosphatase inhibitors (ThermoScientific, Waltham, MA) for 10 mins. Protein lysates were mixed 1:1 with 2X Laemmli buffer (Sigma Aldrich, St. Louis, MO) and boiled for 5 minutes at 95°C. Protein samples were separated by gel electrophoresis using pre-cast polyacrylamide gels and a Mini-PROTEAN electrophoresis chamber (Biorad, Hercules, CA). Proteins were

transferred to a PVDF membrane (Biorad) by wet transfer. Membranes were blocked with 5% BSA (Sigma Aldrich), and primary antibody incubations were performed overnight at 4°C. The following primary antibodies were used to assess vesicle contents: goat polyclonal antibody to RANKL (sc-7627, Santa Cruz Biotechnology, Dallas, TX); goat polyclonal antibody to OPG (sc-8468, Santa Cruz Biotechnology); rabbit polyclonal antibody to LAMP1 (ab24170, Abcam); goat polyclonal to sclerostin (AF-1589, R&D Systems, Minneapolis, MN). Membranes were rinsed well with TBST (Biorad) and then probed with the appropriate secondary antibodies. Detection was performed using the SuperSignal West Femto chemiluminescence detection kit (Thermo Scientific) and a FujiFilm LAS-4000 Luminescent Image Analyzer (FujiFilm, Stamford, CT). Proteins were verified by band size using a molecular weight ladder (Biorad) and specificity using concurrent negative controls.

4.2.5 Statistics

One-way ANOVA with Dunnett's post hoc was used to compare differences in means among the three groups studied relative to the control group. Significance was observed at $p<0.05$.

4.3 Results

4.3.1 Neomycin inhibits Ca^{2+} oscillations in osteocytes exposed to fluid flow

To evaluate the relative role of flow-induced Ca^{2+}_{cyt} oscillations in osteocyte responses to mechanical loading, we treated cells with the phospholipase C (PLC) inhibitor neomycin to reduce the number of Ca^{2+}_{cyt} responses in cells exposed to flow (Figure 4.4). Treatment of MLO-

Y4 cells before and during fluid shear stimulation resulted in a dramatic decrease in the number of responsive cells as well as the number of Ca^{2+}_{cyt} responses in responsive cells.

4.3.2 Fluid flow increases LAMP1 expression

Immunostaining for the secretory vesicle marker LAMP1 revealed punctate staining consistent with the presence of vesicle-like structures (Figure 4.5). Exposure of MLO-Y4 osteocytes to fluid flow increased the expression of LAMP1, with more abundant punctate stains visible in cells and staining present further throughout the cell body. Inhibition of Ca^{2+} oscillations using neomycin diminished this response.

4.3.3 Flow induces the release of extracellular vesicles in a Ca^{2+}-dependent fashion

Mechanical stimulation of osteocytes induced significant release of extracellular vesicles into the culture medium (Figure 4.6A), with nearly a 30-fold increase in the number of detected particles (Figure 4.6B). This response was dramatically blunted in the presence of neomycin. One-way ANOVA with Dunnett's post hoc revealed a difference between control and flow groups. No difference was detected between control and flow with neomycin treatment.

4.3.4 Extracellular vesicles from osteocytes contain proteins related to bone adaptation

Western blots on osteocyte EV protein lysates detected LAMP1 within the vesicles. In addition, the bone regulatory proteins RANKL, OPG, and sclerostin were among the proteins contained within these EVs (Figure 4.7A). Densitometric analysis of detected bands (Figure 4.7B) showed increased levels of all detected proteins by flow.

4.3.5 Particle size

The average diameter of all released EVs was 175nm. A representative distribution of EV sizes is shown in Figure 4.8A. The EV diameters were not significantly different among groups (Figure 4.8B).

4.4 Discussion

Our most intriguing finding is that load-induced, Ca^{2+}-dependent actomyosin contractions in osteocytes facilitate the release of EVs. Our data suggests that fluid flow modulates osteocyte protein expression by enhancing the production and release of EVs which contain key bone-regulatory proteins such as RANKL, OPG, and sclerostin. This load-induced response is Ca^{2+}-dependent, as treatment with neomycin, which significantly reduces the number of Ca^{2+} responses, diminishes LAMP1 expression as well as EV release. Interestingly, vesicle-like structures have been identified in osteocytes and shown to be enriched in bone regulatory proteins[72]. Though actin networks had been previously implicated in mechanically-induced protein responses in osteocytes, this is the first study to explore the regulation of EV production by mechanical loading as a potential mechanism for these observations.

In a recent morphological study, RANKL and OPG showed strong co-localization to vesicles of osteocytes, indicated by lysosomal-associated membrane protein 1 (LAMP1)[161]. The presence of several OPG-positive structures in canaliculi prompted the group to measure canaliculi diameter in TEM images. They reported a mean canaliculi diameter of 219 ± 45 nm in the cortical bone of mice[161], which is in line with previously published values[162,163]. It is still unknown how osteocytes send biochemical signals from within the bone matrix to cells on the bone surface, and EV transport represents a compelling potential mechanism. Our preliminary *in*

vitro data has found RANKL, OPG, and sclerostin in EVs with an average diameter of 175 nm; thus transport of these proteins through the LCS is a plausible and intriguing means by which osteocytes may coordinate tissue-level bone adaptation.

This is one of few studies to demonstrate that Ca^{2+}-mediated vesicle release can be mechanically-regulated. Most recent studies coupling Ca^{2+} dynamics with exocytosis focus on agonist-induced Ca^{2+} signaling and exocytosis. In an early study of surfactant secretion in lung epithelial cells, substrate stretch was shown to induce Ca^{2+} transients and concurrent exocytosis[164]. Furthermore, the response was dose-dependent. In the musculoskeletal system, dynamic compression was shown to induce exocytosis in chondrocytes[165], and Ca^{2+} signaling has been established as an important biochemical response in these cells as well. It is well established that mechanical loading induces a dose-dependent increase in Ca^{2+}_{cyt} transients in osteocytes[65,66,68]; thus, this further supports the role of EV release in regulating responses to mechanical loading.

There are a few limitations to the current study. First, though we identified sclerostin within EVs released from mechanically stimulated MLO-Y4 cells, this cell line historically expresses limited levels of this protein. Therefore, future work examining the regulation of sclerostin expression by load and Ca^{2+}_{cyt} signaling should translate these experiments to primary cells or more appropriate cell lines[74,75]. Many studies have generated data to support the role of actomyosin contractility in exocytosis, and we have shown actin contractility following Ca^{2+}_{cyt} responses in our cells, but we did not directly show a relationship between actin contractions and EV release in osteocytes. Repeating these studies with an inhibitor of actomyosin contractility would help to solidify this hypothesis. Numerous studies have shown that the actin-stabilizing

compound jasplakinolide interrupts exocytosis[125]; therefore, this is a promising drug for future studies explored EV release in osteocytes.

4.5 Conclusions

This study uncovered a novel and direct consequence of mechanically-induced Ca^{2+} signaling in osteocytes and connected this early biochemical response to subsequent protein responses under mechanical loading. We added insights into the regulation and release of proteins involved in bone adaptation to mechanical loading. Better understanding these mechanisms may inform the pharmacodynamics of current treatments targeting RANKL, OPG and sclerostin and potentially help optimize treatment strategies.

4.6 Figures

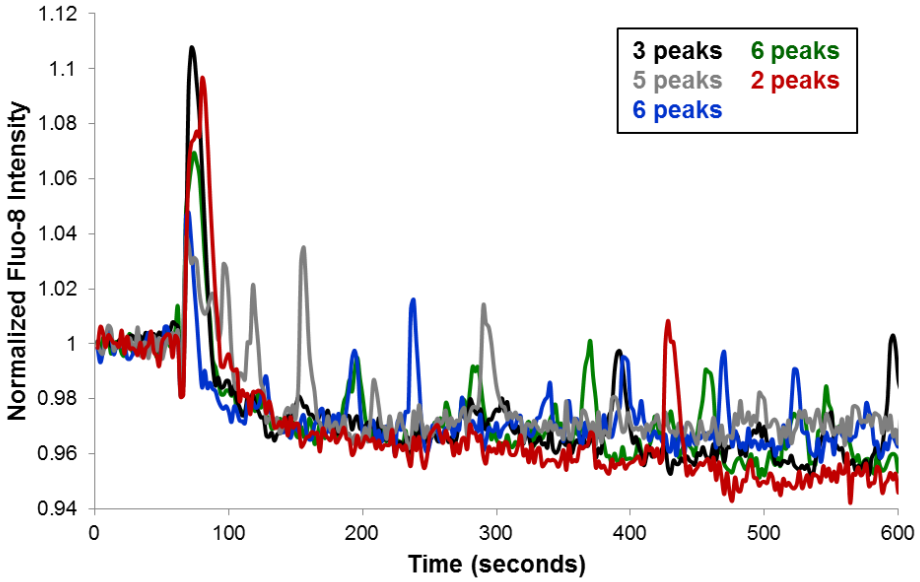

Figure 4.1. Ca^{2+}_{cyt} oscillations in MLO-Y4 cells exposed to fluid shear in medium supplemented with exosome-depleted FBS. Representative time courses are shown for 5 cells exposed to flow. Flow onset was at 60s.

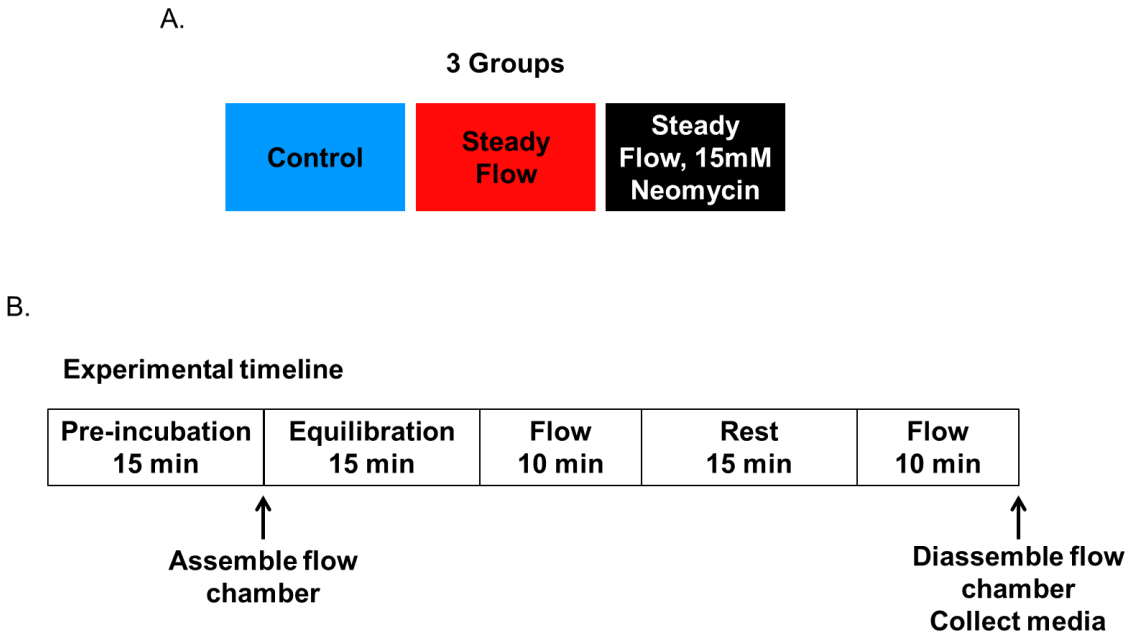

Figure 4.2. Overview of the experimental design. (A) Three experimental conditions were examined in this study. Cells were exposed to fluid shear, and one group was treated with neomycin to prevent flow-induced Ca^{2+}_{cyt} oscillations. Untreated cells under static conditions served as controls. (B) Cells were exposed to two bouts of steady flow with an inserted rest period. Flow duration was 10 minutes. Neomycin was present in the medium for both pre-incubation and equilibration steps, resulting in 30 minutes exposure to the drug prior to mechanical stimulation.

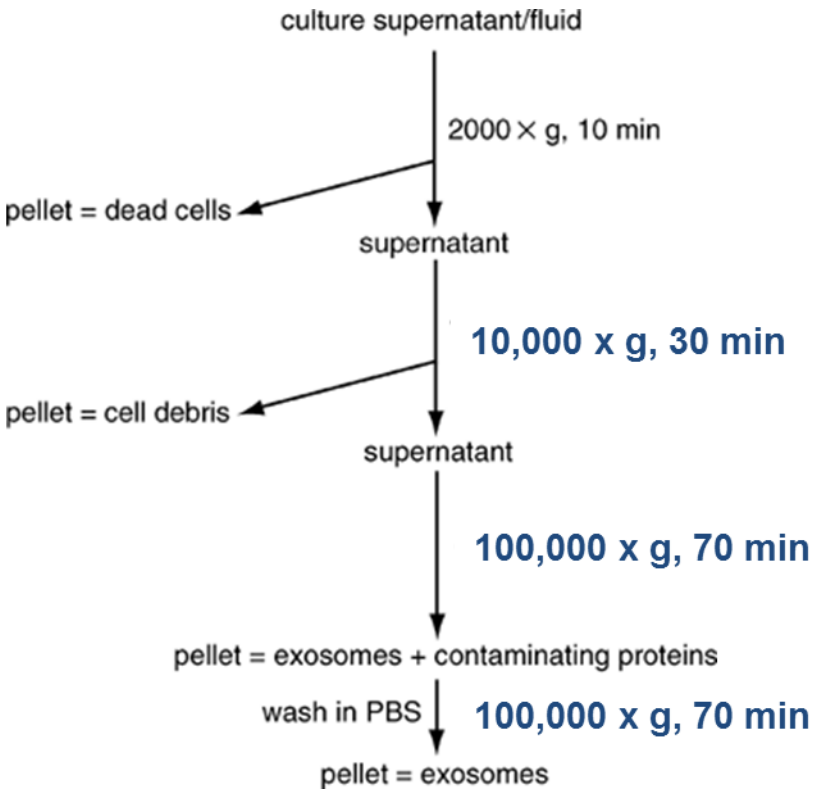

Figure 4.3. Differential ultracentrifugation procedure for isolating extracellular vesicles. Extracellular vesicles were isolated from conditioned medium and subjected to a 10,000 x g centrifugation step to eliminate cell debris and two 100,000 x g centrifugation steps to wash and pellet vesicles. *Image adapted from Reference 151.*

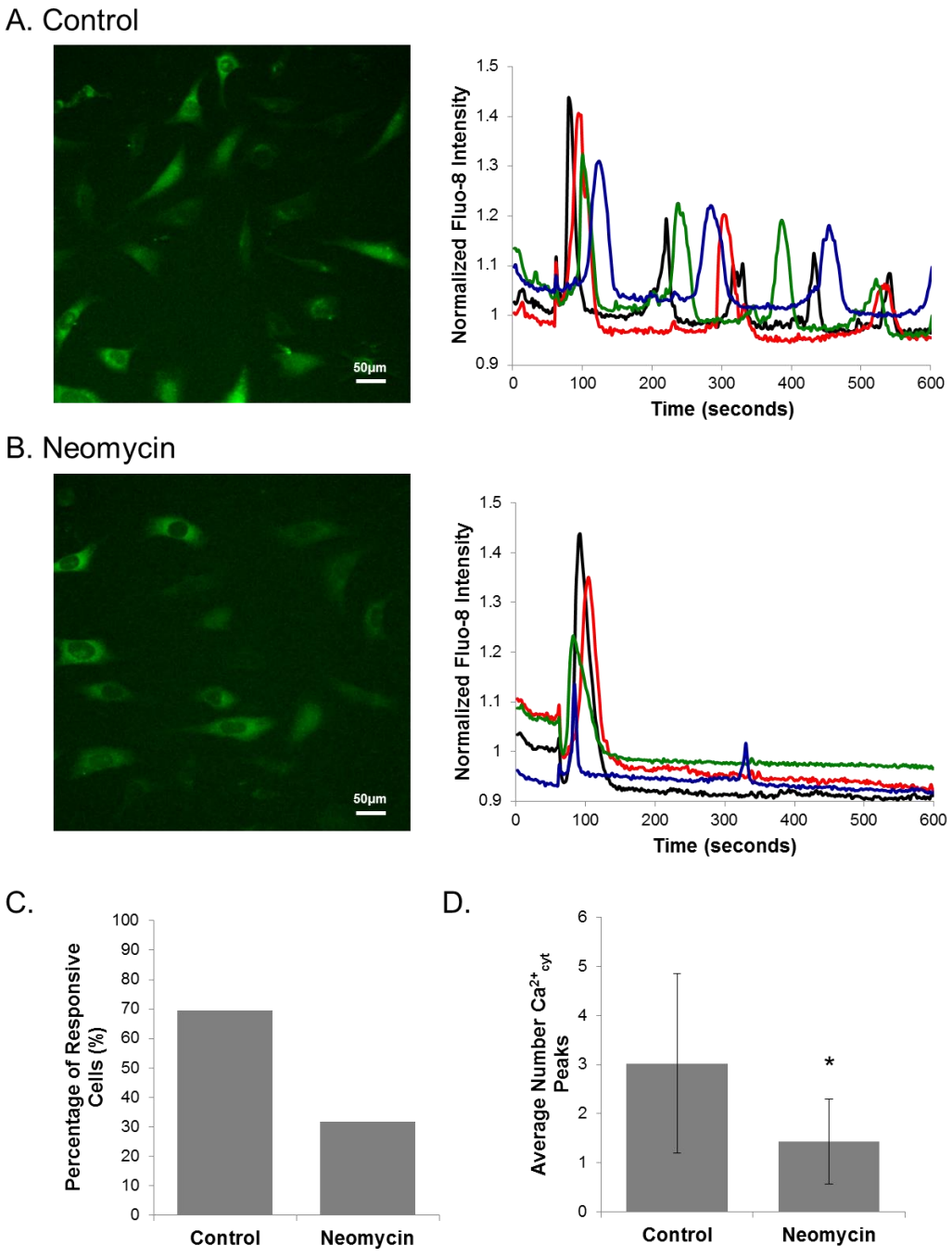

Figure 4.4. Inhibition of Ca^{2+}_{cyt} signaling by treatment with neomycin. Representative MLO-Y4 cells stained with the Fluo-8 Ca^{2+}_{cyt} indicator and exposed to steady flow at t=60s under (A) control conditions or (B) with 15mM neomycin treatment for 15 minutes prior to flow. The drug was also included in the flow medium. The normalized intensity for 4 representative cells is

shown on the right. (C) Percent of cell exhibiting at least one Ca^{2+}_{cyt} transient following flow onset. (D) Average number of Ca^{2+}_{cyt} transients per cell in responsive cells. Error bars are standard deviations. Student's t-test was used to assess differences between the two groups. *$p<0.05$

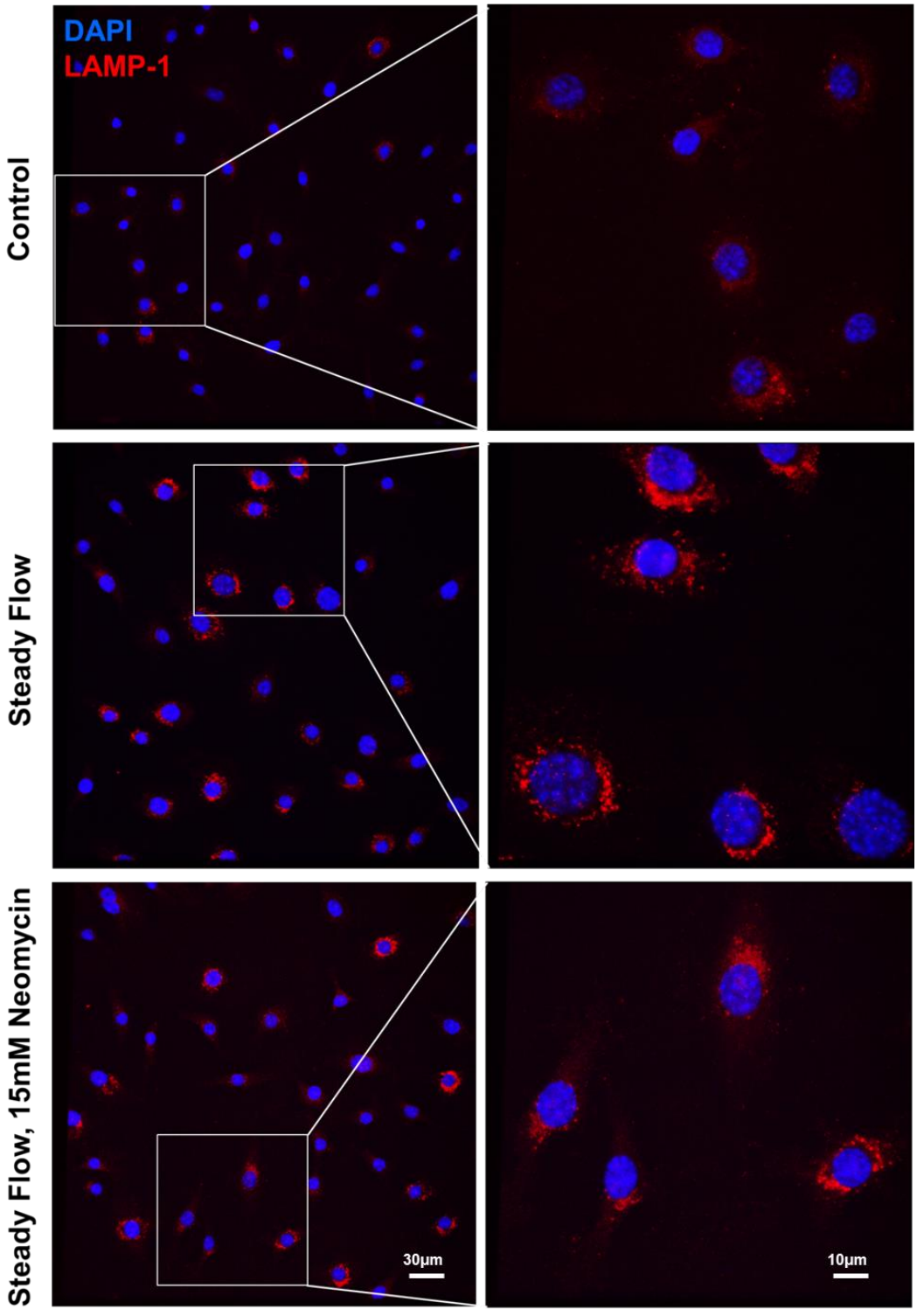

Figure 4.5. LAMP1 immostaining in MLO-Y4 cells exposed to fluid shear. MLO-Y4 cells were fixed immediately following the experiment and immunostained for LAMP1 expression

with a secondary antibody conjugated to AlexaFluor-594. Nuclei were indicated with a DAPI counterstain. Representative 20X (left panel) and higher magnification 60X (insets, right panel) images were taken for each group.

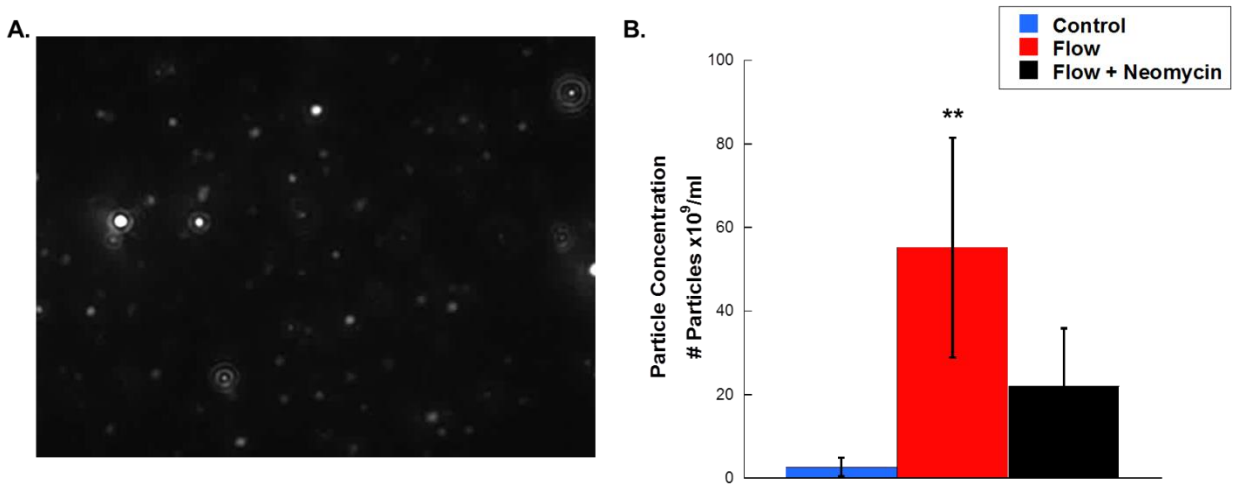

Figure 4.6. Flow-induced extracellular vesicle release. Nanoparticle tracking analysis was used to determine the concentration of particles in samples prepared by differential ultracentrifugation. (A) Representative frame of particles in a sample exposed to fluid flow. (B) Particle concentration. One-way ANOVA with Dunnett's post hoc was used to assess differences among groups compared to control samples. Error bars are standard deviations. **$p<0.01$

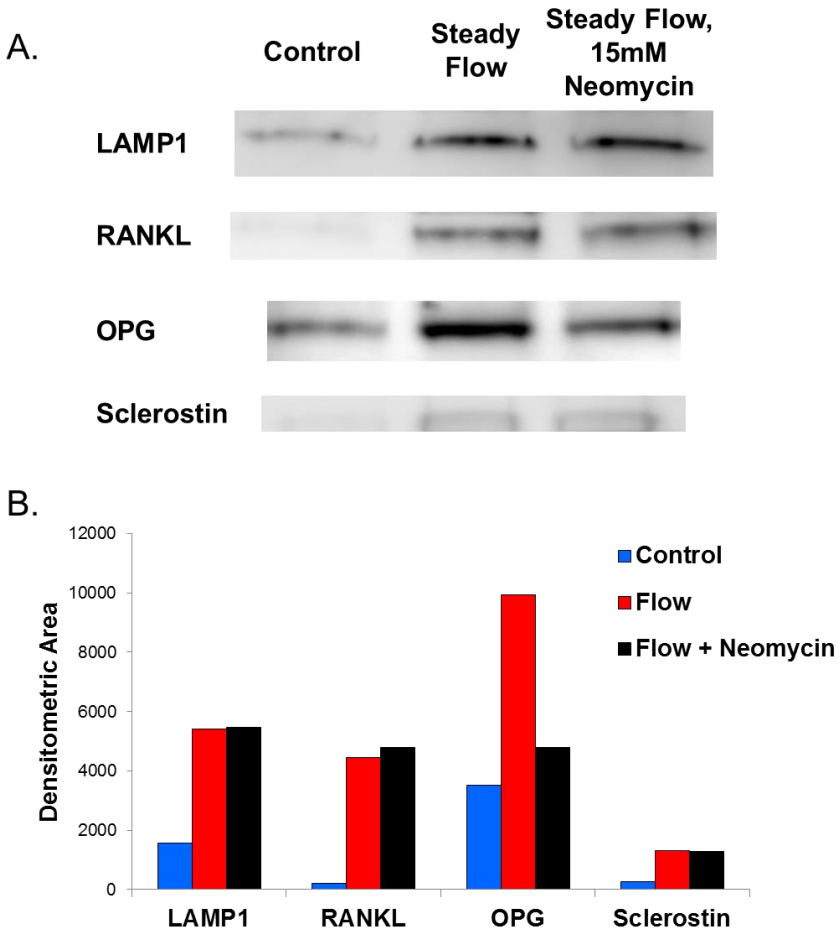

Figure 4.7. Immuno-detection of extracellular vesicle contents. (A) Vesicles fractions were isolated by differential ultracentrifugation and resuspended in lysis buffer to extract protein for Western blots. The proteins examined included the vesicle marker LAMP1 and the bone regulatory proteins RANKL, OPG, and slerostin. (B) Quantification of detected bands for each protein.

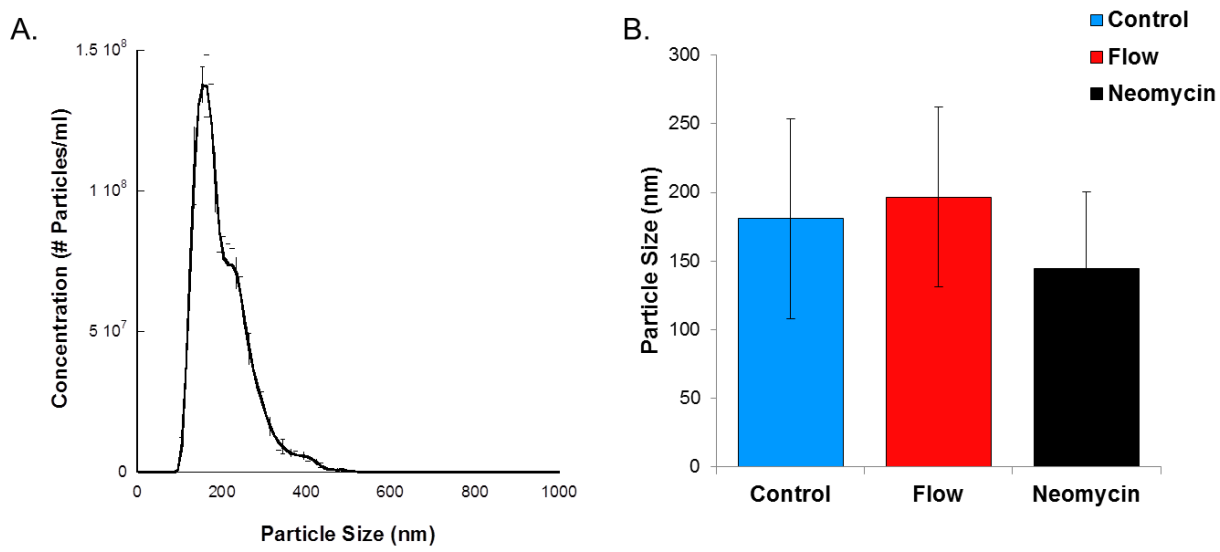

Figure 4.8. Size distribution of osteocyte-derived extracellular vesicles. (A) Representative distribution of particle size for a sample of vesicles isolated from cells exposed to flow. (B) Average particle size for each group. Error bars are standard deviations. Differences were evaluated by one-way ANOVA with Dunnett's post hoc. No differences were detected among groups.

Chapter 5

Validation of Ca^{2+} signaling patterns in the Ocy454 and IDG-SW3 cell lines

5.1 Introduction

Osteocytes are abundant cells buried within the bone with an essential role in maintaining skeletal health[11]. They are widely regarded as mechanosensors and are considered the primary source of sclerostin and receptor activator of nuclear factor κB ligand (RANKL), which control osteoblast and osteoclast activities, respectively. However, the mechanisms underlying osteocyte control of bone adaptation are not completely clear, limiting our ability to effectively treat diseases underpinned by reduced sensitivity, such as osteoporosis.

Due to the nature of their location in the bone, osteocytes are difficult to study. Isolation of primary cells requires intensive digestion treatments to extract cells from the bone matrix[166], resulting in low yields. However, a few studies using primary osteocytes have considerably furthered our understanding of how osteocyte responses to mechanical loading can regulate osteoblast and osteoclast activities. In studies subjecting primary chick osteocytes to pulsatile fluid flow (PFF), conditioned medium was shown to inhibit osteoblast proliferation, promote osteoblast differentiation, upregulate the expression of Wnt proteins, and inhibit osteoclast formation and resorptive capacity[32,35,36]. In a study by the same group on primary human osteocytes, conditions of inflammation such as rheumatoid arthritis were shown to upregulate the ratio of RANKL and its decoy receptor, osteoprotegerin (OPG), and PFF reduced the ratio back to control levels[167]. The introduction of the MLO-Y4 osteocyte-like cell line in 1997 revolutionized the study of osteocytes, making it feasible to study the biology of this important cell type *in vitro* and the regulation of key osteocyte proteins by mechanical load. For instance,

exposure to oscillatory fluid flow was found to reduce the ability of osteocytes to support osteoclastogenesis by decreasing the ratio of RANKL to OPG mRNA[33,34,168], and PFF had similar effects[169]. In another study using low-magnitude, high-frequency vibration, RANKL protein expression was decreased as well, though very early, suggesting to the authors that loading likely inhibited RANKL release from the membrane rather than new protein synthesis[170].

Indeed, our laboratory recently discovered that load-induced Ca^{2+}_{cyt} oscillations and actomyosin contractions in osteocytes facilitate the release of extracellular vesicles (EVs) containing bone regulatory proteins. In addition to RANKL and OPG, we detected sclerostin in these MLO-Y4-derived EVs. However, MLO-Y4 cells historically express low levels of sclerostin, limiting the ability to study the mechanical regulation of this important protein. A better understanding of sclerostin expression by mechanical load is needed. Previous in vivo studies have shown mechanical loading downregulates (and unloading upregulates) expression of sclerostin, and that this down-regulation is required for bone formation responses to loading[40,41,75]. However, recent studies indicate that sclerostin knockout mice still respond to anabolic loading in vivo[42], and wild-type animals treated with anti-sclerostin antibody can still sense disuse environments[43,75]. Thus, there is conflicting evidence regarding whether sclerostin is important in bone mechanoregulation.

Two new osteocyte cell lines have been established recently to address the lack of sclerostin expression in MLO-Y4 (Figure 5.1). The Ocy454 cell line exhibits a mature osteocyte phenotype, characterized by high levels of DMP1 and sclerostin relative to MLO-Y4 cells[75]. Furthermore, sclerostin expression is modulated by both mechanical and hormonal stimulation in these cells, with microgravity inducing increases in both sclerostin and RANKL expression in mature Ocy454, and parathyroid hormone (PTH) and prostaglandin E_2 (PGE_2) suppressing

sclerostin levels upstream of these mechanical responses. The cell line IDG-SW3 exhibits a late-osteoblast phenotype capable of differentiating into a mature osteocyte phenotype in osteogenic conditions[74]. Over time, IDG-SW3 cells decrease the expression of alkaline phosphatase, turn on expression of early osteocyte markers such as E11, and gradually increase the expression of DMP1, sclerostin, and FGF23. This cell line is therefore a useful system for studying phenotypic differences between these two cell types. Both cell lines provide new models for studying the mechanical regulation of sclerostin and opportunities to overcome limitations of MLO-Y4 cells.

As our laboratory is interested in connecting Ca^{2+}-mediated mechanosensitivity to downstream protein responses in osteocytes, we sought to characterize the Ca^{2+} signaling patterns in immature and mature Ocy454 and early- and late-stage IDG-SW3 to determine if they resemble the previously characterized patterns observed in MC3T3-E1 and MLO-Y4 cells, respectively[65]. Given the consistency among our prior *in vitro* and *ex vivo*[68] studies, we hypothesized mature osteocytes would exhibit oscillations in Ca^{2+}_{cyt} in response to fluid shear, while immature cells would be less sensitive.

5.2 Methods

5.2.1 Cell culture and differentiation

Ocy454 cells were allowed to proliferate at 33°C in minimum essential alpha medium (α-MEM, Life Technologies, Carlsbad, CA) supplemented with 10% fetal bovine serum (FBS, Gibco, Life Technologies) and 1X antibiotic/antimycotic (Anti-Anti, Life Technologies) on 0.15mg/ml collagen-coated tissue culture dishes (rat-tail type I, BD Biosciences, San Jose, CA). Upon confluence, cells were transferred to 37°C to differentiate. Cells were cultured for an additional 14 days with routine medium changes.

IDG-SW3 cells were allowed to proliferate at 33°C in α-MEM with 10% FBS containing recombinant mouse interferon-γ (IFN-γ, Life Technologies, Carlsbad, CA) on collagen-coated dishes. Confluent IDG-SW3 were then transferred to 37°C with medium without IFN-γ and supplemented with 50μg/mL ascorbic acid and 4mM β-glycerophosphate to induce differentiation. Cells were grown for 21 days under these conditions.

MLO-Y4 cells were cultured to confluence in α-MEM with 5% FBS (Hyclone Laboratories, Inc., Logan, UT) and 5% calf serum (Life Technologies).

5.2.2 Ca^{2+} indicators

To observe Ca^{2+}_{cyt} changes in Ocy454 cells, plated cells were stained with Fluo-8 AM (AAT Bioquest, Sunnyvale, CA) dissolved in 20% Pluronic F-127 in DMSO (Invitrogen, Carlsbad, CA). Fluo-8 was excited at 488nm, and fluorescence emission was collected at 527nm. IDG-SW3 cells were stained with the red-shifted Ca^{2+}_{cyt} indicator Fura Red-AM (20μM, Life Technologies, Carlsbad, CA) in DMSO and Kolliphor® EL (Sigma-Aldrich, St. Louis, MO) prior to fluid flow stimulation. Fura-Red was excited at 430nm, and fluorescence emission was collected at 641nm, resulting in increases in Fura-Red emission upon Ca^{2+} binding. Ca^{2+}_{cyt} transients were defined by increases in intensity at least 4 times the magnitude of noise prior to flow onset.

5.2.3 Fluid flow stimulation

Differentiated cells were digested by serial collagenase (200 U/ml, Gibco, Life Technologies, Carlsbad, CA) treatments and trypsin-EDTA (0.05%, Life Technologies) and re-plated onto collagen-coated glass slides in antibiotic-free medium. Immature cells were

subcultured onto glass slides using trypsin-EDTA dissociation. Cells were stained with the appropriate Ca^{2+} indicators and then assembled into a custom parallel-plate fluid flow chamber. Cells were exposed to laminar, unidirectional steady flow at 35 dynes/cm^2 using a magnetic gear pump (Ismatec, Cole-Parmer, Vernon Hills, IL). Baseline fluorescence intensity was captured for 1 minute prior to fluid shear stimulation for 9 minutes.

To evaluate the influence of fluid shear on sclerostin expression, cells were exposed to fluid shear at 35 dynes/cm^2 for two 10-minute bouts of steady flow separated by a 15 minute rest period. Slides were post-incubated in flow-conditioned medium for 24 hours, and total protein was extracted. To investigate the role of flow-induced Ca^{2+}_{cyt} oscillations in these responses, an additional group was treated with 15mM neomycin (Sigma Aldrich, St. Louis, MO), which we have shown in earlier studies to impair Ca^{2+} responsiveness.

5.2.4 Immuno-detection

Immediately following flow exposure, cells were fixed and permeabilized in ice-cold acetone. Cells were probed for the expression of sclerostin using standard immunocytochemistry techniques. Briefly, cells were blocked in 2.5% normal horse serum and incubated overnight with a goat polyclonal antibody to sclerostin (AF-1589, R&D Systems, Minneapolis, MN). The VectaFluor Detection system with DyLight 594 Anti-goat Ig reagent (Vector Laboratories, Burlingame, CA) was used to probe the antibody for sclerostin.

Cellular expression of sclerostin was assessed by Western blot. Protein lysates were prepared by lysing 100mm dishes of confluent cells in RIPA lysis and extraction buffer supplemented with protease and phosphatase inhibitors (ThermoScientific, Waltham, MA) for 30 mins. Protein lysates were mixed 1:1 with 2X Laemmli buffer (Sigma Aldrich, St. Louis, MO)

and boiled for 5 minutes at 95°C. Protein samples were separated by gel electrophoresis using pre-cast polyacrylamide gels and a Mini-PROTEAN electrophoresis chamber (Biorad, Hercules, CA). Proteins were transferred to a PVDF membrane (Biorad) by wet transfer. Membranes were blocked with 5% BSA (Sigma Aldrich), and incubation with the primary anti-sclerostin antibody was performed overnight at 4°C. Membranes were rinsed well with TBST (Biorad) and then probed with a rabbit anti-goat IgG secondary antibody (Abcam, Cambridge, MA). Detection was performed using the SuperSignal West Femto chemiluminescence detection kit (Thermo Scientific) and a FujiFilm LAS-4000 Luminescent Image Analyzer (FujiFilm, Stamford, CT). Proteins were verified by band size using a molecular weight ladder (Biorad) and specificity using concurrent negative controls.

5.2.5 Statistics

Differences in the number of Ca^{2+}_{cyt} peaks between mature and immature cells were evaluated with student's t-tests. Significance was detected at $p<0.05$.

5.3 Results

5.3.1 Ocy454 differentiation

The differentiation of Ocy454 cells was verified by monitoring DMP1-GFP expression. Few cells exhibited DMP1-GFP expression at 33°C, even after 14 days post-confluence. At 37°C, Ocy454 cells exhibited considerable DMP1-GFP expression by Day 12 (Figure 5.2).

We also evaluated sclerostin expression in these cells. Sclerostin was not detected in immature (undifferentiated) Ocy454 cells, while mature (differentiated for 14 days) cells showed strong immunoreactivity between 20 and 30 kDa (Figure 5.3A). In addition, sclerostin

expression was stronger in Ocy454 cells than in protein extracted from MLO-Y4 (Figure 5.3B). Negative controls without primary antibody verified antibody specificity (Figure 5.3C).

5.3.2 Ca^{2+}_{cyt} signaling in the Ocy454 cell line

Due to the moderate GFP expression in these cells, cells were stained with the Fluo-8 Ca^{2+}_{cyt} indicator to evaluate Ca^{2+} responses to fluid flow (Figure 5.4). Representative traces of 3 cells are shown in Figure 5.4.

Approximately 50% of immature cells responded to fluid shear with at least one Ca^{2+}_{cyt} transient, and on average cells exhibited 1 or 2 Ca^{2+}_{cyt} peaks (n=126 cells, 7 slides; Figure 5.5). Mature cells were more responsive, with more than 75% of cells responding to flow (n=442 cells, 5 slides; Figure 5.5A). The average number of Ca^{2+}_{cyt} transients in mature Ocy454 cells was nearly 4 peaks, though some cells exhibited up to 19 Ca^{2+} transients in a single stimulation period (Figure 5.5B).

5.3.3 Influence of Ca^{2+} signaling on slerostin changes in response to fluid shear

We next sought to determine whether these flow-induced Ca^{2+}_{cyt} oscillations were critical for downstream regulation of sclerostin by mechanical stimulation. Mature Ocy454 cells exhibited strong sclerostin expression, while sclerostin was no longer detectable in cells exposed to fluid shear (Figure 5.6). Sclerostin was also down-regulated to undetectable levels in neomycin-treated cells.

5.3.4 Ca^{2+}_{cyt} signaling in the IDG-SW3 cell line

After 21 days in culture, IDG-SW3 cells exhibited strong expression of DMP1-GFP (Figure 5.7A). Cells were stained with the Fura-Red Ca^{2+}_{cyt} indicator to characterize Ca2+ responses (Figure 5.7B). Representative time courses of the Ca^{2+}_{cyt} responses of these cells are shown in Figure 5.8. Undifferentiated IDG-SW3, which represent a late-osteoblast, exhibited a strong peak after the onset of flow, with a few subsequent smaller responses. Day 21 IDG-SW3, which represent an osteocyte, exhibited Ca^{2+}_{cyt} oscillations in response to flow.

5.4 Discussion

In this study, we demonstrated that mature Ocy454 and IDG-SW3 cells are more responsive to fluid shear than their immature counterparts, with a higher percentage of responsive cells and higher average number of Ca^{2+}_{cyt} transients. These results are consistent with previous data using the MLO-Y4 and MC3T3-E1 cell lines as well as studies performed on explanted mice tibia from our laboratory. Taken together, these results suggest that these Ca^{2+}_{cyt} signaling patterns are inherent to osteocyte behavior.

We also showed that the Ocy454 cell line in particular is useful for studying mechanisms underlying sclerostin downregulation in response to levels of mechanical stimuli *in vitro* that can stimulate bone formation responses *in vivo*[68]. The only previous study using Ocy454 evaluated changes in sclerostin mRNA to very low levels of fluid shear (maximum 8 dynes/cm^2)[75]. Our results more closely mirror the dramatic decreases in sclerostin protein expression that others have shown in loaded limbs of mice by immunohistochemistry[40,41]. Interestingly, we found that inhibition of Ca^{2+}_{cyt} oscillations, i.e. inhibiting the osteocyte response closely linked to mechanosensing, has no influence on sclerostin downregulation. Therefore, sclerostin expression

itself may not be finely regulated by mechanical load, which would explain some of the discrepancies in knockout and sclerostin inhibited animals subjected to loading. Additional validation of the signaling patterns under various levels and profiles of fluid shear in these cells may clarify this behavior.

The limitations of this study are largely due to the limitations that exist in the culture of these cells. Mature cells of both cell lines were digested from their deposited matrix and replated for fluid shear stimulation. This was chosen to ensure accurate transmission of fluid shear to the cell monolayers; however, the procedure certainly influenced the morphology of the cells and modified their environment. Indeed, three-dimensional culture enhanced the osteocytic phenotype of Ocy454 cells in a previous study[75], so digestion would presumably influence the phenotype of the cells. However, the similarity to our characterization of mature cells across the cell lines and *ex vivo* suggests we are recapitulating a true osteocyte behavior. Another limitation lies in the detection of the sclerostin protein. The expected molecular weight of the sclerostin monomer is 23-28kDa, and we detected immuno-reactivity at a slightly lower molecular weight. Though we verified specificity with negative controls, we have no other explanation for this observation. A recent publication demonstrated that sclerostin can be expressed in multiple molecular weight forms corresponding to dimer and trimeric forms of the protein in addition to other bands, and a band was detected in bone cells at this molecular weight[171]. Future work will aim to clarify this observation by testing other antibody manufacturers and using blocking peptides.

5.5 Conclusion

In this study, we highlighted that load-induced Ca^{2+}_{cyt} oscillations are a hallmark of osteocyte mechanosensitivity by exploring the Ca^{2+} signaling patterns of two relatively new osteocyte cell lines. We also recapitulated the *in vivo* time course of sclerostin suppression by mechanical load in an *in vitro* system, providing a platform for future studies to explore finer aspects of osteocyte regulation of bone adaptation.

5.6 Figures

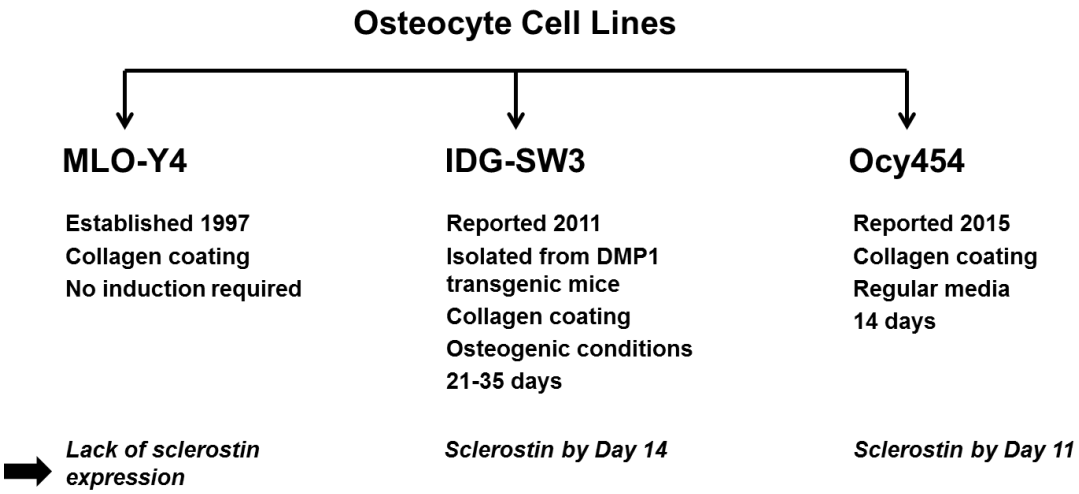

Figure 5.1 Summary of available osteocyte cell lines. Highlighted is the lack of sclerostin expression in the MLO-Y4 cells line, which is the most common cell line used for studying osteocyte mechanobiology.

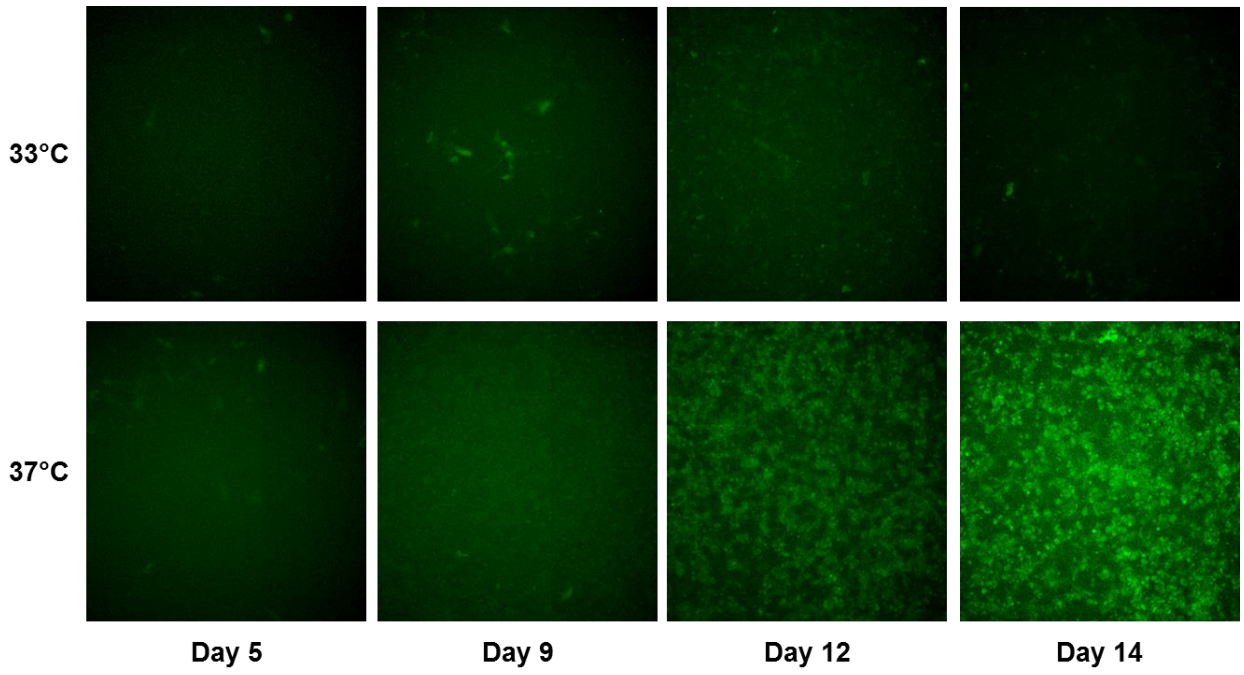

Figure 5.2. Ocy454 differentiation. Expression of GFP driven by the DMP1 promoter in Ocy454 cells grown at 33°C and 37°C for 5, 9, 12, and 14 days.

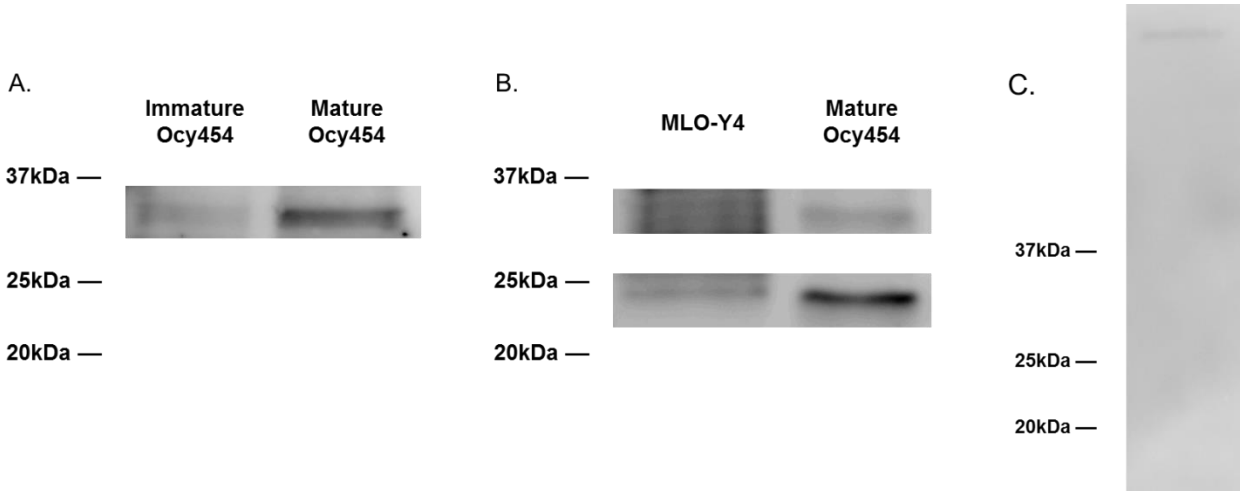

Figure 5.3. Immuno-detected of sclerostin protein. (A) Increase in sclerostin expression with differentiation of Ocy454 cells. (B) Sclerostin expression is more abundant in mature Ocy454 cells than in the MLO-Y4 cell line. (C) Negative control with no 1° antibody.

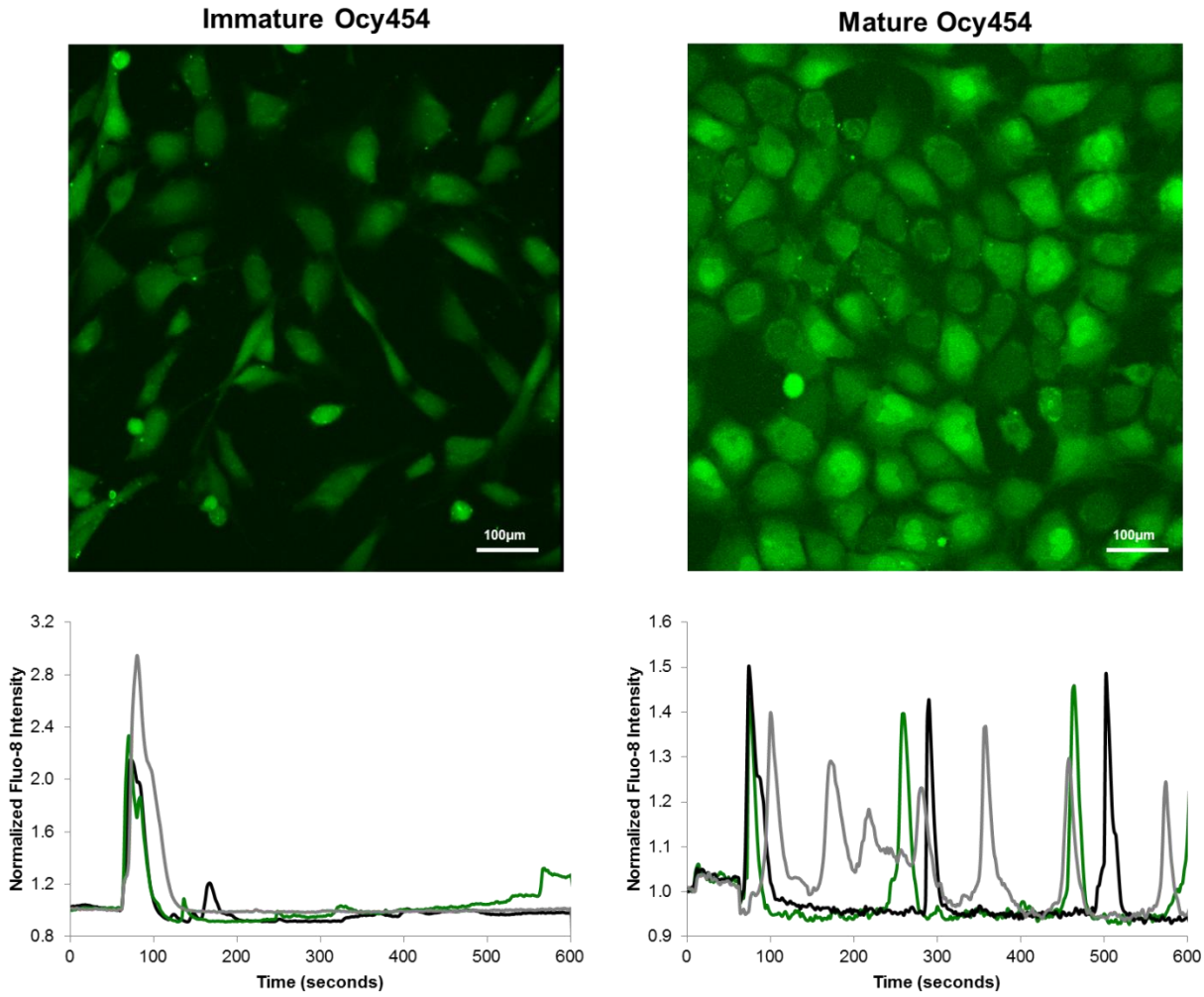

Figure 5.4. Ca^{2+}_{cyt} signaling in immature and mature Ocy454 cells. The top panel shows Fluo-8 staining in immature and mature Ocy454 cells under fluid shear stimulation. Representative time courses of Ca^{2+}_{cyt} responses in three cells from each group are shown below.

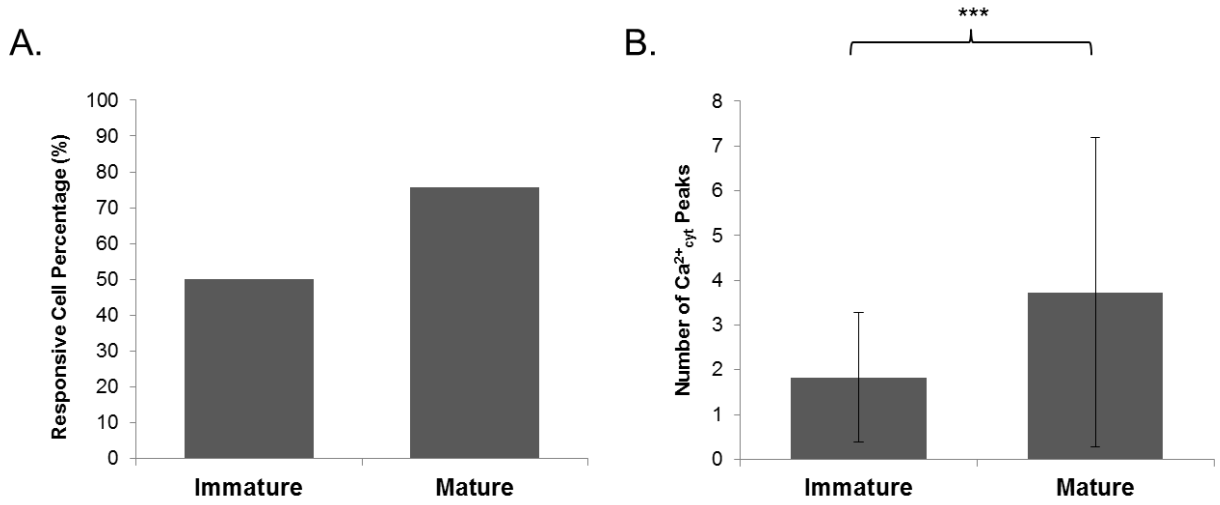

Figure 5.5. Quantification of differences in Ca^{2+} signaling behavior between immature and mature Ocy454 cells. (A) Responsive cell percentage. (B) The number of Ca^{2+}_{cyt} peaks following flow onset in responsive cells. Error bars are standard deviations. Differences were assessed by student's t-test. ***$p<0.001$

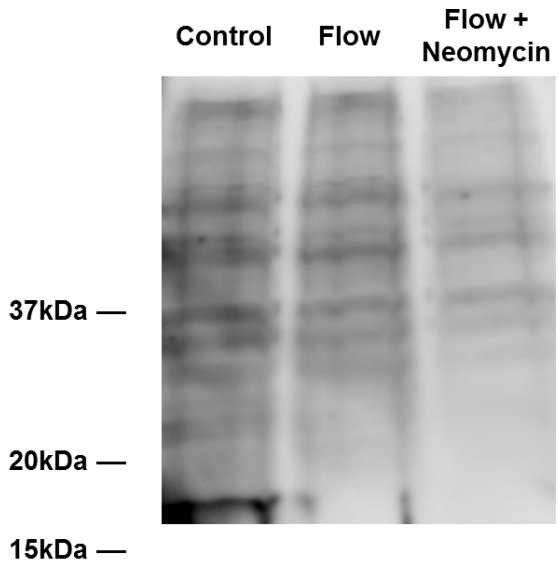

Figure 5.6. Regulation of sclerostin expression by mechanical loading and Ca^{2+}_{cyt} oscillations. Mature Ocy454 cells were exposed to fluid flow in the presence or absence of neomycin and compared with static controls. Whole cell protein was extracted and probed for sclerostin expression by Western blot.

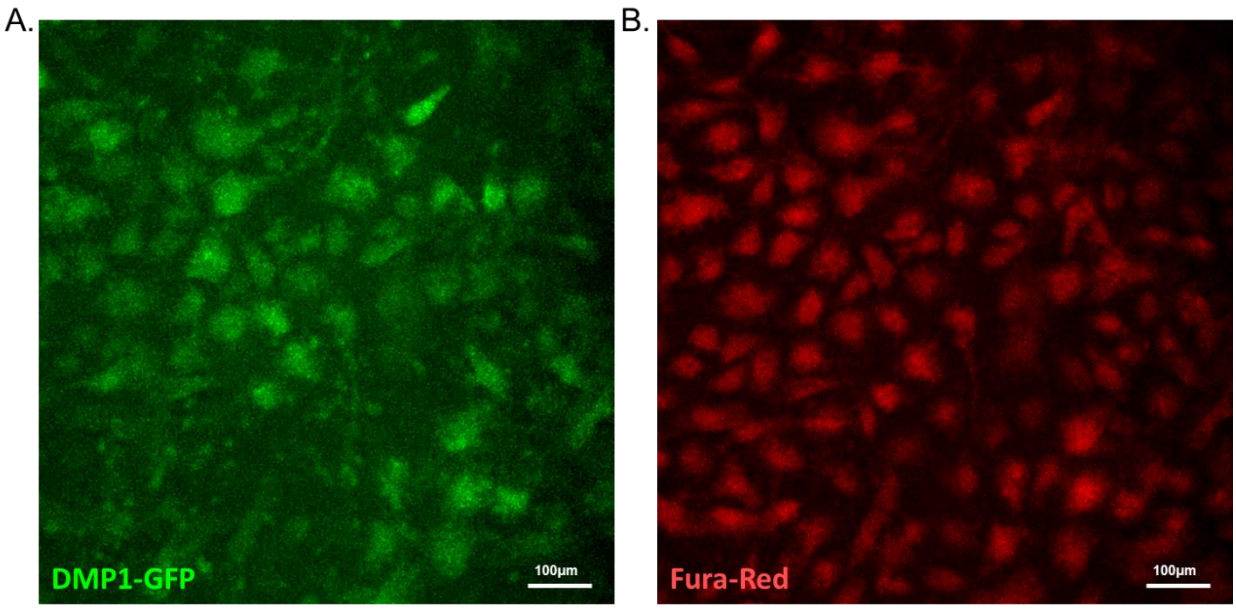

Figure 5.7. IDG-SW3 cell line. (A) After 21 days of differentiation under osteogenic conditions, cells express high levels of GFP driven under the DMP1 promoter. (B) Fura-Red staining in IDG-SW3 cells to indicate Ca^{2+}_{cyt}.

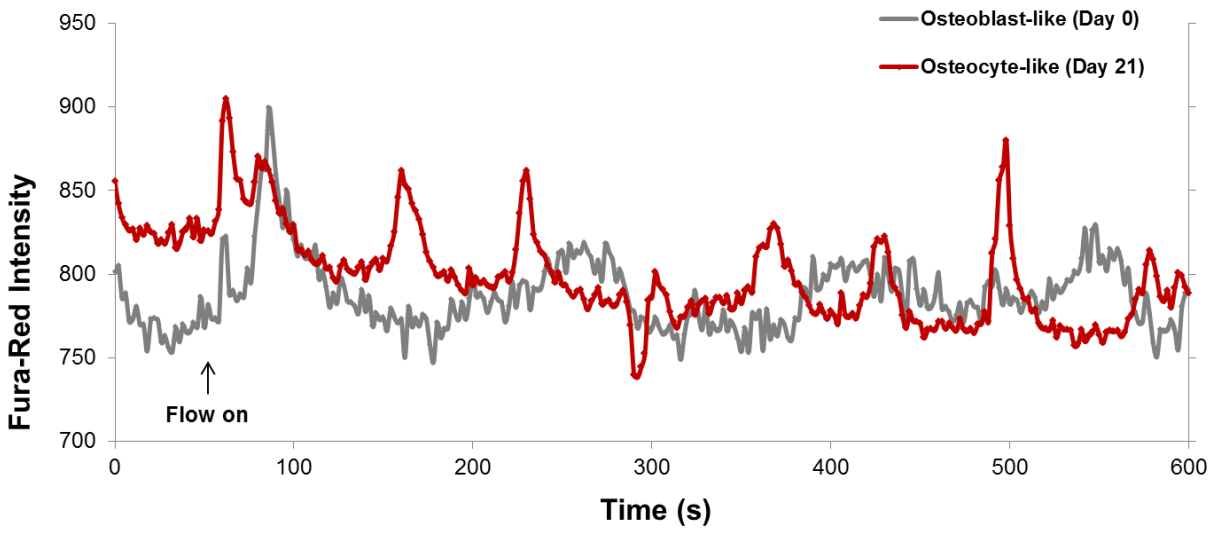

Figure 5.8. Ca^{2+} signaling patterns in early- (Day 0) and late- (Day 21) stage IDG-SW3 cells. Fura-Red staining was used to indicate Ca^{2+}_{cyt}, and plotting the Fura-Red intensity over time reveals transient Ca^{2+} activity.

Chapter 6

A Loadable Perfusion Bioreactor for the Long Term Culture of Bovine Bone Explants

This thesis chapter has been previously published, in part, in the manuscripts:

> *Silvia Marino, Katherine Ann Staines, Genevieve Brown, Rachel Anne Howard-Jones, and Magdalena Adamczyk. "Models of ex vivo explant cultures: applications in bone research." BoneKEy Reports 5, Article number 818, 2016.*

and

> *Genevieve N. Brown, Rachel L. Sattler, and X. Edward Guo. "Experimental studies of bone mechanoadaptation: bridging in vitro and in vivo studies with multiscale systems." Interface Focus 6, 2016.*

6.1 Introduction

The observation that bone can adapt its internal structure to the external mechanical demands placed upon it dates back to more than a hundred years ago[172]. Yet, a clear understanding of the mechanisms underlying mechanoadaptation remains unknown. This is in part due the complexity of studying a process involving numerous cell types interacting in a complex loading environment over varying time scales. Bone adaptation involves changes in bone structure and composition over weeks achieved through coordinated changes at sites of resorption, formation, and remodeling. It is thought that osteocytes – the mechanosensors in bone – direct these processes by regulating osteoclast and osteoblast activities[1]. However, in traditional *in vivo* or *in vitro* approaches, it can be difficult to marry the short-term sensing and longer-term responding timescales, and preserving the spatial relationship between bone cells is

challenging. The cellular network formed by osteocytes in the LCS integrates information from whole bone deformation at different locations in the organ, communicates biochemical responses to bone surfaces where effector cell populations reside, and coordinates the sites of bone formation and resorption responses to adapt the bone structure. Therefore, there exists a need for experimental systems that can couple early osteocyte network responses to mechanical loading to later tissue level changes.

The introduction of three-dimensional (3D) cell cultures has added some complexity to *in vitro* studies and has proven immensely valuable in unveiling cell behaviors that are intricately tied to the native morphology and parameters of the microenvironment[74,104,173-175]. However, the opposite approach – stripping down native tissues to fewer, more controllable features – has also provided unique platforms for connecting these scales. By nature of their source, major advantages of these *ex vivo* or explanted tissues are that they maintain native tissue architecture, cellular composition, and cell-cell arrangement. Thus, explants that can approximate this environment in a controlled experimental setting offer a unique opportunity to study the load-regulated processes in bone biology.

Few bone explant cultures have been established to investigate the adaptive response of bone tissue to mechanical cues, largely due to the requirement to sustain viability of the explanted tissue in culture over long enough periods. The introduction of the ZetOS bioreactor overcame these limitations by providing a system to simultaneously perfuse nutrients through trabecular bone explants and apply dynamic loading[176,177]. Bovine bone cores complete with surface cells and bone marrow were sustained for three weeks in culture, with osteocyte viability remaining above 60% and osteoblast/osteoclast populations responding to mechanical and chemical stimuli[178]. The application of simulated jumping strains resulted in increased bone

formation parameters in some samples, and most importantly, architectural changes in the trabecular bone tissue[178]. Furthermore, application of load resulted in changes in the apparent stiffness of the bone samples[179]. Similar results were reported in a rabbit trabecular bone explant model cultured in a perfusion/loading system, where mechanical loading resulted in new bone deposition demonstrated by osteoid formation and the presence of double fluorochrome labeled surfaces[180]. Comparable systems have been developed to sustain viability in whole bone organ cultures[181]. These improvements in culture conditions lay a strong foundation for using trabecular bone explants to study the mechanisms underlying mechanical adaptation.

A major advantage of transferring tissues to culture environments is the ability to adapt the tissue to remove confounding variables and isolate critical interactions. Our laboratory developed a trabecular bone explant model of osteocyte-osteoblast interactions to evaluate histological and mechanical property changes in response to loading that had been built on previous explants used for short term loading experiments[182-186]. In this system, bovine trabecular bone cores were thoroughly cleaned to remove bone marrow, disrupted nerves, and vasculature, as experimental studies have demonstrated an influence of these systems in bone. The explants were also treated to remove any surface cells, which have been shown to populate the bone surface after a few days in culture in an uncontrolled manner[187]. A controlled number of primary osteoblasts could then be seeded back onto the surface. The resulting explant provides a system in which osteocytes in their native environment can send signals to osteoblasts, and bone deposition and changes in mechanical properties can be measured in response to load. For instance, we demonstrated that dynamic deformational loading resulted in early biochemical responses, such as the release of PGE_2, as well as the deposition of osteoid and changes in

apparent elastic modulus of the explant after 4 weeks. Blocking the PGE_2 response abrogated the anabolic effects of loading[188].

In this earlier study, mechanical loading and tissue perfusion were applied by a custom loadable perfusion bioreactor based upon previously reported systems for bovine bone cores[176-179], and similar systems have been recently reported for rabbit trabecular bone explants and whole bone organ cultures[180,181]. However, these systems as well as those that are commercially available have several limitations. First, many loadable perfusion systems do not accommodate the culture of individual specimens, limiting the statistical methods that can be employed for evaluating multiple experimental conditions. Second, some of these systems cannot de-couple the effects of flow perfusion, which itself can be a mechanical stimulus to osteocytes, from the dynamic applied loads[189]. Though the ZetOS system addresses these limitations, the design necessitates stimulating bone under displacement control[178,179], which can result in inaccurate loading of trabecular bone due to the unsupported struts of the trabeculae along the cut explant boundaries. Indeed, in previous studies from this group, they found higher increases in stiffness in dead bone cores than living ones cultured in ZetOS bioreactors[189], suggesting to us that end-crushing is symptomatic in this design. Finally, though our early custom bioreactor attempted to overcome these limitations, too many manipulations to remove the bone for mechanical testing complicated the experimental setup, increasing risks of contamination throughout the long culture period.

Therefore, the goal of this study was to design an easy-to-use loadable perfusion bioreactor for individual bovine trabecular bone explants to maintain cell viability over long culture periods and permit routine mechanical stimulation and testing of specimens.

6.2 Methods

6.2.1 Explant and cell culture reagents

Explants and primary osteoblasts were cultured in minimum essential alpha medium (α-MEM, Life Technologies, Carlsbad, CA) supplemented with 10% fetal bovine serum (FBS, Hyclone Laboratories, Inc., Logan, UT) and antibiotics (100 U/ml penicillin, 100 µg/ml streptomycin, Life Technologies). Cells were maintained at 5% CO_2 and 37°C in a humidified incubator.

6.2.2 Obtaining bovine trabecular bone cores

Bovine wrists with intact carpal-metacarpal joint capsules from 6 week old calves were obtained from a local slaughterhouse shipped overnight on ice. The hoof was removed at the fetlock joint along with tendons along the shaft of the metacarpus. Joints were sterilized in diluted Roccal-D Plus (Zoetis, Florham Park, NJ) for 30 minutes and 70% ethanol for an

The flat articular surface of the metacarpus was exposed and cleaned of synovial fluid using gauze soaked in 70% ethanol, and the carpal bone was secured into a vise. Using a diamond-tipped coring tool (Starlite Industries, Rosemont, PA) and a hand drill, 7-mm diameter bone cores were drilled from the articular surface through to the medullary cavity with constant PBS irrigation. Bone cores were transferred to petri dishes with pre-warmed, fully supplemented media.

6.2.3 Preparing individual bone explants

Trabecular bone cores were lightly cleaned with PBS jet rinsing (Interplak water jet, Conair, Stamford, CT) and then cut to the appropriate size (7-mm height) using a IsoMet low

speed saw with high carbon (HC) wafering blade (Buehler, Lake Bluff, IL) (Figure 6.1). The individual bone explants were then thoroughly cleaned using repeated PBS rinses and 0.25% trypsin-EDTA (Gibco, Life Technologies, Grand Island, NY) treatments to remove marrow components, damaged vasculature and nerves, and any surface cells. The remaining cells are osteocytes embedded within the bone matrix. This procedure results in thorough cleaning such that few resident surface cells repopulate the bone, even after weeks in culture (Figure 6.2).

6.2.4 Obtaining primary osteoblasts by explant outgrowth

The "excess" bone cores pieces from trimming the cores were thoroughly rinsed with PBS, cut into 2-3 mm bone chips, and transferred to tissue culture dishes with pre-warmed, fully-supplemented media. The bone chips were kept at 37°C and 5% CO_2 to allow for outgrowth of primary cells. The second population of cells migrating from the chips was considered a more homogeneous population of osteoblasts. Upon confluence, cells were switched to osteogenic media supplemented with 10 mM β-glycerophosphate and 50 μg/ml ascorbic acid (Sigma Aldrich, St. Louis, MO).

6.2.5 Seeding primary osteoblasts onto explants

The primary osteoblasts isolated by explant outgrowth were used to seed a controlled number of cells back onto the bone cores at a concentration of 2.5×10^5 cells/explant in fully-supplemented media using a custom cell-seeder with slow stirring for 1 hour. Explants were then transferred to 6-well plates prior to assembling into bioreactors. Seeding of bone cores with primary osteoblasts results in uniform distribution of cells, which gradually populate the bone surface (Figure 6.3).

6.2.6 Loadable perfusion bioreactor

To sustain the viability of osteocytes in culture periods long enough to observe changes in bone formation and elastic modulus in response to mechanical loading, we designed a loadable perfusion bioreactor. The design consisted of a polyetherimide perfusion base and cap with a 316L stainless steel piston to transmit load (Zero Hour Parts, Ann Arbor, MI). A compression spring with threaded button and retractable stainless steel plungers were used to easily lock the positions of the piston and cap (McMaster-Carr, Elmhurst, IL). Silicon O-rings were used to create a tight seal for perfusion (McMaster-Carr). Ceramic discs custom-cut from 4-bore ceramic tubes (McMaster-Carr) were used to provide an even surface for loading the bone cores through which fluid could perfuse. All stainless steel components were passivated with 10% w/v citric acid for 30 minutes at 65°C.

Low-level perfusion at 0.01 ml/min was driven by a multichannel peristaltic pump (Ismatec, Cole-Parmer, Vernon Hills, IL) to supply the bone tissue with nutrients and enhance waste exchange to keep osteocytes embedded within the bone alive[190]. Tubing was connected between the pump, reservoir, and bioreactor by luer adapters (Cole-Parmer). The bioreactor was coupled to a mechanical testing (Bose Electroforce, Bose, Eden Prairie, MN) for mechanical interventions and testing of mechanical properties. The average of 5 separate measurements of height and diameter were used to determine the geometric properties of the explant. On Day 0, the apparent elastic modulus was determined for each specimen from the slope of the stress-strain curve constructed from the last 5 loading cycles of a 20 second 1Hz sinusoidal bout of loading from -5 to -10N. From this information, the load necessary to apply a stimulus of 2400 microstrain (με) was calculated. Subsequently, samples were subjected to daily loading with a

1Hz sinusoidal compressive waveform from a pre-load of -2N to the determined load. On the final day of experimentation, the apparent elastic modulus of each specimen was determined again.

6.2.7 Validation of mechanical testing in the bioreactor

Solid ultra-high molecular weight polyethylene (UHMWPE) cylinders were machined to the size of the explants (7 mm diameter, 7 mm height) and used as standard materials to evaluate mechanical testing in the bioreactor, as the moduli is comparable to that of trabecular bone. Apparent elastic moduli were determined in three different configurations: a standard unconfined compression test between two stainless steel platens, a compression test between the load piston with the sample in the bioreactor base, and an additional compression test with the bioreactor cap attached to the loading piston (the intended configuration for using the bioreactor). To correct for compliance of the polyetherimide base (C_{base}), an adjusted displacement for the sample was calculated by:

$$\delta_{explant} = \delta_{total} - F \times C_{base}$$

C_{base} was calculated as the inverse of stiffness determined from the slope of the force-displacement curve for the base only (average of 5 independent tests). In each configuration, 5 UHMWPE samples were tested.

To evaluate whether mechanical testing, routine loading, and long term culture caused artificial increases in apparent moduli of bovine bone cores throughout the duration of the experiment, we loaded devitalized bone cores for 1, 3, 5, and 10 days and compared the percent difference in apparent elastic modulus after 4 weeks in culture to non-loaded explants and tissue culture controls. Bone cores were harvested as described and then devitalized by repeated freeze-

thawing. Loads corresponding to 2400με were determined for each sample to apply dynamic loading of similar strains across all groups.

6.2.8 Analysis of osteocyte viability

Explants were cut vertically in half using the Isomet saw prior and stained with Molecular Probes LIVE/DEAD Viability/Cytotoxicity kit (Invitrogen, Carlsbad, CA) to evaluate cell viability. Explants were imaged by confocal microscopy (Olympus FV1000, Olympus, Waltham, MA) ~100μm into the bone tissue.

Traditional histological techniques were also used to complement staining in living explants. The other half of the explants were fixed in neutral buffered formalin (Fisher Scientific, Hampton, NH), embedded in paraffin, sectioned at 8μm thickness, and stained with hematoxylin and eosin (H&E) to evaluate cell viability by morphology. Empty lacunae or shriveled cell nuclei were used to discern dead osteocytes. The number of live osteocytes were counted and normalized to bone area. Counts were performed on non-consecutive sections by three independent blinded observers.

6.2.9 Statistics

One-way ANOVA with appropriate post-hoc analyses were used to evaluate differences across groups. For differences among configurations and the percent change in moduli of devitalized explants, Bonferroni's post hoc analysis was used to compare all pairs. For osteocyte viability, Dunnett's post hoc was performed using the initial group as the control. Significance was detected at $p<0.05$.

6.3 Results

6.3.1 Design of a loadable perfusion bioreactor for individual bovine trabecular bone explants

The exploded and assembly views for the bioreactor design are shown in Figure 6.4. Perfusion is achieved in a bottom-up approach through an inlet in the bioreactor base and an outlet in the loading piston. Silicon O-rings and ceramic discs sit above and below the trabecular bone explant in the base, guiding fluid to perfuse through and not around the bone tissue. Another O-ring serves as a secondary seal between the base and the cap, preventing leaks and avenues for infection. The stainless steel loading piston secures the bone core throughout culture. The threads of the piston are engaged by a button with compression spring to lock the piston into position. For ease of use for mechanical testing, this button can release the threads to allow the piston to come off the bone core. Furthermore, the quick-locking plunger screws allow the cap to be released from the base and moved up along the piston away from the sample. In this configuration, mechanical testing can be performed. The entire assembly, with a single bioreactor connected to the perfusion pump and mechanical testing device, is shown in Figure 6.5.

6.3.2 Validation of frictionless loading and accurate mechanical testing

We first sought to validate that dynamic deformational loads could be delivered to bone explants in this device in a frictionless manner. This is evidenced by smooth load and displacement curves from a representative mechanical test of a trabecular bone explant (Figure 6.6).

We next wanted to verify the accuracy of mechanical testing in this device by comparing mechanical testing results from different configurations on samples of a standard material

(Figure 6.7). Correction for the compliance of the plastic base resulted in no differences in apparent elastic moduli determined between a standard unconfined compression test and one performed in the bioreactor.

Finally, we wanted to ensure that mechanical testing, routine loading, and long term culture did not result in significant artificial increases in apparent moduli of bovine bone cores throughout the duration of the experiment. We loaded devitalized bone cores for 1, 3, 5, and 10 days and compared the percent difference in apparent elastic modulus after 4 weeks in culture to non-loaded explants and tissue culture controls. No differences were detected among groups, and average percent changes were below ±10% for all groups (Figure 6.8).

6.3.3 Confirmation of osteocyte viability over extended culture

We also sought to confirm perfusion could maintain osteocyte viability in culture. After 2 weeks, live osteoblasts appear confluent along the bone surface (Figure 6.9A, B), and beneath this surface layer, live osteocytes can be identified (Figure 6.9C). Static cultures, in comparison, show a number of dead osteocytes (Figure 6.9D). Histological assessment revealed osteocyte viability is maintained in perfused cultures for up to 4 weeks, whereas viability is compromised in static conditions (Figure 6.10).

6.4 Discussion

We have described the design of a loadable perfusion bioreactor permitting the long term culture and characterization of trabecular bone explants capturing osteocyte-osteoblast interactions in response to mechanical load. The bioreactor design permits routine and accurate mechanical testing, precise mechanical interventions, and perfusion to sustain cell viability for at

least the 4 weeks examined in this study. This system sets the stage for studies aimed at determining the role of osteocytes in sensing mechanical loads and coordinating bone adaptation to those loads. As an example, osteocytes embedded within trabecular bone explants have been shown to elicit Ca^{2+} responses (Figure 6.11), which we have shown *in vitro* to be a critical mechanical response to applied loads that modulates the production of bone regulatory proteins. Future studies could explore the role of Ca^{2+} signaling in regulating the expression of proteins involved in osteocyte control of osteoblast activity to better understand how bone formation is initiated.

This bioreactor design overcomes a number of limitations in similar available or previously described systems. Foremost is the ability to evaluate individual specimens for biochemical characterization and study endpoints. Additionally, loading of individual specimens under load control permits the application of similar strains across all samples, similar to strain-matching that is done for *in vivo* experiments.

While powerful as a model system, limitations exist. The added challenge of keeping osteocytes viable makes decoupling the long term effects of loading versus transport difficult. Additionally, while native arrangement of the osteocytes and connection with surface cells is achieved with the explant, the bone core size and shape do not capture the whole bone response to mechanical loading as faithfully as would a whole bone explant, models of which exist, but for shorter term experimentation. Additional limitations relate to the chosen cell types. For instance, both osteocytes and osteoblasts are capable of releasing PGE_2 in response to mechanical stimulation, so it is unclear from our earlier study if this response was mediated primarily through osteocyte mechanosensing. A critical advantage of this explant system, however, is the ability to selectively manipulate the osteoblast population to disrupt signaling pathways in

osteoblasts only, a condition that cannot be created by *in vivo* studies. Finally, the removal of all cell types except osteocytes and the seeded cell type of interest may obscure the essential interactions of other native cells in the adaptive process. Despite these limitations, explanted trabecular bone cultures can be used to probe outcomes of mechanical loading at very different time points with a simplified cell composition in a still intricate arrangement.

6.5 Conclusion

We designed an easy-to-use loadable perfusion bioreactor for trabecular bone explants to capture long-term tissue-level changes in response to mechanical loads mediated by osteocytes. This system enables us to isolate interactions between osteocytes and osteoblasts in a controlled manner to delineate mechanisms underlying load-induced bone formation responses. This bioreactor can serve as a platform for future studies aimed at understanding mechanoadaptation in bone.

6.6 Figures

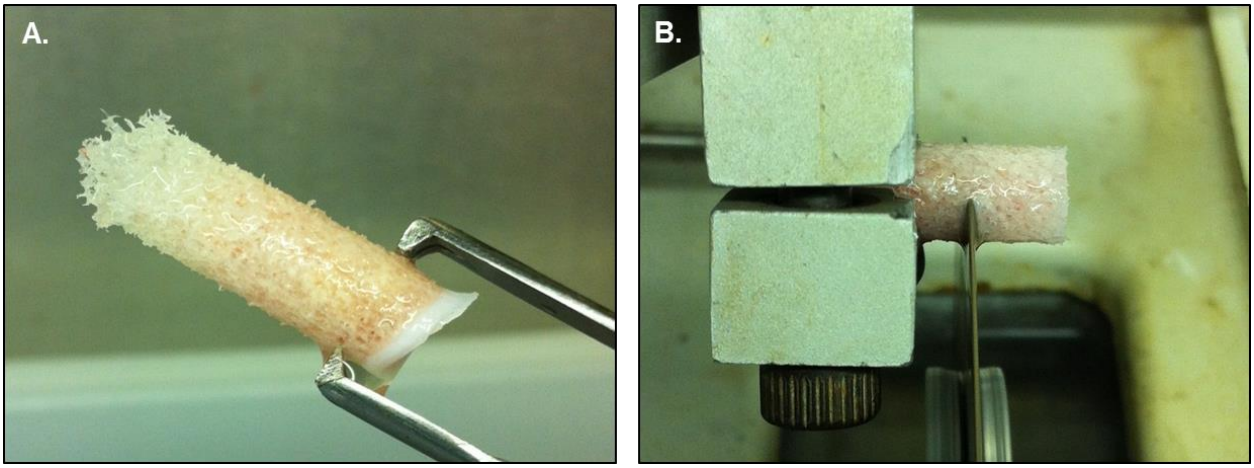

Figure 6.1. Trabecular bone explants. (A) Trabecular bone core drilled from a bovine metacarpus. (B) 7 mm trabecular bone explant cut from the bone core using a low speed saw.

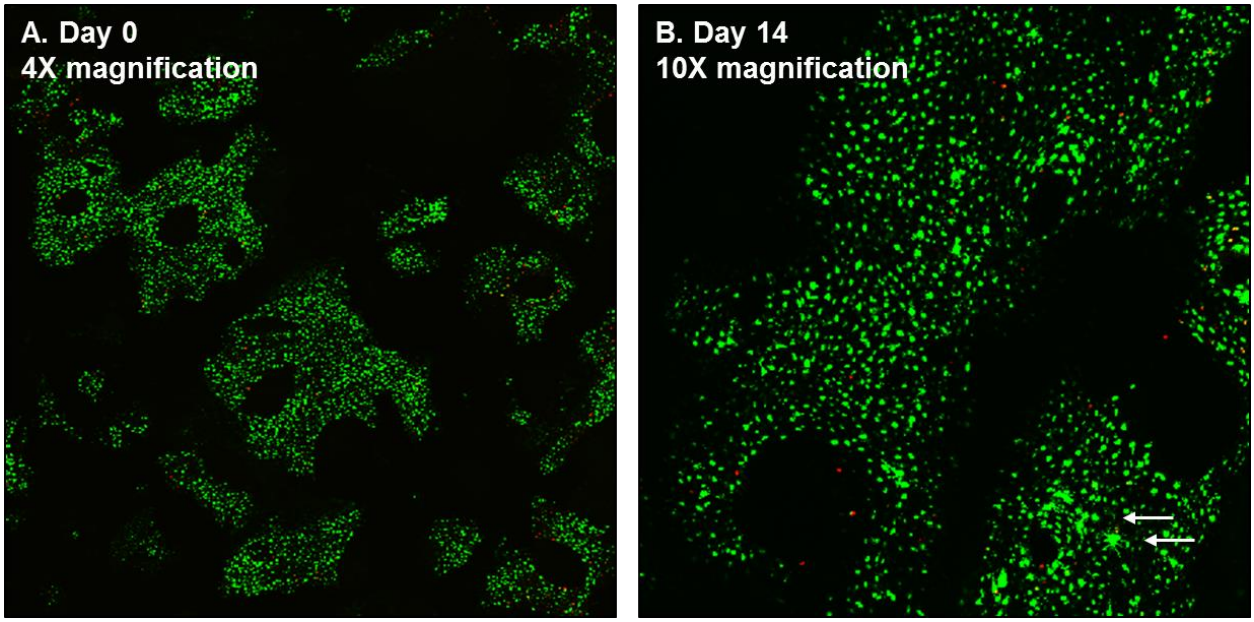

Figure 6.2. Cleaning of trabecular explants. (A) A confocal image of a cleaned trabecular bone explant stained with a LIVE/DEAD cytotoxicity/viability kit. Repeated PBS rinsing and trypsinization removes all surface cells, leaving only live osteocytes embedded in the bone (live cells are green). (B) Cleaned explant after 14 days in culture. Live osteocytes remain in the interior, and rigorous cleaning ensures that few surface cells (arrows) remain to populate the bone surface.

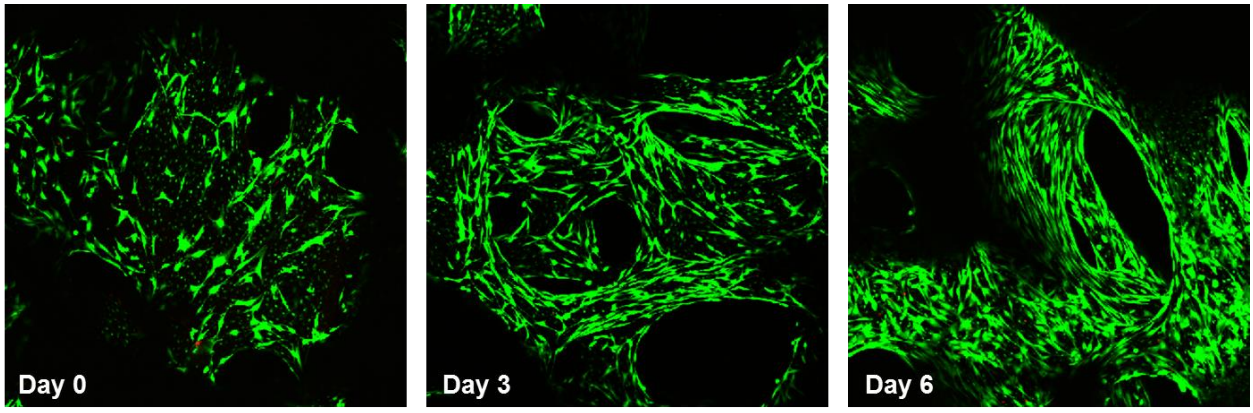

Figure 6.3. Controlled seeding of primary osteoblasts onto trabecular bone explants. Confocal images of trabecular explants stained with a LIVE/DEAD cytotoxicity/viability kit. A defined number of cells are seeded onto explants using a custom cell seeder. Osteoblasts gradually and evenly populate the available bone surfaces.

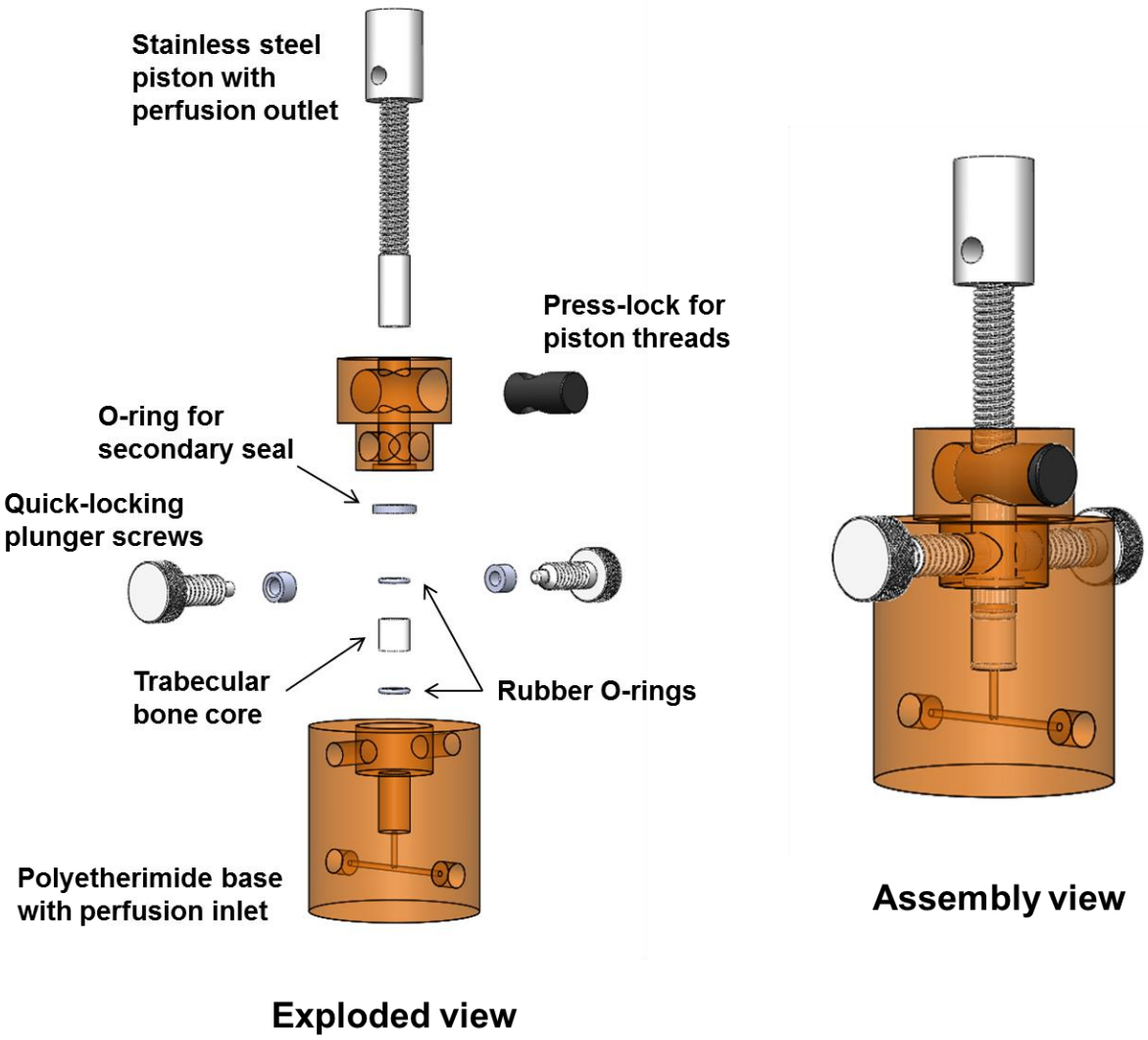

Figure 6.4. Loadable perfusion bioreactor for perfusion and mechanical testing/dynamic loading of trabecular bone explants. The exploded view highlights the main components used to secure the trabecular bone explant (bone core) for loading and perfusion. The assembly view is a schematic of a bioreactor for an individual bone specimen.

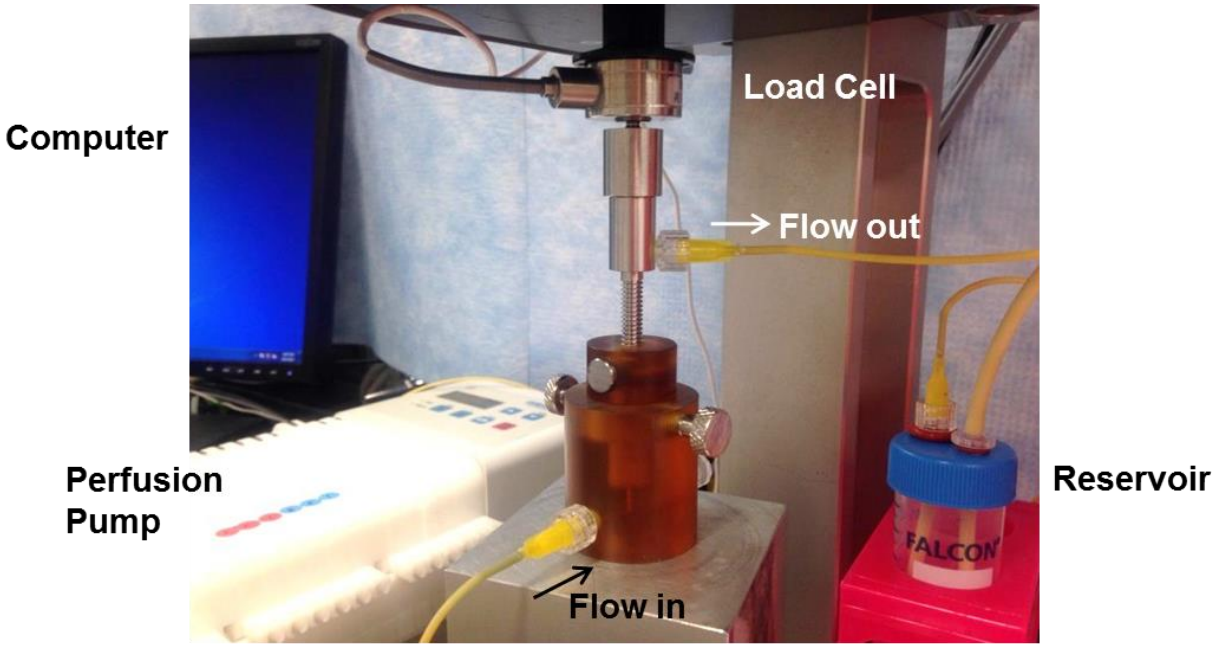

Figure 6.5. Setup of the experimental system. Each loadable perfusion bioreactor is connected to a multi-channel perfusion pump and can be placed in a mechanical testing device for loading or mechanical testing.

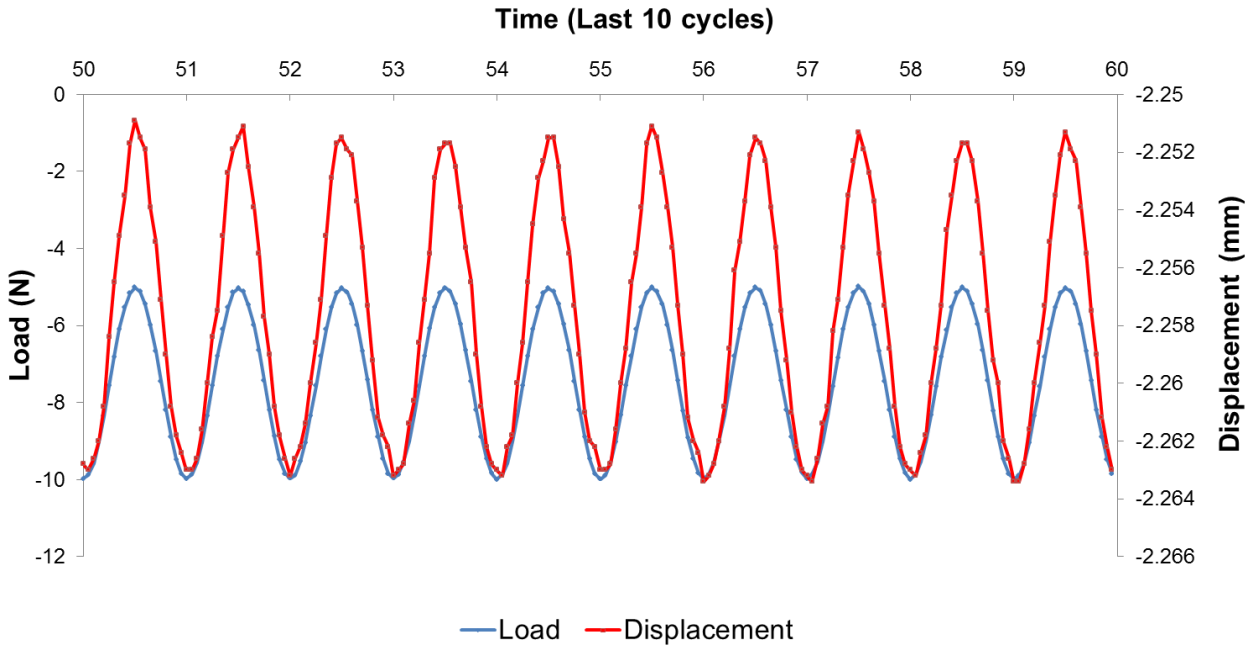

Figure 6.6. Representative load and displacement curve from the last ten cycles of dynamic mechanical testing. The applied waveform was a 1 Hz sinusoidal compressive waveform from --5N (level 1) to -10N (level 2) under load control.

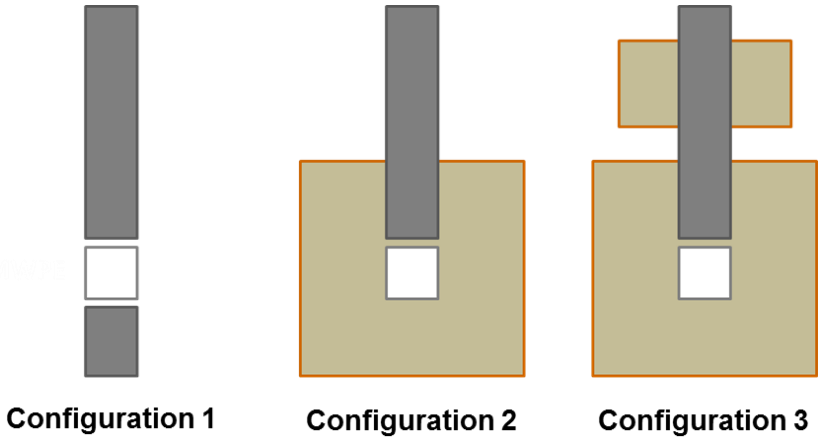

	E1	E2	E3
Original	214.9 ± 4.8	198.0 ± 9.7**	200.1 ± 7.9**
Corrected	546.7 ± 20.4	594.1 ± 81.6	608.8 ± 71.9

p = 0.36

p = 0.16

Figure 6.7. Configurations for mechanical testing of a standard material to evaluate effects of the chamber design on accuracy of mechanical testing. Configuration 1 represents a standard unconfined compression testing configuration between two rigid stainless steel platens. Configurations 2 and 3 are in the polyetherimide chamber base with and without the chamber cap, respectively. Standard ultra-high molecular weight polyethylene solid specimens machined to the same geometry of trabecular bone explants (n=5) were tested in each configuration, and the apparent elastic modulus was determined from the slope of a load-displacement curve constructed from the final compressive cycle of a mechanical test and the specimen geometry. Using one-way ANOVA with Bonferroni's post hoc analysis, significant differences were

detected in the sample moduli determined from specimens in the chamber, but upon correction for the compliance of the plastic base, these differences were no longer significant. **$p<0.01$

A.

Group	Explant Number	Average Height (mm)	Average Diameter (mm)	Average Modulus Day 0 (MPa)	Load Corresponding to 2400με (N)	Average Modulus Day 28 (MPa)	% Change
Tissue Culture Control	8	6.65	7.07	73.4	6.83	70.4	-4.1
	17	6.75	7.10	102.6	9.49	89.4	-12.9
	15	6.55	7.08	92.6	8.52	99.4	7.4
	25	6.66	7.13	107.1	9.92	110.5	3.1
	2	6.81	7.08	102.8	9.77	101.7	-1.1
	3	6.73	7.02	92.2	8.71	85.6	-7.2
Non-loaded	5	6.70	7.07	42.5	4.01	46.0	8.3
	9	6.74	7.02	69.7	6.51	63.2	-9.3
	34	6.71	7.04	84.2	7.86	95.1	13.0
	32	6.55	7.10	90.8	8.39	100.3	10.4
	28	6.69	7.07	103.1	9.58	102.4	-0.6
	26	6.73	7.11	122.2	11.42	127.7	4.5
Loaded 1 Day	7	6.68	7.00	50.9	4.80	57.5	12.9
	12	6.62	7.03	73.6	7.00	50.3	-31.7
	36	6.88	6.99	85.9	8.02	103.8	20.7
	29	6.81	7.08	91.2	8.20	110.1	20.8
	24	6.69	7.00	108.2	10.10	105.9	-2.1
	4	6.65	7.06	127.2	12.19	111.1	-12.7
Loaded 3 Days	16	6.81	7.06	59.3	5.61	64.9	9.4
	18	6.69	7.05	81.9	7.70	102.0	24.5
	20	6.52	7.01	88.1	8.26	88.4	0.4
	30	6.69	7.01	93.6	8.65	82.3	-12.1
	11	6.78	7.04	108.7	10.23	92.6	-14.8
	14	6.70	7.04	131.1	12.22	127.6	-2.7
Loaded 5 Days	21	6.78	7.01	62.0	5.74	*24.6	*-60.2
	19	6.75	7.04	83.3	7.81	75.6	-9.2
	33	6.81	7.02	88.3	8.18	72.8	-17.6
	10	6.76	7.02	96.1	9.14	88.1	-8.3
	22	6.71	6.90	110.4	10.22	122.8	11.2
	31	6.87	7.00	131.3	12.06	110.2	-16.0
Loaded 10 Days	1	6.63	6.98	62.1	5.85	58.2	-6.2
	27	6.81	7.00	83.8	7.78	84.8	1.2
	35	6.64	7.01	89.7	8.30	88.1	-1.8
	6	6.76	7.04	96.3	8.96	80.7	-16.3
	23	6.67	7.01	118.9	11.11	100.3	-15.7
	13	6.69	7.03	133.5	12.35	138.9	4.1

B.

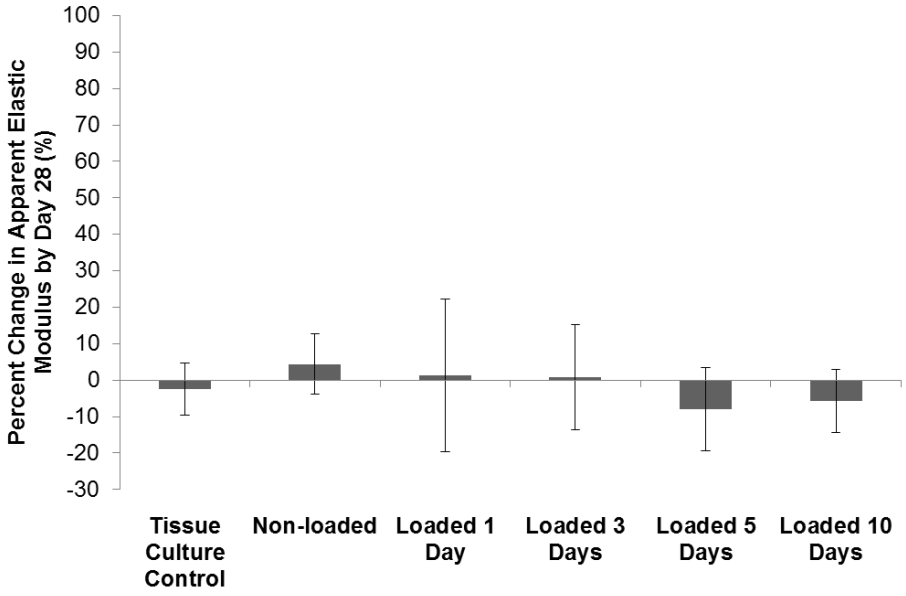

Figure 6.8. Percent change in elastic modulus of devitalized bone cores loaded routinely and culture for 4 weeks. (A) 36 trabecular bone explants were randomly assigned to one of 6 groups (n=6/group): tissue culture control, non-loaded, and loaded for 1, 3, 5, and 10 days. Apparent elastic moduli were determined for each sample at Day 0, and a load level corresponding to 2400με was determined for each sample to apply similar strains across all specimens. The modulus was determined again after 4 weeks (Day 28), and a percent difference

was calculated. (B) Average percent change in apparent elastic modulus for each group. Error bars are standard deviations. One sample was eliminated as an outlier from the 5 day loading group (gray italics). One-way ANOVA with Bonferroni's post hoc analysis was used to determine differences among groups, and $p<0.05$ was set to indicate significance. No differences were detected.

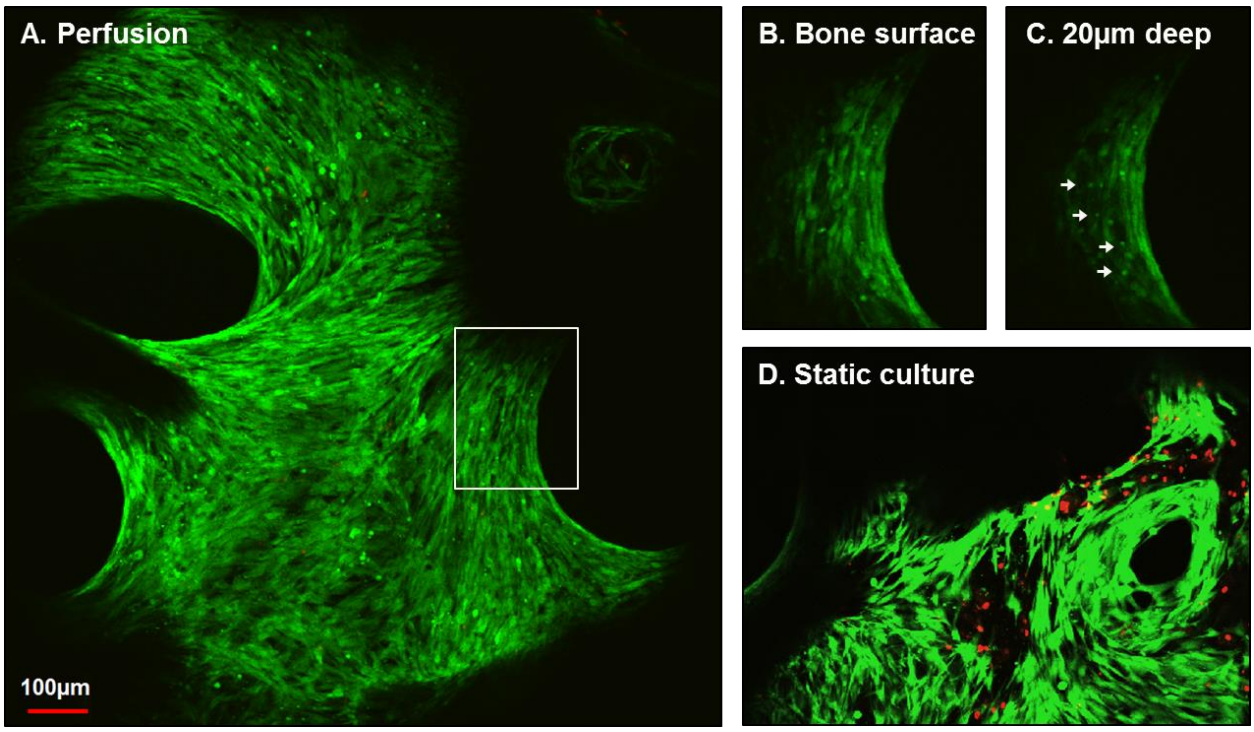

Figure 6.9. Influence of perfusion on osteocyte viability over long term culture. (A) Reconstructed confocal image of an explant perfused for 14 days in the loadable perfusion chamber. (B) Inset of the confocal slice corresponding to the bone surface. (C) Live osteocytes (green cells, white arrows) are observed 20µm below osteoblasts on the bone surface. (D) A number of dead osteocytes (red cells) can be observed in static cultures at the same time point.

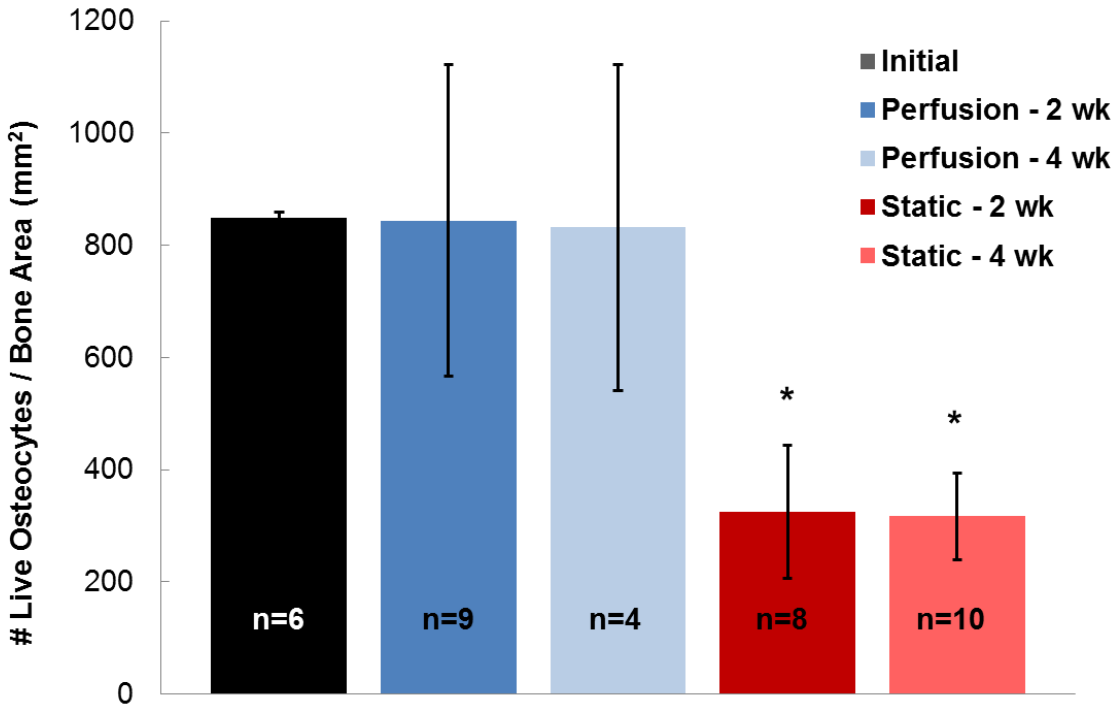

Figure 6.10. Histological assessment of osteocyte viability in explants cultured for 2 or 4 weeks (wk) in loadable perfusion bioreactors compared with static tissue culture controls. Error bars are standard deviations. Sample numbers for each group are indicated. One-way ANOVA with Dunnet's post hoc analysis was used to determine differences in the number of live osteocytes from initial levels. *$p<0.05$

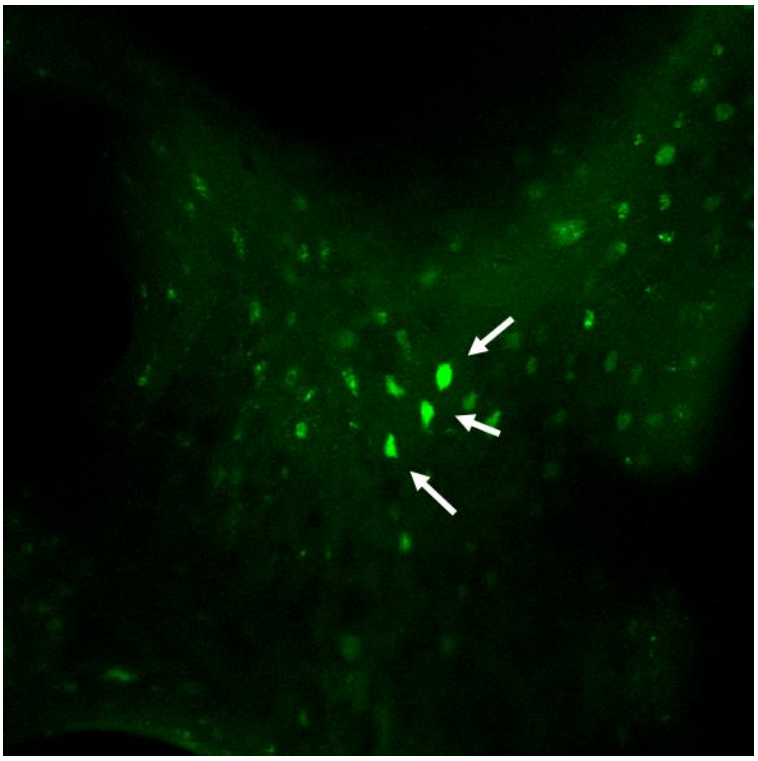

Figure 6.11. Calcium signaling in trabecular bone explants. Confocal image of an explant stained with the Fluo-8 calcium indicator and treated with 50μM ATP. Arrows indicate responsive osteocytes.

Chapter 7

Summary

The work in this thesis solidifies Ca^{2+} signaling as a critical osteocyte response to mechanical loading and adds to the body of work exploring how and why these signals are generated. In Chapter 2, we discovered Ca^{2+}_{cyt} transients are coupled to Ca^{2+}_{ER} dynamics in osteocytes exposed to fluid flow and that T-Type VSCC interact with the ER to effect this behavior. In Chapter 3, we demonstrated that actin cytoskeletal dynamics are involved in Ca^{2+}_{cyt} signal generation and that Ca^{2+} signals in turn activate actomyosin contractions. These contractions can be prevented by the drug jasplakinolide, which has been previously used *in vivo*. In Chapter 4, we identified a new mechanotransduction pathway in which load-induced Ca^{2+}_{cyt} oscillations are facilitating the production and release of extracellular vesicles in osteocytes, which contain key bone regulatory proteins such as RANKL, OPG, and sclerostin. In Chapter 5, we translated our studies to new osteocyte cell lines which more faithfully capture native cell behaviors, namely the expression of sclerostin. Finally, in Chapter 6, we introduced a novel system for exploring interactions between embedded osteocytes and cells on the bone surface which may help translate some of our findings from the cellular level up to the tissue level. Ultimately, a better understanding of the mechanisms behind the robust Ca^{2+}_{cyt} oscillations in osteocytes and how they relate to their roles as coordinators of bone adaptation may improve our ability to prevent or treat bone pathologies underpinned by reduced mechanosensitivity.

References

1 Chen, J.-H., Liu, C., You, L. & Simmons, C. A. Boning up on Wolff's Law: Mechanical regulation of the cells that make and maintain bone. *Journal of Biomechanics* **43**, 108-118 (2010).

2 Wilks, D. C. *et al.* Bone mass and geometry of the tibia and the radius of master sprinters, middle and long distance runners, race-walkers and sedentary control participants: A pQCT study. *Bone* **45**, 91-97 (2009).

3 Jones, H., Priest, J., Hayes, W., Tichenor, C. & Nagel, D. Humeral hypertrophy in response to exercise. *J Bone Joint Surg Am* **59**, 204-8 (1977).

4 Kazakia, G. J. *et al.* The influence of disuse on bone microstructure and mechanics assessed by HR-pQCT. *Bone* **63**, 132-140 (2014).

5 Cowin, S. C. On mechanosensation in bone under microgravity. [Review]. *Bone* **22**, 119S-125S (1998).

6 Smith, S. M. *et al.* Fifty Years of Human Space Travel: Implications for Bone and Calcium Research. *Annual Review of Nutrition* **34**, 377-400 (2014).

7 Spyropoulou, A., Karamesinis, K. & Basdra, E. K. Mechanotransduction pathways in bone pathobiology. *Biochimica et Biophysica Acta (BBA) - Molecular Basis of Disease* **1852**, 1700-1708 (2015).

8 Franz-Odendaal, T. A., Hall, B. K. & Witten, P. E. Buried alive: How osteoblasts become osteocytes. *Developmental Dynamics* **235**, 176-190 (2006).

9 Bonewald, L. F. Establishment and characterization of an osteocyte-like cell line, MLO-Y4. *Journal of Bone and Mineral Metabolism* **17**, 61-65 (1999).

10 Kalajzic, I. *et al.* In vitro and in vivo approaches to study osteocyte biology. *Bone* **54**, 296-306 (2013).

11 Bonewald, L. F. The amazing osteocyte. *J Bone Miner Res* **26**, 229-238 (2011).

12 Bonewald, L. F. & Johnson, M. L. Osteocytes, mechanosensing and Wnt signaling. *Bone* **42**, 606-615 (2008).

13 Jacobs, C. R., Temiyasathit, S. & Castillo, A. B. Osteocyte Mechanobiology and Pericellular Mechanics. *Annual review of biomedical engineering* **12**, 369-400 (2010).

14 Schaffler, M. B., Cheung, W.-Y., Majeska, R. & Kennedy, O. Osteocytes: Master Orchestrators of Bone. *Calcif Tissue Int* **94**, 5-24 (2014).

15 Klein-Nulend, J., Bakker, A. D., Bacabac, R. G., Vatsa, A. & Weinbaum, S. Mechanosensation and transduction in osteocytes. *Bone* **54**, 182-190 (2013).

16 Kamioka, H., Honjo, T. & Takano-Yamamoto, T. A three-dimensional distribution of osteocyte processes revealed by the combination of confocal laser scanning microscopy and differential interference contrast microscopy. *Bone* **28**, 145-149 (2001).

17 Ehrlich, P. J. & Lanyon, L. E. Mechanical strain and bone cell function: a review. *Osteoporosis International* **13**, 688-700 (2002).

18 Owan, I. *et al.* Mechanotransduction in bone: osteoblasts are more responsive to fluid forces than mechanical strain. *The American Journal of Physiology* **273**, C810-815 (1997).

19 Weinbaum, S., Cowin, S. C. & Zeng, Y. A model for the excitation of osteocytes by mechanical loading-induced bone fluid shear stresses. *Journal of Biomechanics* **27**, 339-360 (1994).

20 Piekarski, K. & Munro, M. Transport mechanism operating between blood supply and osteocytes in long bones. *Nature* **269**, 80-82 (1977).

21 Zeng, Y., Cowin, S. & Weinbaum, S. A fiber matrix model for fluid flow and streaming potentials in the canaliculi of an osteon. *Annals of Biomedical Engineering* **22**, 280-292 (1994).

22 Fritton, S. P. & Weinbaum, S. Fluid and Solute Transport in Bone: Flow-Induced Mechanotransduction. *Annual Review of Fluid Mechanics* **41**, 347-374 (2009).

23 Weinbaum, S., Cowin, S. C. & Zeng, Y. A model for the excitation of osteocytes by mechanical loading-induced bone fluid shear stresses. *Journal of Biomechanics* **27**, 339-360 (1994).

24 Price, C., Zhou, X., Li, W. & Wang, L. Real-time measurement of solute transport within the lacunar-canalicular system of mechanically loaded bone: direct evidence for load-induced fluid flow. *J Bone Miner Res* **26**, 277-285 (2011).

25 Kameo, Y. & Adachi, T. Interstitial fluid flow in canaliculi as a mechanical stimulus for cancellous bone remodeling: in silico validation. *Biomech Model Mechanobiol* **13**, 851-860 (2014).

26 Ajubi, N. E. *et al.* Pulsating Fluid Flow Increases Prostaglandin Production by Cultured Chicken Osteocytes—A Cytoskeleton-Dependent Process. *Biochemical and Biophysical Research Communications* **225**, 62-68 (1996).

27 Ajubi, N. E., Klein-Nulend, J., Alblas, M. J., Burger, E. H. & Nijweide, P. J. Signal transduction pathways involved in fluid flow-induced PGE2 production by cultured

osteocytes. *American Journal of Physiology Endocrinology and Metabolism* **276**, E171-E178 (1999).

28 Kamel, M. A., Picconi, J. L., Lara-Castillo, N. & Johnson, M. L. Activation of beta-catenin signaling in MLO-Y4 osteocytic cells versus 2T3 osteoblastic cells by fluid flow shear stress and PGE2: Implications for the study of mechanosensation in bone. *Bone* **47**, 872-881 (2010).

29 Klein-Nulend, J., Semeins, C. M., Ajubi, N. E., Nijweide, P. J. & Burger, E. H. Pulsating Fluid Flow Increases Nitric Oxide (NO) Synthesis by Osteocytes but Not Periosteal Fibroblasts - Correlation with Prostaglandin Upregulation. *Biochemical and Biophysical Research Communications* **217**, 640-648 (1995).

30 Vatsa, A., Smit, T. H. & Klein-Nulend, J. Extracellular NO signalling from a mechanically stimulated osteocyte. *J Biomech* **40 Suppl 1**, S89-95 (2007).

31 Ponik, S. M., Triplett, J. W. & Pavalko, F. M. Osteoblasts and osteocytes respond differently to oscillatory and unidirectional fluid flow profiles. *Journal of Cellular Biochemistry* **100**, 794-807 (2007).

32 Santos, A., Bakker, A. D., Zandieh-Doulabi, B., Semeins, C. M. & Klein-Nulend, J. Pulsating fluid flow modulates gene expression of proteins involved in Wnt signaling pathways in osteocytes. *Journal of Orthopaedic Research* **27**, 1280-1287 (2009).

33 Kim, C. H., You, L., Yellowley, C. E. & Jacobs, C. R. Oscillatory fluid flow-induced shear stress decreases osteoclastogenesis through RANKL and OPG signaling. *Bone* **39**, 1043-1047 (2006).

34 You, L. *et al.* Osteocytes as mechanosensors in the inhibition of bone resorption due to mechanical loading. *Bone* **42**, 172-179 (2008).

35 Tan, S. D. *et al.* Osteocytes subjected to fluid flow inhibit osteoclast formation and bone resorption. *Bone* **41**, 745-751 (2007).

36 Vezeridis, P. S., Semeins, C. M., Chen, Q. & Klein-Nulend, J. Osteocytes subjected to pulsating fluid flow regulate osteoblast proliferation and differentiation. *Biochemical and Biophysical Research Communications* **348**, 1082-1088 (2006).

37 Tatsumi, S. *et al.* Targeted Ablation of Osteocytes Induces Osteoporosis with Defective Mechanotransduction. *Cell Metabolism* **5**, 464-475 (2007).

38 Xiong, J. *et al.* Matrix-embedded cells control osteoclast formation. *Nature Medicine* **17**, 1235-1241 (2011).

39 Nakashima, T. *et al.* Evidence for osteocyte regulation of bone homeostasis through RANKL expression. *Nature Medicine* **17**, 1231-1234 (2011).

40 Robling, A. G. *et al.* Mechanical Stimulation of Bone in Vivo Reduces Osteocyte Expression of Sost/Sclerostin. *Journal of Biological Chemistry* **283**, 5866-5875 (2008).

41 Moustafa, A. *et al.* Mechanical loading-related changes in osteocyte sclerostin expression in mice are more closely associated with the subsequent osteogenic response than the peak strains engendered. *Osteoporosis International* **23**, 1225-1234 (2012).

42 Morse, A. *et al.* Mechanical Load Increases in Bone Formation via a Sclerostin-Independent Pathway. *Journal of Bone and Mineral Research* **29**, 2456-2467 (2014).

43 Spatz, J. M. *et al.* Sclerostin antibody inhibits skeletal deterioration due to reduced mechanical loading. *Journal of Bone and Mineral Research* **28**, 865-874 (2013).

44 Hung, C. T., Pollack, S. R., Reilly, T. M. & Brighton, C. T. Real-time calcium response of cultured bone cells to fluid flow. *Clinical Orthopaedics and Related Research*, 256-269 (1995).

45 Karlstad, J., Sun, Y. & Singh, B. in *Calcium Signaling* Vol. 740 *Advances in Experimental Medicine and Biology*, 143-157 (Springer Netherlands, 2012).

46 Ferreira-Martins, J. *et al.* Spontaneous Calcium Oscillations Regulate Human Cardiac Progenitor Cell Growth. *Circulation Research* **105**, 764-774 (2009).

47 Ohara-Imaizumi, M. *et al.* Pattern of rise in subplasma membrane Ca2+ concentration determines type of fusing insulin granules in pancreatic β cells. *Biochemical and Biophysical Research Communications* **385**, 291-295 (2009).

48 Dolmetsch, R. E., Xu, K. & Lewis, R. S. Calcium oscillations increase the efficiency and specificity of gene expression. *Nature* **392**, 933-936 (1998).

49 Wei, C. *et al.* Calcium flickers steer cell migration. *Nature* **457**, 901-905 (2009).

50 Sun, S., Liu, Y., Lipsky, S. & Cho, M. Physical manipulation of calcium oscillations facilitates osteodifferentiation of human mesenchymal stem cells. *The FASEB Journal* **21**, 1472-1480 (2007).

51 Hwang, S.-Y. & Putney Jr, J. W. Calcium signaling in osteoclasts. *Biochimica et Biophysica Acta (BBA) - Molecular Cell Research* **1813**, 979-983 (2011).

52 Kajiya, H. *et al.* RANKL-induced TRPV2 expression regulates osteoclastogenesis via calcium oscillations. *Cell Calcium* **48**, 260-269 (2010).

53 Kajiya, H. in *Calcium Signaling* Vol. 740 *Advances in Experimental Medicine and Biology*, Ch. 41, 917-932 (Springer Netherlands, 2012).

54 Jacobs, C. R. *et al.* Differential effect of steady versus oscillating flow on bone cells. *J Biomech* **31**, 969-976 (1998).

55 Donahue, S. W., Donahue, H. J. & Jacobs, C. R. Osteoblastic cells have refractory periods for fluid-flow-induced intracellular calcium oscillations for short bouts of flow and display multiple low-magnitude oscillations during long-term flow. *Journal of Biomechanics* **36**, 35-43 (2003).

56 Godin, L. M., Suzuki, S., Jacobs, C. R., Donahue, H. J. & Donahue, S. W. Mechanically induced intracellular calcium waves in osteoblasts demonstrate calcium fingerprints in bone cell mechanotransduction. *Biomech Model Mechanobiol* **6**, 391-398 (2007).

57 Huo, B. *et al.* Fluid Flow Induced Calcium Response in Bone Cell Network. *Cellular and Molecular Bioengineering* **1**, 58-66 (2008).

58 Guo, X. E. *et al.* Intracellular calcium waves in bone cell networks under single cell nanoindentation. *Mol Cell Biomech* **3**, 95-107 (2006).

59 Ishihara, Y. *et al.* In situ imaging of the autonomous intracellular Ca2+ oscillations of osteoblasts and osteocytes in bone. *Bone* **50**, 842-852 (2012).

60 Adachi, T. *et al.* Osteocyte calcium signaling response to bone matrix deformation. *Journal of Biomechanics* **42**, 2507-2512 (2009).

61 Ishihara, Y. *et al.* Ex vivo real-time observation of Ca(2+) signaling in living bone in response to shear stress applied on the bone surface. *Bone* **53**, 204-215 (2013).

62 Adachi, T., Aonuma, Y., Taira, K., Hojo, M. & Kamioka, H. Asymmetric intercellular communication between bone cells: Propagation of the calcium signaling. *Biochemical and Biophysical Research Communications* **389**, 495-500 (2009).

63 Adachi, T. *et al.* Calcium response in single osteocytes to locally applied mechanical stimulus: differences in cell process and cell body. *J Biomech* **42**, 1989-1995 (2009).

64 Thi, M. M., Suadicani, S. O., Schaffler, M. B., Weinbaum, S. & Spray, D. C. Mechanosensory responses of osteocytes to physiological forces occur along processes and not cell body and require αVβ3 integrin. *Proceedings of the National Academy of Sciences* **110**, 21012-21017 (2013).

65 Lu, X. L., Huo, B., Chiang, V. & Guo, X. E. Osteocytic network is more responsive in calcium signaling than osteoblastic network under fluid flow. *J Bone Miner Res* **27**, 563-574 (2012).

66 Jing, D. *et al.* Spatiotemporal properties of intracellular calcium signaling in osteocytic and osteoblastic cell networks under fluid flow. *Bone* (2013).

67 Lu, X. L., Huo, B., Park, M. & Guo, X. E. Calcium response in osteocytic networks under steady and oscillatory fluid flow. *Bone* **51**, 466-473 (2012).

68 Jing, D. *et al.* In situ intracellular calcium oscillations in osteocytes in intact mouse long bones under dynamic mechanical loading. *The FASEB Journal* **28**, 1582-1592 (2014).

69 Baik, A. D. *et al.* Quasi-3D Cytoskeletal Dynamics of Osteocytes under Fluid Flow. *Biophysical Journal* **99**, 2812-2820 (2010).

70 Baik, A. D., Qiu, J., Hillman, E. M., Dong, C. & Edward Guo, X. Simultaneous Tracking of 3D Actin and Microtubule Strains in Individual MLO-Y4 Osteocytes under Oscillatory Flow. *Biochemical and Biophysical Research Communications* (2013).

71 Kamel-ElSayed, S. A., Tiede-Lewis, L. M., Lu, Y., Veno, P. A. & Dallas, S. L. Novel approaches for two and three dimensional multiplexed imaging of osteocytes. *Bone* **76**, 129-140 (2015).

72 Veno, P., Prideaux, M., Dusevich, V., Bonewald, L. & Dallas, S. in *American Society for Bone and Mineral Research* (Minneapolis, MN, 2012).

73 Kato, Y., Windle, J. J., Koop, B. A., Mundy, G. R. & Bonewald, L. F. Establishment of an Osteocyte-like Cell Line, MLO-Y4. *Journal of Bone and Mineral Research* **12**, 2014-2023 (1997).

74 Woo, S. M., Rosser, J., Dusevich, V., Kalajzic, I. & Bonewald, L. F. Cell line IDG-SW3 replicates osteoblast-to-late-osteocyte differentiation in vitro and accelerates bone formation in vivo. *J Bone Miner Res* **26**, 2634-2646 (2011).

75 Spatz, J. M. *et al.* The Wnt-inhibitor Sclerostin is Up-regulated by Mechanical Unloading in Osteocytes in-vitro. *Journal of Biological Chemistry* (2015).

76 Hung, C. T., Allen, F. D., Pollack, S. R. & Brighton, C. T. Intracellular Ca2+ stores and extracellular Ca2+ are required in the real-time Ca2+ response of bone cells experiencing fluid flow. *Journal of Biomechanics* **29**, 1411-1417 (1996).

77 Shao, Y., Alicknavitch, M. & Farach-Carson, M. C. Expression of voltage sensitive calcium channel (VSCC) L-type Cav1.2 (α1C) and T-type Cav3.2 (α1H) subunits during mouse bone development. *Developmental Dynamics* **234**, 54-62 (2005).

78 Thompson, W. R. *et al.* Association of the alpha(2)delta(1) subunit with Ca(v)3.2 enhances membrane expression and regulates mechanically induced ATP release in MLO-Y4 osteocytes. *J Bone Miner Res* **26**, 2125-2139 (2011).

79 Harraz, O. F. *et al.* CaV3.2 Channels and the Induction of Negative Feedback in Cerebral Arteries. *Circulation Research* **115**, 650-661 (2014).

80 Smyth, J. T. *et al.* Activation and regulation of store-operated calcium entry. *Journal of Cellular and Molecular Medicine* **14**, 2337-2349 (2010).

81 Park, C. Y., Shcheglovitov, A. & Dolmetsch, R. The CRAC Channel Activator STIM1 Binds and Inhibits L-Type Voltage-Gated Calcium Channels. *Science* **330**, 101-105 (2010).

82 Wang, Y. *et al.* The Calcium Store Sensor, STIM1, Reciprocally Controls Orai and CaV1.2 Channels. *Science* **330**, 105-109 (2010).

83 Nguyen, N. *et al.* STIM1 participates in the contractile rhythmicity of HL-1 cells by moderating T-type Ca2+ channel activity. *Biochimica et Biophysica Acta (BBA) - Molecular Cell Research* **1833**, 1294-1303 (2013).

84 Miyawaki, A. *et al.* Fluorescent indicators for Ca2+ based on green fluorescent proteins and calmodulin. *Nature* **388**, 882-887 (1997).

85 Qian, T. *et al.* FRET imaging of calcium signaling in live cells in the microenvironment. *Integrative Biology* **5**, 431-438 (2013).

86 Suzuki, J. *et al.* Imaging intraorganellar Ca2+ at subcellular resolution using CEPIA. *Nat Commun* **5** (2014).

87 Costantini, L. & Snapp, E. Probing Endoplasmic Reticulum Dynamics using Fluorescence Imaging and Photobleaching Techniques. *Current Protocols in Cell Biology* (2001).

88 Palmer, A. E. *et al.* Ca2+ indicators based on computationally redesigned calmodulin-peptide pairs. *Chemistry & Biology* **13**, 521-530 (2006).

89 Ishikawa, J. *et al.* A Pyrazole Derivative, YM-58483, Potently Inhibits Store-Operated Sustained Ca2+ Influx and IL-2 Production in T Lymphocytes. *The Journal of Immunology* **170**, 4441-4449 (2003).

90 Chen, Y.-T. *et al.* The ER Ca2+ sensor STIM1 regulates actomyosin contractility of migratory cells. *Journal of cell science* **126**, 1260-1267 (2013).

91 Jairaman, A. & Prakriya, M. Molecular pharmacology of store-operated CRAC channels. *Channels* **7**, 402-414 (2013).

92 Bootman, M. D. *et al.* 2-Aminoethoxydiphenyl borate (2-APB) is a reliable blocker of store-operated Ca2+ entry but an inconsistent inhibitor of InsP3-induced Ca2+ release. *The FASEB Journal* **16**, 1145-1150 (2002).

93 Palmer, A. E., Jin, C., Reed, J. C. & Tsien, R. Y. Bcl-2-mediated alterations in endoplasmic reticulum Ca2+ analyzed with an improved genetically encoded fluorescent sensor. *Proceedings of the National Academy of Sciences* **101**, 17404-17409 (2004).

94 Hara, T. *et al.* Calcium Efflux From the Endoplasmic Reticulum Leads to β-Cell Death. *Endocrinology* **155**, 758-768 (2014).

95 Lee, K. *et al.* The primary cilium functions as a mechanical and calcium signaling nexus. *Cilia* **4**, 7 (2015).

96 Prideaux, M. *et al.* Parathyroid Hormone Induces Bone Cell Motility and Loss of Mature Osteocyte Phenotype through L-Calcium Channel Dependent and Independent Mechanisms. *PloS one* **10**, e0125731 (2015).

97 Cabahug-Zuckerman, P. *et al.* in *Orthopaedic Research Society Annual Meeting* (Las Vegas, NV, 2015).

98 Brown, G. N., Leong, P. L. & Guo, X. E. T-Type voltage-sensitive calcium channels mediate mechanically-induced intracellular calcium oscillations in osteocytes by regulating endoplasmic reticulum calcium dynamics. *Bone* **88**, 56-63 (2016).

99 Kim, T.-J. *et al.* Distinct mechanisms regulating mechanical force-induced Ca2+ signals at the plasma membrane and the ER in human MSCs. **4** (2015).

100 Arnsdorf, E. J., Tummala, P., Kwon, R. Y. & Jacobs, C. R. Mechanically induced osteogenic differentiation – the role of RhoA, ROCKII and cytoskeletal dynamics. *Journal of cell science* **122**, 546-553 (2009).

101 Malone, A. M. *et al.* The role of actin cytoskeleton in oscillatory fluid flow-induced signaling in MC3T3-E1 osteoblasts. *Am J Physiol Cell Physiol* **292**, C1830-1836 (2007).

102 McGarry, J. G., Klein-Nulend, J. & Prendergast, P. J. The effect of cytoskeletal disruption on pulsatile fluid flow-induced nitric oxide and prostaglandin E2 release in osteocytes and osteoblasts. *Biochemical and Biophysical Research Communications* **330**, 341-348 (2005).

103 Tanaka-Kamioka, K., Kamioka, H., Ris, H. & Lim, S.-S. Osteocyte Shape Is Dependent on Actin Filaments and Osteocyte Processes Are Unique Actin-Rich Projections. *Journal of Bone and Mineral Research* **13**, 1555-1568 (1998).

104 Murshid, S. A. *et al.* Actin and microtubule cytoskeletons of the processes of 3D-cultured MC3T3-E1 cells and osteocytes. *Journal of Bone and Mineral Metabolism* **25**, 151-158 (2007).

105 Bacabac, R. G. *et al.* Round versus flat: Bone cell morphology, elasticity, and mechanosensing. *Journal of Biomechanics* **41**, 1590-1598 (2008).

106 Klein-Nulend, J., Bacabac, R. G. & Bakker, A. D. Mechanical Loading and How it Affects Bone Cells: The Role of the Osteocyte Cytoskeleton in Maintaining our Skeleton. *European Cells and Materials* **24**, 278-291 (2012).

107 Chen, N. X. *et al.* Ca2+ regulates fluid shear-induced cytoskeletal reorganization and gene expression in osteoblasts. *Am J Physiol Cell Phsyiol* **278**, C989-997 (2000).

108 Vatsa, A., Semeins, C. M., Smit, T. H. & Klein-Nulend, J. Paxillin localisation in osteocytes—Is it determined by the direction of loading? *Biochemical and Biophysical Research Communications* **377**, 1019-1024 (2008).

109 Kim, T.-J. *et al.* Substrate rigidity regulates Ca2+ oscillation via RhoA pathway in stem cells. *Journal of Cellular Physiology* **218**, 285-293 (2009).

110 Godbout, C. *et al.* The Mechanical Environment Modulates Intracellular Calcium Oscillation Activities of Myofibroblasts. *PloS One* **8**, 1-10 (2013).

111 Pavalko, F. M. *et al.* Fluid shear-induced mechanical signaling in MC3T3-E1 osteoblasts requires cytoskeleton-integrin interactions. *Am J Physiol Cell Physiol* **275**, C1591-1601 (1998).

112 Malone, A. M. D. *et al.* The role of actin cytoskeleton in oscillatory fluid flow-induced signaling in MC3T3-E1 osteoblasts. *Am J Physiol Cell Phsyiol* **292**, C1830-C1836 (2007).

113 Miyauchi, A. *et al.* αVβ3 Integrin ligands enhance volume-sensitive calcium influx in mechanically stretched osteocytes. *Journal of Bone and Mineral Metabolism* **24**, 498-504 (2006).

114 Miyauchi, A. *et al.* Parathyroid Hormone-activated Volume-sensitive Calcium Influx Pathways in Mechanically Loaded Osteocytes. *Journal of Biological Chemistry* **275**, 3335-3342 (2000).

115 Rath, A. L. *et al.* Correlation of cell strain in single osteocytes with intracellular calcium, but not intracellular nitric oxide, in response to fluid flow. *J Biomech* **43**, 1560-1564 (2010).

116 Li, B. *et al.* Development of micropost force sensor array with culture experiments for determination of cell traction forces. *Cell Motility and the Cytoskeleton* **64**, 509-518 (2007).

117 Brown, S. & Spudich, J. Cytochalasin inhibits the rate of elongation of actin filament fragments. *The Journal of Cell Biology* **83**, 657-662 (1979).

118 Holzinger, A. in *Cytoskeleton Methods and Protocols*, 71-87 (Humana Press, 2010).

119 Trendowski, M. Exploiting the cytoskeletal filaments of neoplastic cells to potentiate a novel therapeutic approach. *Biochimica et Biophysica Acta (BBA) - Reviews on Cancer* **1846**, 599-616 (2014).

120 Zouani, O. F., Rami, L., Lei, Y. & Durrieu, M.-C. Insights into the osteoblast precursor differentiation towards mature osteoblasts induced by continuous BMP-2 signaling. *Biology Open* **2**, 872-881 (2013).

121 Honjo, T. *et al.* Promotion of Ccn2 expression and osteoblastic differentiation by actin polymerization, which is induced by laminar fluid flow stress. *J. Cell Commun. Signal.* **6**, 225-232 (2012).

122 Miyawaki, A., Griesbeck, O., Heim, R. & Tsien, R. Y. Dynamic and quantitative Ca(2+) measurements using improved cameleons. *Proceedings of the National Academy of Sciences* **96**, 2135-2140 (1999).

123 Bashour, K. T. *et al.* CD28 and CD3 have complementary roles in T-cell traction forces. *Proceedings of the National Academy of Sciences* **111**, 2241-2246 (2014).

124 Nightingale, T. D. *et al.* Actomyosin II contractility expels von Willebrand factor from Weibel–Palade bodies during exocytosis. *The Journal of Cell Biology* **194**, 613-629 (2011).

125 Wollman, R. & Meyer, T. Coordinated oscillations in cortical actin and Ca2+ correlate with cycles of vesicle secretion. *Nat Cell Biol* **14**, 1261-1269 (2012).

126 Kamioka, H., Sugawara, Y., Honjo, T., Yamashiro, T. & Takano-Yamamoto, T. Terminal Differentiation of Osteoblasts to Osteocytes Is Accompanied by Dramatic Changes in the Distribution of Actin-Binding Proteins. *Journal of Bone and Mineral Research* **19**, 471-478 (2004).

127 Panebra, A. *et al.* Regulation of phospholipase C-γ1 by the actin-regulatory protein villin. *Am J Phsyiol Cell Physiol* **281**, C1046-1058 (2001).

128 Reilly, G., Knapp, H., Stemmer, A., Niederer, P. & Knothe Tate, M. Investigation of the Morphology of the Lacunocanalicular System of Cortical Bone Using Atomic Force Microscopy. *Annals of Biomedical Engineering* **29**, 1074-1081 (2001).

129 Kerschnitzki, M. *et al.* Architecture of the osteocyte network correlates with bone material quality. *Journal of Bone and Mineral Research* **28**, 1837-1845 (2013).

130 Milovanovic, P. *et al.* Osteocytic Canalicular Networks: Morphological Implications for Altered Mechanosensitivity. *ACS Nano* **7**, 7542-7551 (2013).

131 Rubin, C. T., Bain, S. D. & McLeod, K. J. Suppression of the osteogenic response in the aging skeleton. *Calcif Tissue Int* **50**, 306-313 (1992).

132 Turner, C. H., Takano, Y. & Owan, I. Aging changes mechanical loading thresholds for bone formation in rats. *Journal of Bone and Mineral Research* **10**, 1544-1549 (1995).

133 Srinivasan, S. *et al.* Enabling bone formation in the aged skeleton via rest-inserted mechanical loading. *Bone* **33**, 946-955 (2003).

134 Meakin, L. B., Galea, G. L., Sugiyama, T., Lanyon, L. E. & Price, J. S. Age-Related Impairment of Bones' Adaptive Response to Loading in Mice Is Associated With Sex-

Related Deficiencies in Osteoblasts but No Change in Osteocytes. *Journal of Bone and Mineral Research* **29**, 1859-1871 (2014).

135 Meakin, L. B., Udeh, C., Galea, G. L., Lanyon, L. E. & Price, J. S. Exercise does not enhance aged bone's impaired response to artificial loading in C57Bl/6 mice. *Bone* **81**, 47-52 (2015).

136 Holguin, N., Brodt, M. D., Sanchez, M. E. & Silva, M. J. Aging diminishes lamellar and woven bone formation induced by tibial compression in adult C57BL/6. *Bone* **65**, 83-91 (2014).

137 Duncan, R. L. & Turner, C. H. Mechanotransduction and the functional response of bone to mechanical strain. *Calcif Tissue Int* **57**, 344-358. (1995).

138 Rochefort, G. Y. The osteocyte as a therapeutic target in the treatment of osteoporosis. *Therapeutic Advances in Musculoskeletal Disease* **6**, 79-91 (2014).

139 Xiong, J. *et al.* Osteocytes, not Osteoblasts or Lining Cells, are the Main Source of the RANKL Required for Osteoclast Formation in Remodeling Bone. *PloS One* **10**, e0138189 (2015).

140 Burgers, T. A. & Williams, B. O. Regulation of Wnt/β-catenin signaling within and from osteocytes. *Bone* **54**, 244-249 (2013).

141 ten Dijke, P., Krause, C., de Gorter, D. J. J., Löwik, C. W. G. M. & van Bezooijen, R. L. Osteocyte-Derived Sclerostin Inhibits Bone Formation: Its Role in Bone Morphogenetic Protein and Wnt Signaling. *The Journal of Bone & Joint Surgery* **90**, 31-35 (2008).

142 Padhi, D., Jang, G., Stouch, B., Fang, L. & Posvar, E. Single-dose, placebo-controlled, randomized study of AMG 785, a sclerostin monoclonal antibody. *J Bone Miner Res* **26**, 19-26 (2011).

143 McColm, J., Hu, L., Womack, T., Tang, C. C. & Chiang, A. Y. Single- and Multiple-Dose Randomized Studies of Blosozumab, a Monoclonal Antibody Against Sclerostin, in Healthy Postmenopausal Women. *Journal of Bone and Mineral Research* **29**, 935-943 (2014).

144 McClung , M. R. *et al.* Romosozumab in Postmenopausal Women with Low Bone Mineral Density. *New England Journal of Medicine* **370**, 412-420 (2014).

145 Ominsky, M. S. *et al.* Differential temporal effects of sclerostin antibody and parathyroid hormone on cancellous and cortical bone and quantitative differences in effects on the osteoblast lineage in young intact rats. *Bone* **81**, 380-391 (2015).

146 Stolina, M. *et al.* Temporal changes in systemic and local expression of bone turnover markers during six months of sclerostin antibody administration to ovariectomized rats. *Bone* **67**, 305-313 (2014).

147 Zhang, J.-N. *et al.* The role of the sphingosine-1-phosphate signaling pathway in osteocyte mechanotransduction. *Bone* **79**, 71-78 (2015).

148 Liu, C. *et al.* Effects of cyclic hydraulic pressure on osteocytes. *Bone* **46**, 1449-1456 (2010).

149 Li, X. *et al.* Connexin 43 is a potential regulator in fluid shear stress-induced signal transduction in osteocytes. *Journal of Orthopaedic Research* **31**, 1959-1965 (2013).

150 Kennedy, O. D., Laudier, D. M., Majeska, R. J., Sun, H. B. & Schaffler, M. B. Osteocyte apoptosis is required for production of osteoclastogenic signals following bone fatigue in vivo. *Bone* **64**, 132-137 (2014).

151 Plotkin, L. I. *et al.* Inhibition of Osteocyte Apoptosis Prevents the Increase in Osteocytic Receptor Activator of Nuclear Factor κB Ligand (RANKL) but Does Not Stop Bone Resorption or the Loss of Bone Induced by Unloading. *Journal of Biological Chemistry* **290**, 18934-18942 (2015).

152 Cabahug-Zuckerman, P. *et al.* Osteocyte Apoptosis Caused by Hindlimb Unloading is Required to Trigger Osteocyte RANKL Production and Subsequent Resorption of Cortical and Trabecular Bone in Mice Femurs. *Journal of Bone and Mineral Research*, n/a-n/a (2016).

153 Hu, M., Tian, G.-W., Gibbons, D. E., Jiao, J. & Qin, Y.-X. Dynamic fluid flow induced mechanobiological modulation of in situ osteocyte calcium oscillations. *Archives of Biochemistry and Biophysics* **579**, 55-61 (2015).

154 Parajuli, A. *et al.* Bone's responses to mechanical loading are impaired in type 1 diabetes. *Bone* **81**, 152-160 (2015).

155 You, J. *et al.* Osteopontin Gene Regulation by Oscillatory Fluid Flow via Intracellular Calcium Mobilization and Activation of Mitogen-activated Protein Kinase in MC3T3–E1 Osteoblasts. *Journal of Biological Chemistry* **276**, 13365-13371 (2001).

156 Follonier, L., Schaub, S., Meister, J.-J. & Hinz, B. Myofibroblast communication is controlled by intercellular mechanical coupling. *Journal of Cell Science* **121**, 3305-3316 (2008).

157 Kalra, H., Drummen, G. & Mathivanan, S. Focus on Extracellular Vesicles: Introducing the Next Small Big Thing. *International Journal of Molecular Sciences* **17**, 170 (2016).

158 Colombo, M., Raposo, G. & Théry, C. Biogenesis, Secretion, and Intercellular Interactions of Exosomes and Other Extracellular Vesicles. *Annual Review of Cell and Developmental Biology* **30**, 255-289 (2014).

159 Théry, C. Exosomes: secreted vesicles and intercellular communications. *F1000 Biology Reports* **3**, 15 (2011).

160 Théry, C., Amigorena, S., Raposo, G. & Clayton, A. in *Current Protocols in Cell Biology* (John Wiley & Sons, Inc., 2001).

161 Solberg, L. B., Stang, E., Brorson, S. H., Andersson, G. & Reinholt, F. P. Tartrate-resistant acid phosphatase (TRAP) co-localizes with receptor activator of NF-KB ligand (RANKL) and osteoprotegerin (OPG) in lysosomal-associated membrane protein 1 (LAMP1)-positive vesicles in rat osteoblasts and osteocytes. *Histochem Cell Biol* **143**, 195-207 (2015).

162 Wang, L. *et al.* In situ measurement of solute transport in the bone lacunar-canalicular system. *Proceedings of the National Academy of Sciences* **102**, 11911-11916 (2005).

163 Sharma, D. *et al.* Alterations in the Osteocyte Lacunar-Canalicular Microenvironment due to Estrogen Deficiency. *Bone* **51**, 488-497 (2012).

164 Wirtz, H. & Dobbs, L. Calcium mobilization and exocytosis after one mechanical stretch of lung epithelial cells. *Science* **250**, 1266-1269 (1990).

165 Tchivilev, I. V., Graff, R. D. & Lee, G. M. in *Orthopaedic Research Society Annual Meeting* (2003).

166 Stern, A. R. *et al.* Isolation and culture of primary osteocytes from the long bones of skeletally mature and aged mice. *BioTechniques* **52**, 361-373 (2012).

167 Pathak, J. L. *et al.* Mechanical Loading Reduces Inflammation-Induced Human Osteocyte-to-Osteoclast Communication. *Calcif Tissue Int* **97**, 169-178 (2015).

168 Li, J., Rose, E., Frances, D., Sun, Y. & You, L. Effect of oscillating fluid flow stimulation on osteocyte mRNA expression. *Journal of Biomechanics* **45**, 247-251 (2012).

169 Kulkarni, R. N., Bakker, A. D., Everts, V. & Klein-Nulend, J. Inhibition of Osteoclastogenesis by Mechanically Loaded Osteocytes: Involvement of MEPE. *Calcif Tissue Int* **87**, 461-468 (2010).

170 Lau, E. *et al.* Effect of low-magnitude, high-frequency vibration on osteocytes in the regulation of osteoclasts. *Bone* **46**, 1508-1515 (2010).

171 Hernandez, P., Whitty, C., John Wardale, R. & Henson, F. M. D. New insights into the location and form of sclerostin. *Biochemical and Biophysical Research Communications* **446**, 1108-1113 (2014).

172 Wolff, J. *Das Gaesetz der Transformation der Knochen*. (Hirchwild, 1892).

173 Boukhechba, F. *et al.* Human Primary Osteocyte Differentiation in a 3D Culture System. *Journal of Bone and Mineral Research* **24**, 1927-1935 (2009).

174 Honma, M., Ikebuchi, Y., Kariya, Y. & Suzuki, H. Establishment of optimized in vitro assay methods for evaluating osteocyte functions. *Journal of Bone and Mineral Metabolism* **33**, 73-84 (2015).

175 Vazquez, M. *et al.* A New Method to Investigate How Mechanical Loading of Osteocytes Controls Osteoblasts. *Frontiers in Endocrinology* **5**, 208 (2014).

176 Jones, D. B., Broeckmann, E., Pohl, T. & Smith, E. L. Development of a mechanical testing and loading system for trabecular bone studies for long term culture. *Eur Cell Mater* **5**, 48-59; discussion 59-60 (2003).

177 Davies, C. M. *et al.* Mechanically loaded ex vivo bone culture system 'Zetos': systems and culture preparation. *Eur Cell Mater* **11**, 57-75; discussion 75 (2006).

178 David, V. *et al.* Ex Vivo Bone Formation in Bovine Trabecular Bone Cultured in a Dynamic 3D Bioreactor is Enhanced by Compressive Mechanical Strain. *Tissue Eng Part A* **14**, 117-126 (2008).

179 Vivanco, J. *et al.* Apparent elastic modulus of ex vivo trabecular bovine bone increases with dynamic loading. *Proceedings of the Institution of Mechanical Engineers, Part H: Journal of Engineering in Medicine* **227**, 904-912 (2013).

180 Zong ming, W. *et al.* Bone formation in rabbit cancellous bone explant culture model is enhanced by mechanical load. *BioMedical Engineering OnLine* **12**, 35-35 (2013).

181 Davidson, E. H. *et al.* Flow perfusion maintains ex vivo bone viability: a novel model for bone biology research. *Journal of Tissue Engineering and Regenerative Medicine* **6**, 769-776 (2012).

182 Haj, A. J. E., Minter, S. L., Rawlinson, S. C. F., Suswillo, R. & Lanyon, L. E. Cellular responses to mechanical loading in vitro. *Journal of Bone and Mineral Research* **5**, 923-932 (1990).

183 Rawlinson, S. C. *et al.* Loading-related increases in prostaglandin production in cores of adult canine cancellous bone in vitro: A role for prostacyclin in adaptive bone remodeling? *Journal of Bone and Mineral Research* **6**, 1345-1351 (1991).

184 Pitsillides, A. *et al.* Mechanical strain-induced NO production by bone cells: a possible role in adaptive bone (re)modeling? *FASEB J.* **9**, 1614-1622 (1995).

185 Rawlinson, S. C. F., Mosley, J. R., Suswillo, R. F. L., Pitsillides, A. A. & Lanyon, L. E. Calvarial and limb bone cells in organ and monolayer culture do not show the same early responses to dynamic mechanical strain. *Journal of Bone and Mineral Research* **10**, 1225-1232 (1995).

186 Rawlinson, S. C. F., Mohan, S., Baylinli, D. J. & Lanyon, L. E. Exogenous prostacyclin, but not prostaglandin E2;, produces similar responses in both G6PD activity and RNA

production as mechanical loading, and increases IGF-II release, in adult cancellous bone in culture. *Calcif Tissue Int* **53**, 324-329 (1993).

187 Takai, E., Mauck, R. L., Hung, C. T. & Guo, X. E. Osteocyte Viability and Regulation of Osteoblast Function in a 3D Trabecular Bone Explant Under Dynamic Hydrostatic Pressure. *Journal of Bone and Mineral Research* **19**, 1403-1410 (2004).

188 Chan, M. *et al.* A Trabecular Bone Explant Model of Osteocyte–Osteoblast Co-Culture for Bone Mechanobiology. *Cellular and Molecular Bioengineering* **2**, 405-415 (2009).

189 Endres, S., Kratz, M., Wunsch, S. & Jones, D. B. Zetos: a culture loading system for trabecular bone. Investigation of different loading signal intensities on bovine bone cylinders. *J Musculoskelet Neuronal Interact* **9**, 173-183 (2009).

190 Cartmell, S. H., Porter, B. D. & Guldberg, R. E. Effect of Media Perfusion Rate on Cell Seeded 3D Constructs In Vitro. *in 2002 Annual BMES Fall Meeting* (2002).